
UNITED KINGDOM · CHINA · MALAYSIA

# Colouring Naphthalene Diimides

Samuel J Quinn

## Abstract

Naphthalene diimides have been explored in a wide variety of ways; They are a promising candidate for organic electronics, boasting the ability to form n-type semiconductor materials, the stability of their anions further aiding in this regard. Their electron poor aromatic core can be used in host guest chemistry to generate interlocked species. The ability to tune their electronic properties and how this could be manipulated to create photovoltaic devices is primarily focus of this thesis.

A series of naphthalene diimides substituted at the core with morpholine moieties have been synthesized and their optical and electronic properties have been probed. Interestingly these species were found to not follow the typical trends for core substituted naphthalene diimides. Through further investigation it was revealed that this unexpected behavior was due to the conformation of core substituents, typically considered unimpactful.

In addition to these species, more complex naphthalene diimide systems, core substituted with phenothiazine and phenoxazine, have been synthesized. By combination of the electron deficient naphthalene diimide with the electron rich phenothiazine and phenoxazine electron donor-acceptor species have been created. These species can be excited by visible light and upon excitation have the potential to generate a charge separated state, which could be used to generate current in a photovoltaic device.

Finally a naphthalene diimide furnished with two BODIPY units was synthesized in an attempt to utilize it as the central rod of a rotaxane. The electronic properties of this rod species were also attempted to be modulated via thionation of the naphthalene diimide core. These species would be used to assess the viability of utilizing BODIPY as a light harvesting antenna for naphthalene diimide systems.

“The prudent text-books give it
In tables at the end
'The stress that shears a rivet
Or makes a tie-bar bend-
'What traffic wrecks macadam-
What concrete should endure-
but we, poor Sons of Adam
Have no such literature,
*To warn us or make sure! ”*

Rudyard Kipling – Hymn of Breaking Strain

# Acknowledegements

There is no way that this book could never have been written if it was not for all the help I received from so many people along the way. First foremost Professor Neil Champness, who provided me with inspiration, encouragement and was always there to talk about how ridiculous it all was.

Dr Stephen Davies for his expert help with CV, Spectroelectrochemistry and EPR, but also some excellent walking recommendations.

Dr William Lewis for all his help with crystallography service. Also all the people involved in running all the analytical services at Nottingham I used throughout my PhD.

The excellent postdocs who I have worked with: Dr Lixu Yang, for all her synthetic insight and brutal one-liners, Dr Constance Pfeiffer for teaching me crystallography and being an excellent secretary and Dr Nic Pearce primarily for dad jokes but also for a huge amount of help with my thesis writing.

Also all of my B52 lab mates. Firstly Ben, he knows what he did, Tim Hames for his unending optimism, Harry for reminding me how much work goes into a PhD, Sarah for helping me yell at my molecules, Charlie for asking the right questions, Harry for not being sick on me, Phillllliiippipppi for being my contender for the silliest laugh, Arjun for teaching me so many new words and Maggie for also

being so kind. Jim and Jack for being excellent partners in crime throughout the whole process, along with the rest of Irene. Finally my family for their support throughout the whole endeavor.

# List of abbreviations

| | |
|---|---|
| **BODIPY** | 4,4-difluoro-4-bora-3a,4a-diaza-s-indacene |
| **cNDI** | Core substituted naphthalene diimide |
| **cPDI** | Core substituted perylene diimide |
| **CV** | Cyclic voltammetry |
| **d** | Day |
| **DCM** | Dichloromethane |
| **DDQ** | 2,3-Dichloro-5,6-dicyano-1,4-benzoquinone |
| **DFT** | Density functional theory |
| **DMF** | Dimethylformamide |
| **DMSO** | Dimethyl sulfoxide |
| **DNA** | Deoxyribonucleic acid |
| $E_{1/2}$ | Redox potential |
| **EPR** | Electron paramagnetic resonanc |
| **$Fc^+$ /Fc** | Ferrocenium/ Ferrocene |
| **FD** | Field desorption |
| $g_{iso}$ | Isotropic g-factor |
| **h** | Hour |
| **HDI** | Hexarylene diimide |
| **HOMO** | Highest occupied molecular orbital |
| **LUMO** | Lowest unoccupied molecular orbital |
| **min** | Minute |
| **MALDI** | Matrix assisted laser desorption/ionization |
| **MS** | Mass spectrometry |
| **NDA** | 1,4,5,8-Naphthalenetetracarboxylic dianhydride |
| **NDI** | Naphthalene diimide |
| **NMR** | Nuclear magnetic resonance |
| **ODI** | Octaarylene diimide |
| **OFET** | Organic field effect transistor |
| **OLED** | Organic light emitting diode |
| **PDA** | Perylene-3,4,9,10-tetracarboxylic dianhydride |
| **PDI** | Perylene diimide |
| **PET** | Photoinduced electron transfer |
| **PIO** | Photoinduced oxidation |
| **PIR** | Photoinduced reduction |
| **RT** | Room temperature |
| **TBCA** | Tribromoisocyanuric acid |
| **TFA** | Trifluoroacetic acid |
| **THF** | Tetrahydrofuran |
| **TMS** | Trimethylsilyl |
| **TMSA** | Trimethylsilylacetylene |

| | |
|---|---|
| **UV** | Ultraviolet |
| **vis** | Visible |
| **ε** | Molar absorption extinction coefficient |
| **λ** | Wavelength |
| **Δ** | Change in |

# Contents

# Chapter 1 : Introduction

## 1.1: Organic dye molecules

Colours have always fascinated mankind; the ability to change the colour of our environment is something appealing to humans. Historically this was achieved by utilizing metals salts[1] or by extracting naturally produced organic pigments from organisms[2] to generate dyes. This changed after industrialisation with William Perkin's accidental discovery of the Mauveine family of purple dyes (Figure 1-1).[3,4] Up until this time purple dyes could only be generated via the extraction of pigment from around 12000 sea snails.[5] Industrialisation allowed for large scale production of Mauveine[6] and launched the synthetic dye industry, proving that synthetic dyes could be produced in larger quantities and more cheaply than dyes extracted from natural stocks.

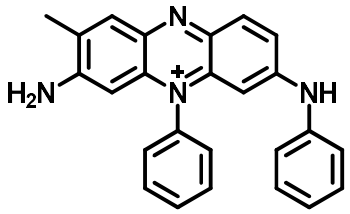


Figure 1-1: Structure of Mauveine A one of the 12 discovered members of the Mauveine dye family[6]

The potential of organic dyes has been explored much further since this initial success, and dyes are now available in shades across the entire visible range. Perhaps more importantly however, organic dye molecules have been incorporated into more complex systems allowing them to go beyond colouring agents and become tools. Such uses have included the tagging of biological samples,[7] allowing for

the easy detection of species in both medicinal and biological fields without the need for complex detection machinery. Dyes have also been shown to be instrumental in increasing the detection limit of optical spectroscopy, seen in the Nobel prize worthy work of Betzig, Hell and Moerner.[8] Organic dyes have also infiltrated modern electronic devices notably in revolutionary laser light sources,[9] OLEDs[10] and are being used in photovoltaic devices.[11]

The origin of colour in organic dyes arises from their extended conjugated π systems, enabling the electronic transitions of the molecule to be lowered in energy into the visible range. The extended π systems' electronics can be fine-tuned by synthetic manipulation, such as using electron donating or withdrawing groups to change the energy of the highest occupied molecular orbital (HOMO) and the lowest unoccupied molecular orbital (LUMO).[12] For example, a group that stabilises and lowers the energy of the HOMO increases the energy gap between the HOMO and the LUMO (assuming the LUMO remains unaffected), thus shortening the wavelength of the light absorbed. Many organic dyes also exhibit fluorescence due to a stabilised excited state with limited ways to relax non-radiatively, opening the possibility of utilising the energy of such excited states for other purposes. This thesis focuses upon exploring two families of organic dyes: rylene diimides and BODIPYs.

## 1.2: Rylene tetracarboxylic diimides

Rylene tetracarboxylic diimides[13] are a family of organic dyes consisting of a number of naphthalene units joined together, capped with an imide group on either end of the oligomer at the 1 and 8 positions of the terminal naphthalenes (Figure 1-2). Initial interest in these species was built around their physical properties, which cause them to form n-type semiconductor materials.[14] Rylene diimides have also been found to have high electron affinities and mobilities, and in addition they exhibit highly absorbing optical bands whilst retaining a high level of thermal and photochemical stability.[15-17] This combination of properties makes rylene diimides excellent candidates for organic electronics.[18]

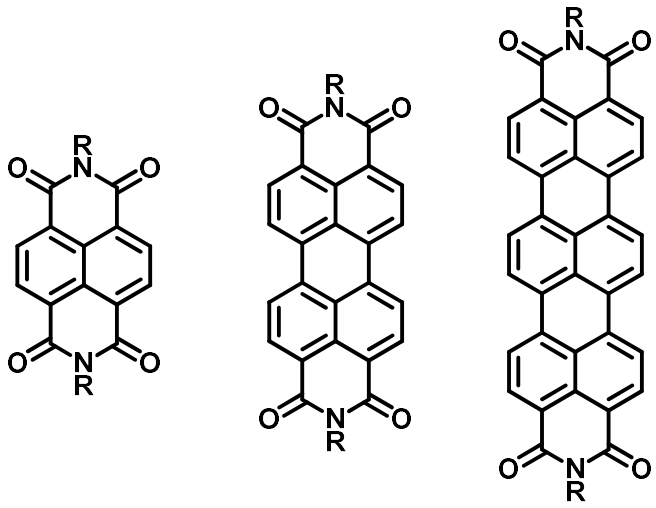


Figure 1-2: General structures of rylene diimides NDI, PDI and TDI (left to right)

The typical synthesis of these species involves heating of the dianhydride to a moderately high temperature with an excess of the desired amine,[19] resulting in a condensation reaction that forms the diimide. Though larger rylene diimides have been synthesized, with the largest being the 8 naphthyl unit ODI,[20] only 1,4,5,8-naphthalenetetracarboxylic dianhydride (NDA) and perylene-3,4,9,10-tetracarboxylic dianhydride (PDA) are commercially available and as a result naphthalene diimide (NDI) and perylene diimide (PDI) have been widely studied.

## 1.3: Naphthalene diimides

The structure of an NDI consists of a single naphthyl unit capped with two imide rings on opposite sides of the molecule. There are 3 locations where an NDI may be synthetically modified (Figure 1-3): the imide residue, the aromatic core and the carbonyls. The synthesis of NDI was first reported from pyrene in the 1930s by Vollman,[21] who later also reported upon how the "practically colourless" nature of NDI could be altered to generate dye species via core subsitution.[22] Asymmetric substitution of the imide residues of NDIs is not straightforward, generally requiring the mono imide to be less reactive than the di, the exception being the Ghadiri method[23] which allows for asymmetric substitution of NDIs with alkyl substituents.

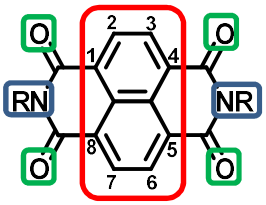


Figure 1-3: Structure and numbering system of NDIs, showcasing the aromatic core (red), imide residue (blue) and carbonyl (green)

Examination of the redox properties of NDIs (Figure 1-4) reveals that they undergo two reversible reductions at relatively mild potentials, the first at -1.1 V (vs $Fc^+/Fc$) to create a stable radical anion, and the second at -1.5 V (vs $Fc^+/Fc$) to generate the dianion.[19,24] The nature of the imide residue plays little role in the redox properties of the NDI core as the nitrogen atom acts as a node of electron density, electronically separating the core from the imide residue. As a result either the aromatic core or the carbonyls must be altered to change its redox properties or absorbance.

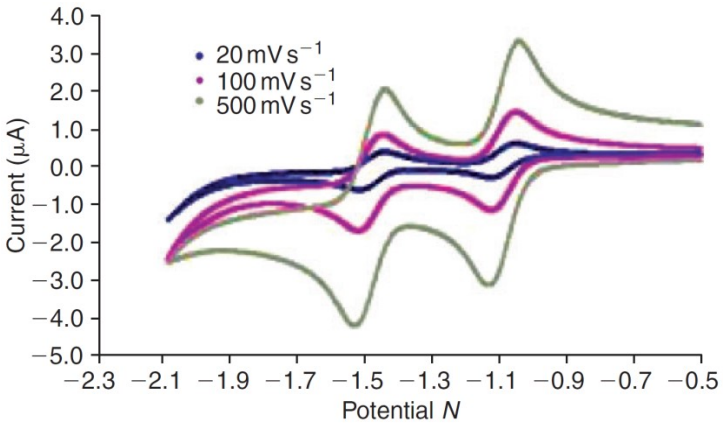


Figure 1-4: A typical set of cyclic voltammograms of a NDI at differing scan rates[25]

The optical absorption profile (Figure 1-5) of NDIs show an intense absorbance in the near-ultraviolet region, with the main peaks arising from the 0 → 0, 0 → 1 and 0 → 2 vibronic bands.[19] Dialkyl

substituted NDIs can also be seen to give mirror fluorescence emission with a Stokes shift of 7 nm.[25] When substituted with aromatic amines however, this mirror fluorescence is either extremely weak or not observed. When reduced, the NDI's radical anion is more strongly absorbing, typically with a $\lambda_{max}$ red shifted into the visible spectrum, and a series of less strongly absorbing bands at lower energies.

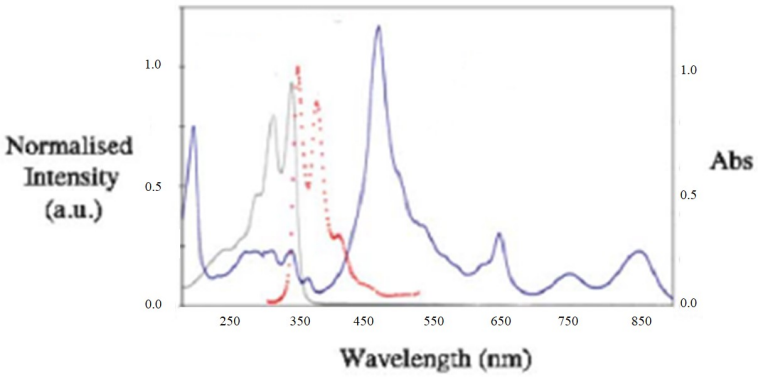


Figure 1-5: UV/Visible Spectra of a typical NDI (grey), the fluorescence spectra of the NDI (red) and its radical anion (blue)[19]

In the late 20th century NDIs began seeing use in supramolecular assemblies, beginning with work using NDIs as a DNA binder (Figure 1-6).[26] The aromatic core promotes intercalation between base pairs and the imides forming hydrogen bonds with the base pairs, as it resembles the acceptor-donor-acceptor pattern of thymine and uracil.[27]

Figure 1-6: Model of NDI –DNA binding showing the intercalation of NDI (red) into DNA (grey)[27]

The electron transport properties of NDIs have been explored and it has been demonstrated that the radical anions can exist in π-stacks allowing for electrical conduction along these nanowires.[28] NDIs are also considered one of the most promising candidates for organic based semiconductors, showing good stability in air.[29] These electronic properties have been harnessed to create devices such as OFETs[30,31] and organic photovoltaics.[32,33]

## 1.4: BODIPY

The first example of a BODIPY was reported in 1968[34] by Treibs and Kreuzer, however little was done with the species until the 1980s[35] when its potential as a biological dye was realised,[36] replacing the popular fluorescein. At the start of the 21st century large amounts of work was conducted exploring BODIPYs and in 2006 alone 729 patents and 1074 journal articles describing the dyes were published, showing the extent of interest in these species.[37]

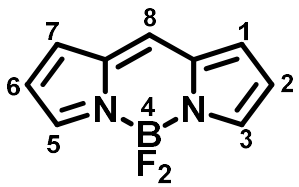


Figure 1-7: The structures of and BODIPY

The basic structure of a BODIPY is numbered in a similar manner to that of indacene (Figure 1-7). An important structural difference is the inclusion of the $BF_2$ unit, which stops the BODIPY from being a truly aromatic species. Instead the BODIPY becomes quasi-aromatic: the π electrons are unable to form the expected cyclic currents.[38] This quasi-aromaticity lowers the amount of intersystem crossing and thereby lowers fluorescence quenching. As the BODIPY structure is rigidly locked by the conjugation, as shown by molecular modeling[39] and crystallography,[40] there are limited ways the excited molecule can perturb to release this energy. These two structural elements endow BODIPYs with their most useful properties: sharp intense absorption bands (ε~50,000 $mol^{-1}dm^3cm^{-1}$), and a mirror

fluorescence with a small Stokes shift and high quantum yields[41,42] (Figure 1-8) caused by a low number of non-radiative deactivation pathways. Typically, BODIPYs exhibit a single reversible one electron reduction,[43-45] however such anions can prove to be unstable over long time periods.

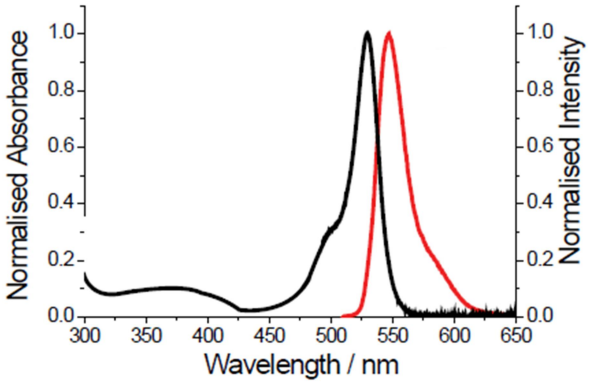


Figure 1-8: UV/visible spectra (black) and fluorescence spectra (red) of a BODIPY dye[46]

What makes BODIPYs appealing over other dye molecules is the ease with which they can be synthetically tailored towards a specific purpose through a suite of reactions which allow for every position to be synthetically malleable. Synthesis of BODIPY species (Figure 1-9) typically involves a condensation between pyrrole and an electrophilic carbonyl species to generate a dipyrromethane.[47] This dipyrromethane is then oxidised, after which it is complexed with $BF_3.OEt_2$, substituted pyrroles and carbonyl offer the first avenue to synthetically tailor BODIPYs.[45,48] The BODIPY core readily undergoes electrophilic substitution to generate halogen substituted BODIPYS [42,49] which can undergo typical cross-coupling reactions.[50] The boron centre can also undergo substitution, by reacting with an alcohol in

the presence of $AlCl_3$ replacing the F atoms with ethers.[44,51] Methyl groups substituted at the 5 and 3 positions can be deprotonated and so undergo reactions with electron rich aldehydes[36,52,53] to form styryl species.

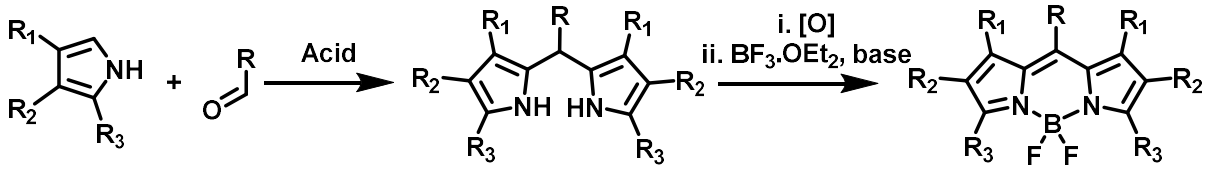


Figure 1-9: Example of typical synthesis of a BODIPY

A result of their synthetic malleability,[37] intense absorbance and highly fluorescent nature BODIPYs have found applications in many fields beyond simple fluorescent biological dyes. For instance, BODIPYs have proven to be excellent candidates for dye based lasers which use their high quantum yields and tight emission bands.[54,55] There are also many dye sensitized photovoltaic cells for which a BODIPY acts as a light harvesting antenna.[56,57]

## 1.5: Thesis overview

The primary focus of this thesis is the tuning of the properties of dye molecules. The primary the family of molecules explored are the NDIs, and how the molecular orbitals of these species can be tuned via synthesis. The ultimate aim of this work is to gain control over the optical and redox properties of these species. This would allow them to be tailored organic electronic, namely photovoltaic devices.

Chapter 2 explores a synthetic route towards the core substitution of NDIs. Morpholine, a commercially available substituent is used to screen reaction conditions and a series of tertiary amine substituted sterically crowded cNDIs are prepared (Figure 1-10). These species are found to deviate from the typical trend seen with most amine substitution and instead show that the conformation of the substituents can affect modulation of molecular orbitals.

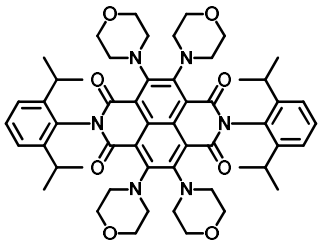

Figure 1-10: An example molecule from Chapter 2 (**2.12**)

Chapter 3 uses the synthetic tool box developed in Chapter 2 to generate a series of electron donor-acceptor species. Herein the electron accepting properties of NDIs are combined with the electron donating phenothiazine and phenoxazine species (Figure 1-11). A novel synthetic pathway for the production of N-substituted

phenoxazine species is created and the electronic and optical properties of the donor acceptor species are explored. This body of work intends to show how the HOMO LUMO gap of these species could be controlled via core substitution. This allows these species to absorb visible light and therefore allows them to be suitable candidates for photovoltaic devices.

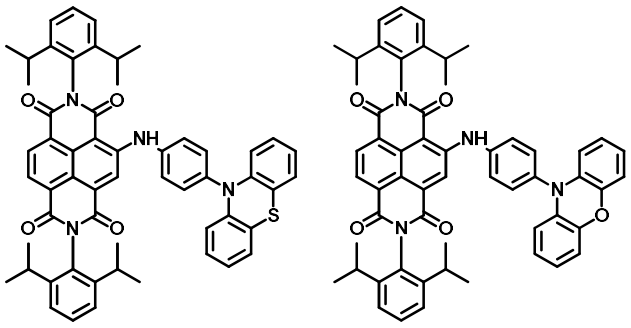

Figure 1-11: Example molecules from Chapter 3 (left: **3.6** right: **3.7**)

Chapter 4 explores the synthesis of a light harvesting rotaxane using a rod based on a NDI capped with BODIPY (Figure 1-12). In addition to there is an attempt made to modulate the molecular orbitals of the rod via thionation of the NDI. The work primarily explores the viability of using thionated NDIs under conditions similar to those of NDIS and examines the robustness of the NDI to be used as a guest molecule.

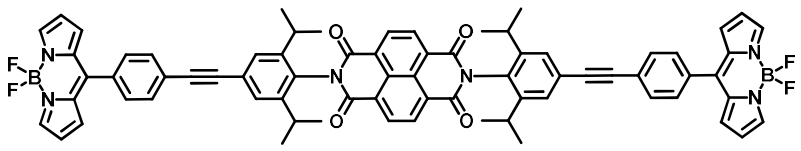

Figure 1-12: The rod molecule from Chapter 4 (**4.3**)

Chapter 5 summaries the results of the thesis and highlights the impact of the results and the scope for future study.

## 1.6: References


(1) L.Dayeta, J. T. Daniela, *J. Archaeol. Sci,* **2013**, *40*, 3492.

(2) S. B. Ester, A. N. H. Ferreira, H. McNab, A. Quye *Chem. Soc. Rev,* **2004**, *33*, 329.

(3) K.Hübner, *Chem. unserer Zeit,* **2006**, *40*, 274.

(4) A. S.Travis, *Technol. Cult,* **1990**, *31*, 51.

(5) D.Jacoby, *DOP,* **2004**, *58*, 197.

(6) M. M. Sousa, M. J.Melo, A. J.Parola, P. J. T.Morris, H. S.Rzepa,; J. S. S.de Melo, *Chem. Eur. J.,* **2008**, *14*, 8507.

(7) N. Boens, V. L.W. Dehaen, *Chem Soc Rev*, **2011**, *41*, 1130.

(8) "The Nobel Prize in Chemistry 2014". *Nobelprize.org.* Nobel Media AB 2014. Web. 21 Feb 2018. <http://www.nobelprize.org/nobel_prizes/chemistry/laureates/2014/>

(9) L. W.Hillman, P. F.Liao, P.Kelley, F. J.Duarte, *Dye laser principles: with applications*, 1990.

(10) C. W.Tang, S. A.VanSlyke, *Appl. Phys. Lett.*, **1987**, *51*, 913.

(11) B.O'Regan, M.Gratzel, *Nature* **1991**, *353*, 737.

(12) J.Clayden, N.Greeves, S.Warren, P.Wothers *Organic Chemistry,* **2008**, *1*, 151.

(13) T. Weil, J.Hofkens, K.Peneva, K.Müllen, *Angew. Chem. Int. Ed.,* **2010**, *49*, 9068.

(14) J. H Oh, S. L Suraru, W.Y Lee, M.Könemann,; H. W.Höffken, C.Röger, R.Schmidt, Y.Chung, W.C.Chen, F.Würthner, Z.Bao, *Adv. Funct. Mater,* **2010**, *20*, 2148.

(15) F.Wurthner, *Chem Commun,* **2004**, 1564.

(16) Z.Chen, U.Baumeister, C.Tschierske, F.Würthner, *Chem. Eur. J,* **2007**, *13*, 450.

(17) G.Seybold, G.Wagenblast, *Dyes Pigm,* **1989**, *11*, 303.

(18) X.Zhan, A.Facchetti, S.Barlow, T. J.Marks, M. A.Ratner, M. R.Wasielewski, S. R.Marder, *Adv. Mater*, **2011**, *23*, 268.

(19) S. V.Bhosale, C. H.Jani, S. J.Langford, *Chem. Soc. Rev,* **2008**, *37*, 331.

(20) Z.Yuan, S.L.Lee, L.Chen, C.Li, K. S.Mali, S.De Feyter, K.Müllen, *Chem. Eur. J,* **2013**, *19*, 11842.

(21) G.Kranzlein, H.Vollmann,; Google Patents: 1933.

(22) H.Vollmann, Google Patents: 1937.

(23) W.S.Horne, N.Ashkenasy, M. R. Ghadiri, *Chem. Eur. J,* **2005**, *11*, 1137.

(24) S.-L.Suraru, F.Würthner, *Angew. Chem. Int. Ed,* **2014**, *53*, 7428.
(25) G.Andric, J. F.Boas, A. M.Bond, G. D.Fallon, K. P.Ghiggino, C. F.Hogan, J. A.Hutchison, M. A.-P.Lee, S. J.Langford, J. R.Pilbrow, G. J.Troup, C. P Woodward,. *Aust. J. Chem,* **2004**, *57*, 1011.
(26) S.Takenaka, M.Mamabe, M.Yokoyama, M.Nishi, J.Tanaka, H.Kondo, *Chem Commun,* **1996**, 379.
(27) V.Guelev, J.Lee, J.Ward, S.Sorey, D. W.Hoffman, B. L.Iverson, *Chemistry & Biology,* **2001**, *8*, 415.
(28) L. L.Miller, K. R.Mann, *Acc. Chem. Res.* **1996**, *29*, 417.
(29) H. E.Katz, A. J.Lovinger, J.Johnson, C.Kloc, T.Siegrist, W.Li, Y. Y.Lin, A.Dodabalapur, *Nature,* **2000**, *404*, 478.
(30) M. M.Durban, P. D. Kazarinoff, C. K.Luscombe, *Macromolecules* **2010**, *43*, 6348.
(31) T. B.Singh, S.Erten, S.Günes, C.Zafer, G.Turkmen, B.Kuban, Y.Teoman, N. S.Sariciftci, S.Icli, *Org. Electron,* **2006**, *7*, 480.
(32) M.Schubert, D.Dolfen, J.Frisch, S.Roland, R.Steyrleuthner, B.Stiller, Z.Chen, U.Scherf, N.Koch, A.Facchetti, D.Neher, *Adv. Energy Mater,* **2012**, *2*, 369.
(33) T.Earmme, Y.-J.Hwang, N. M.Murari, S.Subramaniyan, S. A.Jenekhe, *JACS,* **2013**, *135*, 14960.
(34) A.Treibs, F.-H.Kreuzer, *Justus Liebigs Ann Chem,* **1968**, *718*, 208.
(35) H. J.Wories, J. H.Koek, G.Lodder, J.Lugtenburg, R.Fokkens, O.Driessen, G. R.Mohn, *Recl. Trav. Chim. Pays-Bas*, **1985**, *104*, 288.
(36) F. J.Monsma, A. C.Barton, H.Chol Kang, D. L.Brassard, R. P.Haugland, D. R.Sibley, *J. Neurochem,* **1989**, *52*, 1641.
(37) G.Ulrich, R.Ziessel, A.Harriman, *Angew. Chem. Int. Ed,* **2008**, *47*, 1184.
(38) T. G.Pavlopoulos, *Prog Quantum Electron* , **2002**, *26*, 193.
(39) J.B. Prieto, F.L.Arbeloa, V.M. Martínez, I.L. Arbeloa, *Chem. Phys***, 2004**, *296*, 13.
(40) Y.-H.Yu, Z.Shen, H.-Y.Xu, Y.-W.Wang, T.Okujima, N.Ono, Y.-Z Li. X.-Z You, *J. Mol. Struct,* **2007**, *827*, 130.
(41) J. B.Prieto, F. L.Arbeloa, V. M.Martı, T. A.López,; F.Amat-Guerri, M.Liras, I. L.Arbeloa, *Chem. Phys. Lett,* **2004**, *385*, 29.
(42) T.Yogo, Y.Urano, Y.Ishitsuka, F.Maniwa, T.Nagano, *JACS,* **2005**, *127*, 12162.

(43) A. B.Nepomnyashchii, M.Bröring, J.Ahrens, A. J.Bard, *JACS,* **2011**, *133*, 8633.
(44) V. J.Richards, A. L. Gower, J. E Smith, E. S.Davies, D.Lahaye,; A. G Slater, W.Lewis, A. J.Blake, N. R.Champness, D. L.Kays, *Chem Commun,* **2012**, *48*, 1751.
(45) A.Burghart, H.Kim, M. B.Welch, L. H.Thoresen, J.Reibenspies, K.Burgess, F.Bergström, L. B. Johansson, *J. Org. Chem,* **1999**, *64*, 7813.
(46) A. C.Benniston, Anal. Bioanal. Chem, **2014**, *5*, 2155.
(47) B. J.Littler, M. A.Miller, C.-H.Hung, R. W.Wagner, D. F.O'Shea, P. D.Boyle, J. S Lindsey, *J. Org. Chem,* **1999**, *64*, 1391.
(48) M.Baruah, W.Qin, N.Basarić, W. M.De Borggraeve, N.Boens, *J. Org. Chem,* **2005**, *70*, 4152.
(49) K.Rurack, M.Kollmannsberger, J.Daub, *New J. Chem,* **2001**, *25*, 289.
(50) T.Rohand, W.Qin, N.Boens, W.Dehaen, *Eur. J. Org. Chem*, **2006**, *2006*, 4658.
(51) C.Tahtaoui, C.Thomas, F.Rohmer, P.Klotz, G.Duportail, Y.Mély, D.Bonnet, M.Hibert, *J. Org. Chem,* **2007**, *72*, 269.
(52) N.Saki, T.Dinc, E. U.Akkaya, *Tetrahedron* **2006**, *62*, 2721.
(53) G.Sathyamoorthi, L. T.Wolford, A. M.Haag, J. H.Boyer, *Heteroat. Chem,* **1994**, *5*, 245.
(54) J.Bañuelos, V.Martín, C. F. A.Gómez-Durán, I. J. A.Córdoba, E.Peña-Cabrera, I.García-Moreno, Á.Costela, M. E.Pérez-Ojeda, T.Arbeloa, Í. L.Arbeloa, *Chem. Eur. J,* **2011**, *17*, 7261.
(55) D.Zhang, V.Martin, I.Garcia-Moreno, A.Costela, Perez-M. E. Ojeda, Y. Xiao, *PCCP,* **2011**, *13*, 13026.
(56) S.Erten-Ela, M. D.Yilmaz, B.Icli, Y.Dede, S.Icli, E. U.Akkaya, *Org Lett,* **2008**, *10*, 3299.
(57) S.Kolemen, O. A.Bozdemir, Y.Cakmak, G.Barin, S.Erten-Ela, M.Marszalek, J.H Yum, S. M.Zakeeruddin, M. K.Nazeeruddin, M.Gratzel, E. U. Akkaya, *Chem. Sci,* **2011**, *2*, 949.

# Chapter 2 : Morpholated Naphthalene Diimides

# 2.1: Introduction

## 2.1.1: Tuning Rylene absorbance

### *2.1.1.1: The Need for Control*

The need for highly coloured dye molecules within the visible range keeps expanding. The reason for this is that the majority of light that makes its way through the Earth's atmosphere is in the visible spectra,[1] in order to utilise this light molecules that can efficiently absorb it must be synthesised. These molecules can then find homes as light harvesters; collecting light energy for useful work such as in photovoltaic systems,[2,3] or acting as easily identifiable visual stimuli for the detection of specific species.[3,5] To this end it is important that the available catalogue of these dyes be extended so that dyes can be correctly chosen for their particular wavelength and purpose.

NDIs typically can be found to absorb within the UV making most NDIs less suited to being incorporated into photovoltaic devices, as they cannot absorb the majority of light that makes it to earth. However if the electronic transitions are modulated to lower energy, their high extinction coefficients could be exploited, allowing them to efficiently absorb visible light. Rylenes have been repeatedly shown to be excellent candidates for organic electronics due to their superb stability as n-type semiconductors.[6-9] Gaining further understanding and control over these electronic properties allows for tailoring of highly specific materials.

In order to alter the energy of these transitions some electronic perturbation must be caused to the aromatic centre of the rylene. This can be achieved by direct synthetic modification to the aromatic chromophore of the molecule.

### *2.1.1.2: Extending the Aromatic Core*

The most common feature shared by organic chromophores is an extended π system which allows for the electronic transitions of these molecules to be shifted into the visible range. It therefore stands to reason that the amount of conjugation plays a crucial role in energy of these electronic transitions.[10]

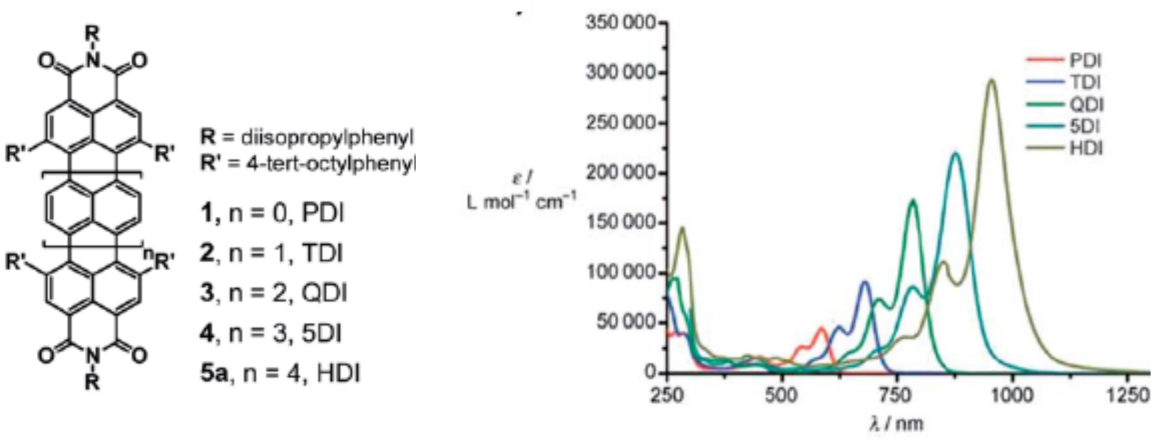


Figure 2-1: Structures of longitudinally extended rylene diimides (left) and the UV/Vis/NIR spectra showing both increasing wavelength of absorption and increasing molar absorption coefficient with extension (right)[11]

This phenomenon has been studied in relation to rylene diimides by utilising series of cross coupling reactions to create successively larger aromatic centres. As the molecules increase in size from PDI to the 6 naphthyl cored hexarylene diimides (HDIs)[11] a bathochromic shift of around 100 nm can be observed with each additional core,

from 580 nm to 953 nm (Figure 0-1). Furthermore this aromatic extension is also accompanied by a large increase in the extinction coefficient, from 30,000 to 300,000 $mol^{-1}dm^3cm^{-1}$.

Unfortunately while this approach does give an excellent modulation of the rylene diimides' electronic properties, the synthesis[12,13] and characterisation of these molecules has proved to be incredibly challenging. Compounding these problems, these extended molecules typically have poor solubilities limiting their practical use and so other synthetic routes need to be explored to generate more useful materials.

#### *2.1.1.3: Thionation of Rylene Diimides*

A way of modifying rylene diimides using a more subtle synthetic approach is to alter the nature of the diimides. Typically this is achieved *via* substitution with sulphur (thionation) to generate a thiocarbonyl rylene diimide. This exchange has a large effect on the electron withdrawing ability of the diimides, as sulphur is less electronegative than oxygen. This in turn affects the frontier orbitals of chromophore, modulating redox and optical properties. This substitution was first reported in a patent by the Facchetti group in 2011.[14] The patent covers the preparation of a number of thionated NDIs and PDIs. Thionation was achieved by reacting rylene diimide, in the case of the NDIs cyclohexyl and 2-ethylhexyl aliphatic imide substituents were used, with a commercially available thionating

reagent, Davy's reagent (Figure 2-2) gave rise to a series of partially thionated NDIs.

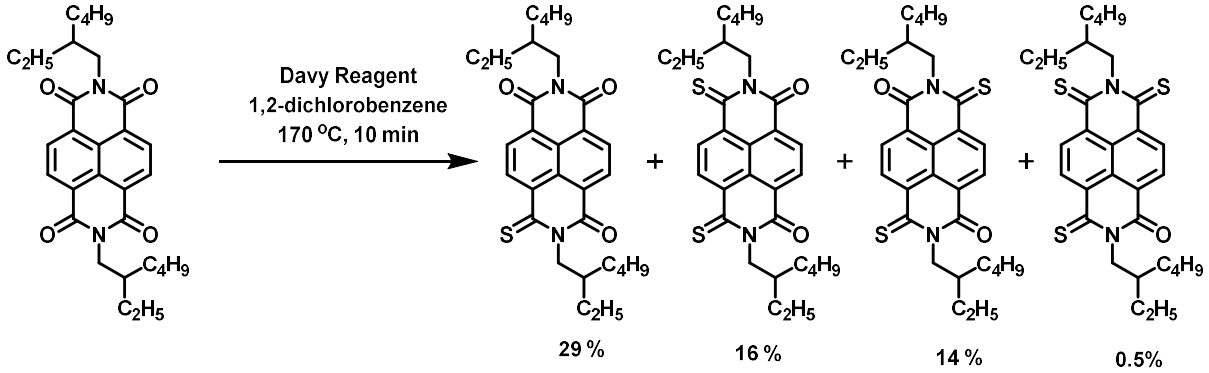


Figure 2-2: Synthesis of partially thionated NDIs

The patent also reported some initial findings on the optical properties of these molecules showing a bathochromic shift upon thionation. Increasing thionation lead to a higher λmax of the molecules. Interestingly in the case of the NDIs, the absorbance maximum moves from the ultraviolet range and into the visible range.

Since this discovery further series of thionated rylene diimides have been synthesised and studied. The typical method for thionation has shifted towards Lawessons reagent in refluxing toluene,[15-17] due to the increased reactivity, ease of use and ready availability of this relatively stable reagent. Further examination of the electronic properties of thionated NDIs was carried out by the Seferos group[15] and revealed a stepwise increase in the of the reduction potential with successive thionation (Table 2-1). This gave rise to a high first reduction potential of - 0.65 V (vs $Fc^+/Fc$) for a tri thionated NDI.

This control over the reduction potential further expands the use of NDIs as n-type electronic materials for OFET applications.

| | $E_{1/2}{}^{-1}$ (V) | $E_{1/2}{}^{-2}$ (V) | $E_{HOMO}{}^{a,b}$ (eV) | $E_{LUMO}{}^{a,c}$ (eV) |
|---|---|---|---|---|
| **P** | −1.11 | −1.53 | −6.97 (−7.42) | −3.79 (−3.87) |
| **S1** | −0.92 | −1.30 | −6.38 (−6.71) | −3.95 (−4.09) |
| ***cis*-S2** | −0.79 | −1.11 | −6.46 (−6.71) | −4.11 (−4.27) |
| ***trans*-S2** | −0.80 | *d* | −6.50 (−6.69) | −4.15 (−4.25) |
| **S3** | −0.65 | *d* | −6.47 (−6.62) | −4.30 (−4.44) |

Table 2-1: Summarising the electronic properties of a series of thionated NDIs reduction potentials given $Fc^{+}/Fc$[15]

While the control of electronic and optical properties these modifications afford is exceptional, the reactions themselves are troublesome. Thionation of rylene diimides still has some trouble with selectivity and generally multiple thionated products are produced from each reaction. The products favoured seem to be determined by the parent diimide, however, unfortunately there seems to be little pattern to be exploited for a more controlled synthesis.

### *2.1.1.4: Core Substituted Rylene diimides*

The final way to synthetically modify the electronic properties of rylene diimides involves substitution directly onto the aromatic naphthyl core. This class of molecule was first reported in 1937[18] however it was not until much later that it was realised these systems could generate interesting electronic and optical properties, so exploration of these species was delayed.

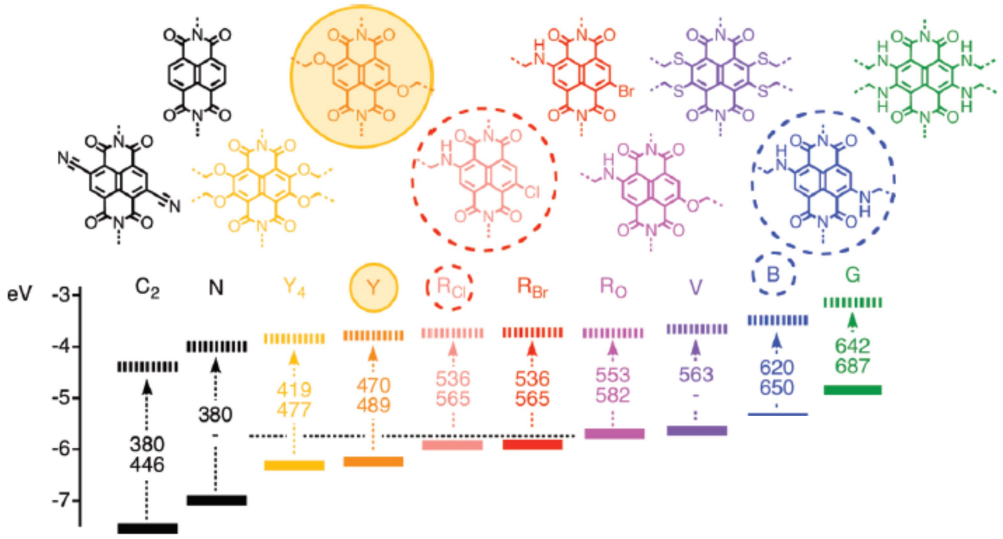


Figure 2-3: Structures of a rainbow series of core substituted NDIs, their maximum absorption (top) and emission wavelength (bottom) in nm and the HOMO (bold) and LUMO (dashed) energy[19]

Perhaps the best example of control of the optical properties of cNDIs can be seen when looking at the rainbow series of cNDIs (Figure 2-3).[19] These species clearly demonstrate the effect of combining electron donating species with an aromatic core furnished with electron withdrawing imides to generate a highly tuneable push-pull chromophore. The new visible absorbance is generally associated with a new charge-transfer band. This tunability is derived from the strength, nature and number of the electron donors substituted to

the core. By using mixtures of donor species, a large range of visible absorbance profiles have been accessed. Not only can a specific absorbance be selected, but also a specific emission, owing to a relatively small Stokes shift observed for NDI fluorescence. This ability to tune the optical properties of cNDIs is one of their most desirable traits. For example the green molecule is considered to be the smallest, most atom efficient, mimic of chlorophyll known.[20]

Inspection of the redox properties of cNDIs shows a clear dependence upon the nature of the substitution. Increasing the electron donating character of the substituent further lowers the reduction potential of the species, while electron withdrawing substituents have the opposite effect. By increasing the number (Figure 0-14) of either type of substituent the effect upon the potential becomes more pronounced.[4,21,22]

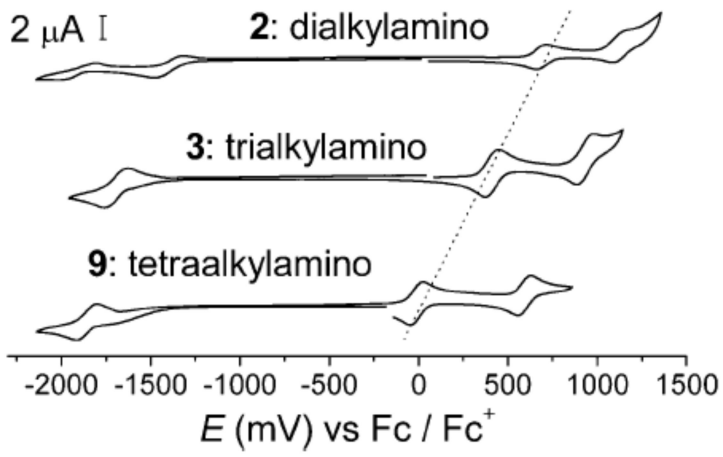


Figure 2-4: Cyclic voltammograms showing the change in redox properties with increasing amino substitution onto the core of a cNDI[4]

Also cNDIs typically retain their planar core, unlike their larger sister compounds cPDIs in which core substitution causes the aromatic core to become twisted.[23] This means that the aromatic core can still be exploited with ease in order to create ordered π-stacked structures[24] with high conductivity desired for molecular electronic purposes. Synthetically a large amount of work was initially done towards expanding the preparation of cPDIs.[25] These synthetic methods adapted toward the preparation of cNDIs.[26-28]

### 2.1.2: Aims and Objectives

As discussed earlier, rylene diimides are amongst the most promising organic molecules for use in optoelectronic devices. By gaining control over the electronics of these molecules this family could be tuned towards specific purposes. Notably, shifting the optical properties of these compounds, into the visible or near IR spectrum, allows for their uses to be extended, to find a home in organic photovoltaics.

Despite extensive research there are few examples of tertiary amine substituted cNDIs within the literature.[21] In order to explore how this affects the properties of these species the target molecules **2.10**-**2.12** (Figure 2-5) were proposed. Morpholine is both highly electron donating and readily available so made an excellent candidate for this exploratory study. Furthermore synthesis of these species would also allow for the exploration of synthetic conditions to readily access cNDIs allowing for more complex species to be synthesised in the future.

The optical and electrochemical properties of these species could then be explored. This would show how these properties have been affected by the substitution, allowing examination of the tertiary amine substitution. It was proposed that these species could create a near IR absorbing molecule which could then be incorporated as a dye in photovoltaic devices allowing for a greater proportion of light to be converted to electricity.

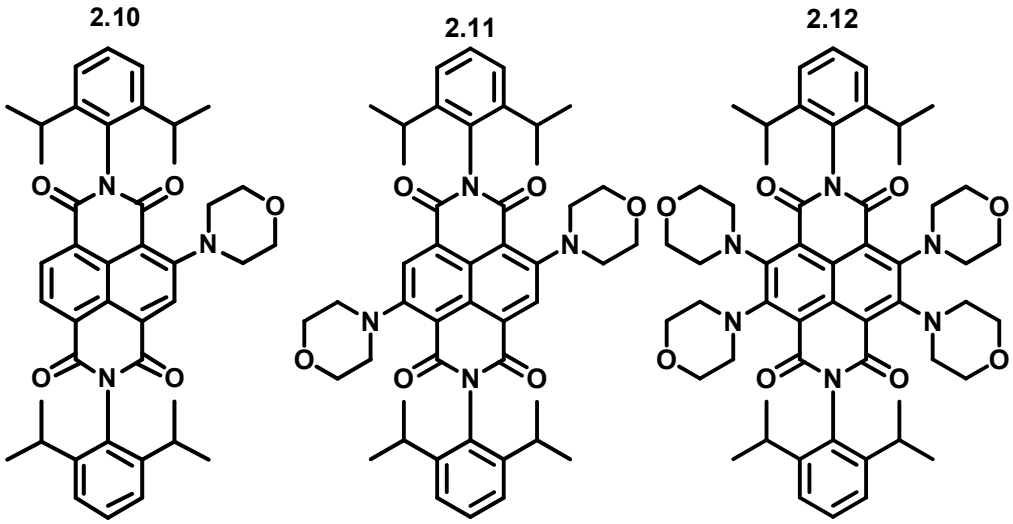


Figure 2-5: Target molecules of Chapter 2

## 2.2: Results and Discussion

### 2.2.1: Synthesis

The total synthesis of 3 novel secondary amine core substituted NDIs is discussed herein. The synthesis of these compounds can be split into three steps: bromination, imidization and substitution.

In the case of all 3 compounds tribromocyanuric acid (TBCA, **2.1**) was used as the bromine source. Cyanuric acid was easily brominated (Scheme 2-1), following a literature preparation,[29] with KBr in the presence of an oxidizing agent, potassium peroxymonosulfate (oxone).

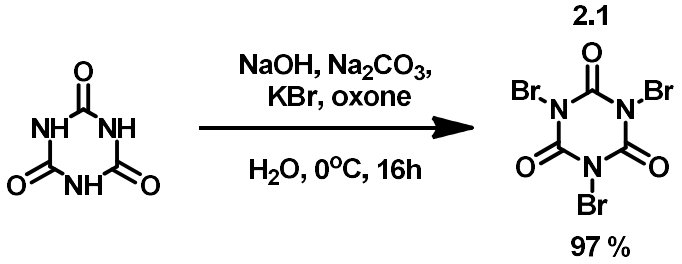


Scheme 2-2: Synthesis of **2.1** (TBCA)

**2.1** is used for the bromination of these NDIs because it is easier to handle and higher in activity than other sources (such as $Br_2$). This higher activity allows for the avoidance of the typically reported harsh conditions involving heating in oleum,[30] instead using concentrated sulfuric acid. The progress of all bromination reactions were monitored *via* MALDI MS.

Both **2.2** and **2.3** where synthesized at room temperature using these conditions (Scheme 2-3). Unfortunately, owing to the absolute

insolubility of these NDA species these compounds were non-isolatable, and cannot be characterized other than by MALDI MS.

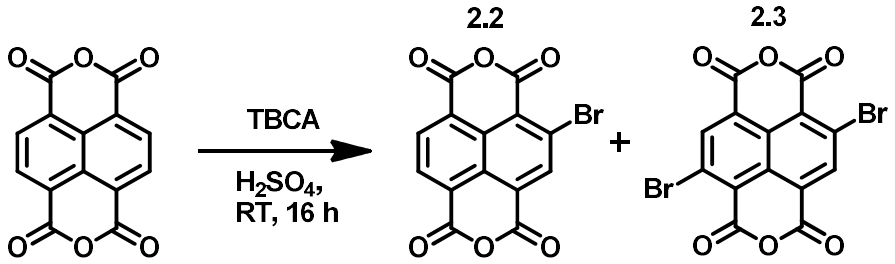


Scheme 2-4: Synthesis of **2.2** and **2.3**

In order to access more brominated species, increased temperature, reaction time and equivalents of **2.1** are required. By doing so **2.4** can be selectively prepared without the presence of the less brominated species (Scheme 2-5). This product was also insoluble and so extensive characterisation beyond MALDI MS was impractical.

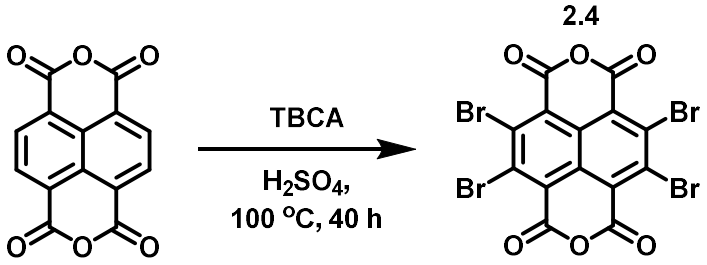


Scheme 2-6: Synthesis of **2.4**

By far the largest success of this bromination method can be seen when brominating PDA to generate **2.5** (Scheme 2-7). This preparation was carried out utilizing a pressure tube in order to push the reaction to completion, encouraging complete bromination of the aromatic core. This was achieved in a much shorter time period than previously reported and started from a non-brominated

PDA which was not previously reported, taking 92 h instead of 150 h.[31]

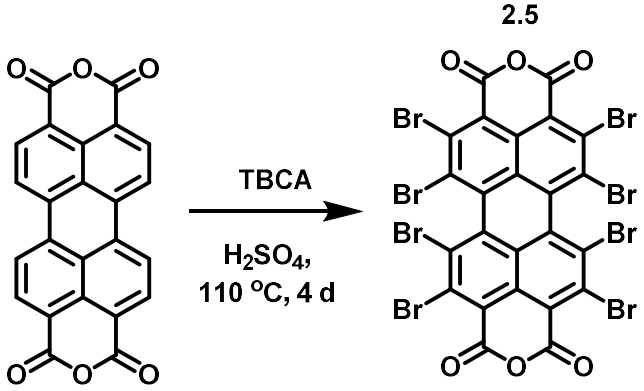


Scheme 2-8: Synthesis of **2.5**

In order to increase solubility to allow for these compounds to be characterized and synthetically manipulated they were imidized. These compounds present two problems in relation to this reaction. First the addition of bromine onto the aromatic core removes electron density from the species and thereby deactivates the anhydrides towards nucleophilic attack. Secondly, as amines have nucleophilic character there is a possibility for unwanted $S_NAr$ reactions onto the core, which would create an unwanted core substituted unwanted side product. In order to limit these side reactions minimum amounts of the amine were used, rather than the typical excess. The amine 2,6-diisopropylaniline was selected, as its sterically bulky aromatic nature should reduce its tendency to act as a nucleophile displacing a Br. It is also fit for purpose as it limits intermolecular π-π interactions, as the isopropyl groups sit perpendicular to the aromatic core, greatly improving solubility thereby making further synthetic manipulation simpler.

Typical methods of imidization, heating in DMF or imidazole, unfortunately lead to the elimination of the bromine atoms giving the non-brominated NDI. Generation of **2.6** and **2.7** was achieved *via* an alternative synthetic method, using an altered literature preparation.[32] Heating a mixture of **2.2** and **2.3** with 2,6-diisopropylaniline to 80 °C in acetic acid (Scheme 2-9) limited the elimination reactions successfully. **2.6** and **2.7** were then isolated and characterized.

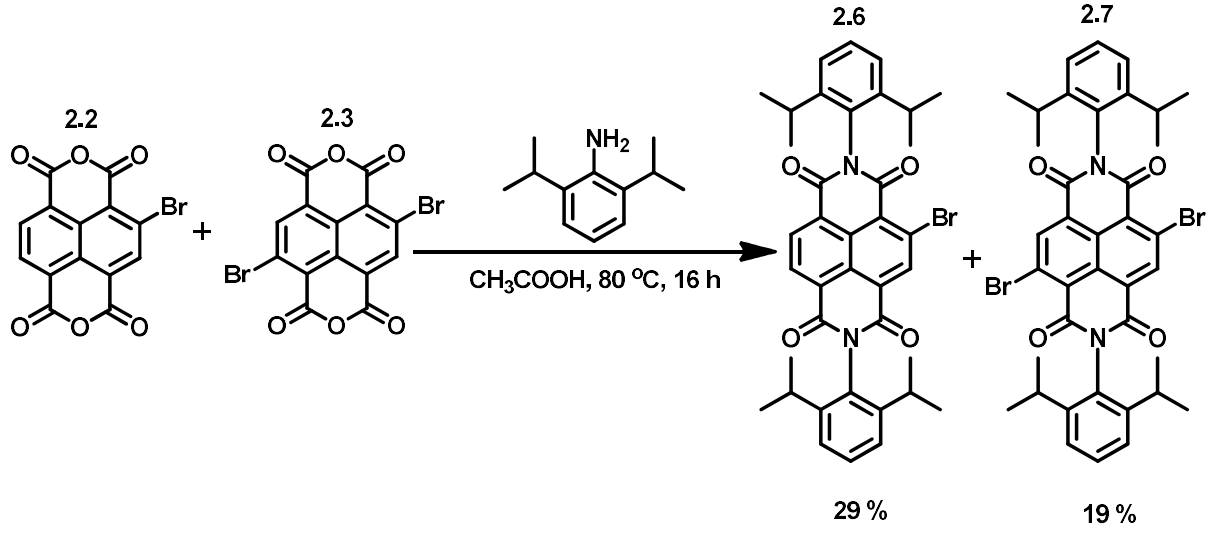


Scheme 2-10: Synthesis of **2.6** and **2.7**

**2.4** required more aggressive treatment to generate **2.8**, as the increased bromination lowers its reactivity. These conditions involved a higher temperature of 80 °C and using multiple equivalents of the amine in order to force the reaction towards completion, overcoming the drastically reduced reactivity of the anhydrides (Scheme 2-11). Unfortunately, the increased proportion of amine lead to the generation unwanted products, due to core substitution of 2,6-

diisopropylaniline. These conditions also seem to encourage some partial elimination of bromine from the aromatic core creating more side products. Isolating **2.8** from this extensive mixture of products unfortunately proved impossible *via* standard purification techniques.

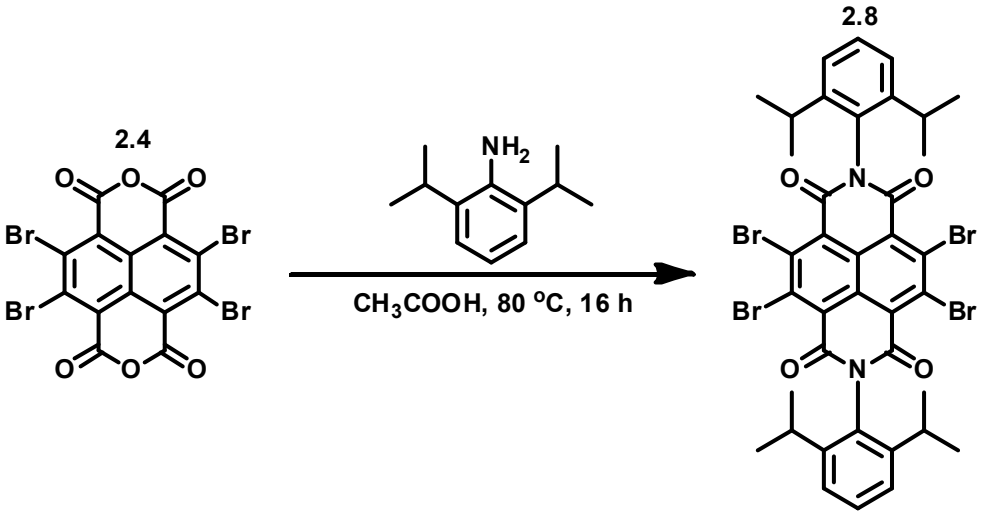


Scheme 2-12: Synthesis of **2.8**

Imidization of **2.5** also presented a challenge as standard conditions led to elimination of the bromines and using the conditions for **2.6**-**2.8** resulted in no reaction and retention of the starting material. This was overcome and **2.5** was imidized with *n*-octylamine following a literature procedure.[31] This involves first generating the amide *in situ* then catalysing the ring closure with $PBr_3$, generating an acyl bromide *in situ* (Scheme 2-13). This method worked well with n-octylamine and **2.9** was isolated and characterised. When these conditions were attempted with other amines, 2,6-diisopropylaniline and isopentylamine, not even trace amounts of the desired diimide

was observed. This is perhaps due to the increase steric bulk making it harder to generate the acyl bromide.

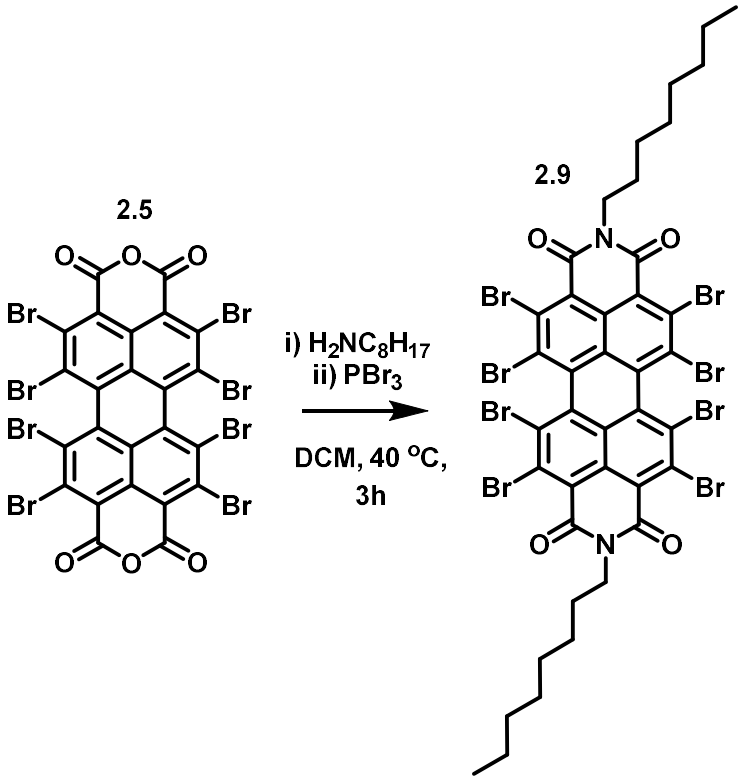


Scheme 2-14: Synthesis of **2.9**

Morpholation of **2.6**-**2.8** was achieved using simple $S_NAr$ chemistry, reacting the brominated species with morpholine. It was found that by using DMF as a solvent, rather than excess of morpholine unwanted elimination of Br could be minimised, reducing unwanted products.

**2.10** was generated using modest conditions (Scheme 2-15), **2.6** was reacted with one equivalent of morpholine in DMF at room temperature. Upon addition of the morpholine a distinct change in colour, from beige to pink, due to the presence of **2.10** was observed.

Preparation of **2.11** required more aggressive conditions, as addition of the first morpholine reduces the reactivity of the remaining bromine. **2.11** was generated in DMF with two equivalents of morpholine at 135 $^{o}$C. Once again a colour change from beige to dark blue was observed.

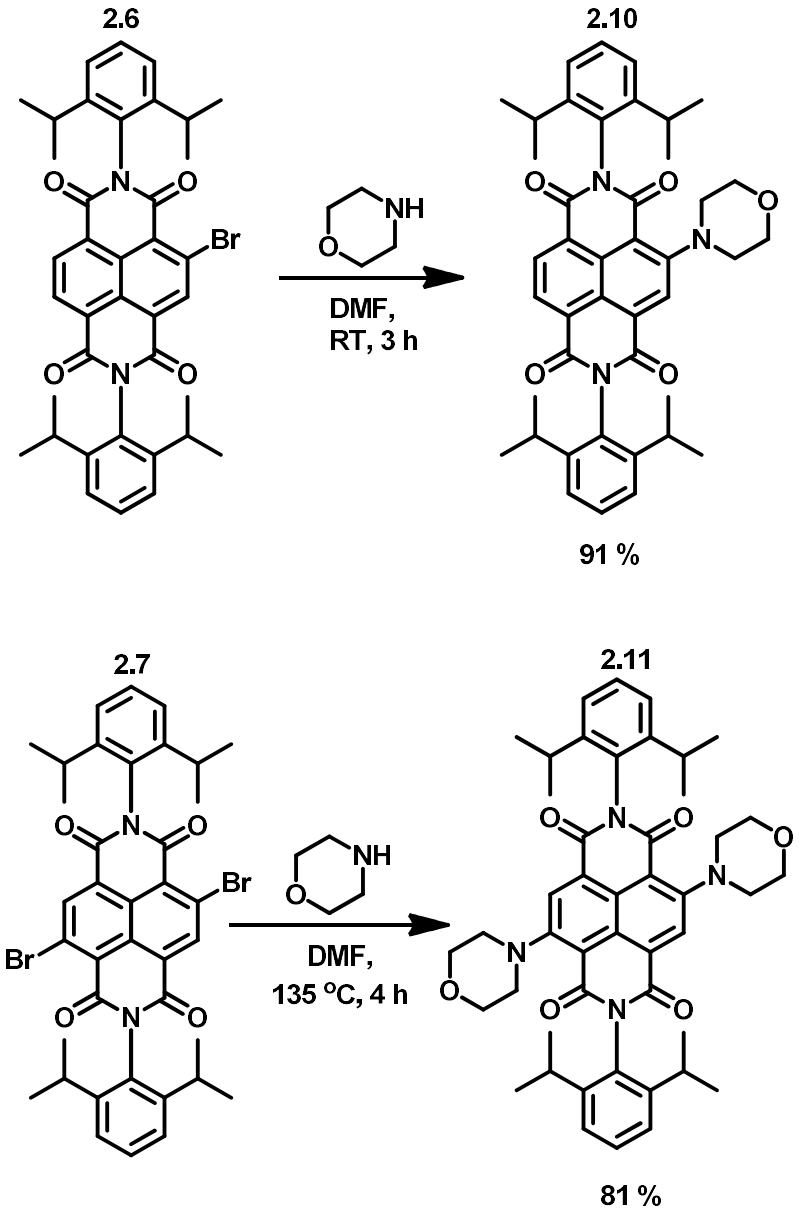


Scheme 2-16: Synthesis of **2.10** and **2.11**

Preparation of **2.12** was achieved utilising a longer reaction time and a large excess of morpholine. This was required to overcome the unfavourable sterics of the final product and the reduced reactivity of the bromines after partial substitution. As **2.8** was not isolated prior to the reaction, many unwanted products were formed, also under these conditions a further elimination of the bromines was observed. However owing to **2.12** being more polar than other less morpholated products it could be isolated and characterised, though in an understandably low yield (Scheme 2-17).

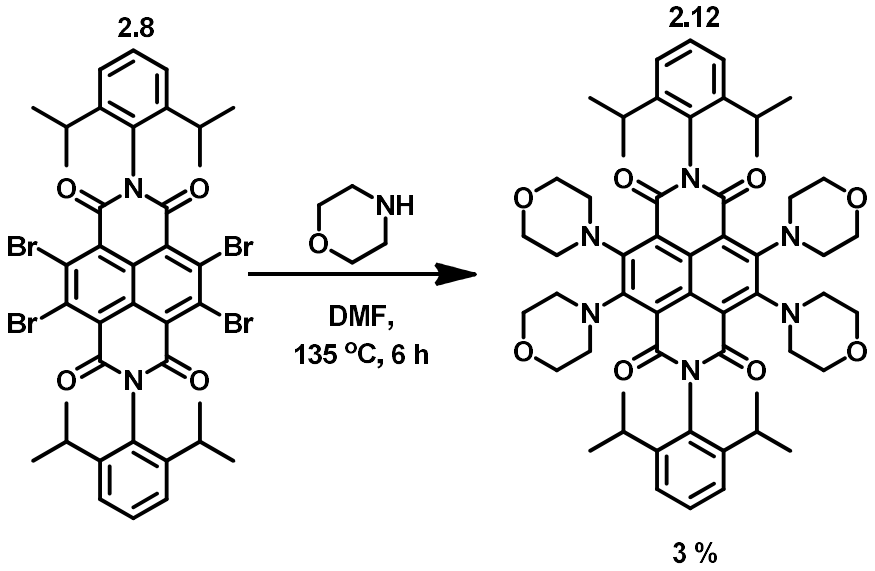


Scheme 2-18: Synthesis of **2.12**

Morpholation of **2.9** was unfortunately unsuccessful. The reaction with morpholine in DMF was attempted at a variety of temperatures, between RT and 130 °C (Scheme 2-19). This universally this led to creation of a large amount of partially substituted products, identified only *via* MALDI MS of the crude samples. Though all typical purification techniques were attempted, isolation of a product

was not achieved. Given the number of partially substituted isomers that are possible this is not suprising as all of the dimorpholated isomers for instance would have similar properties and therefore be extremely difficult to separate. The fully morpholated product **2.13** was not observed in any reaction, this is not unexpected as the level of steric hindrance around the aromatic core is so great, also the increased electron density upon the aromatic core would deactivate it towards complete substitution.

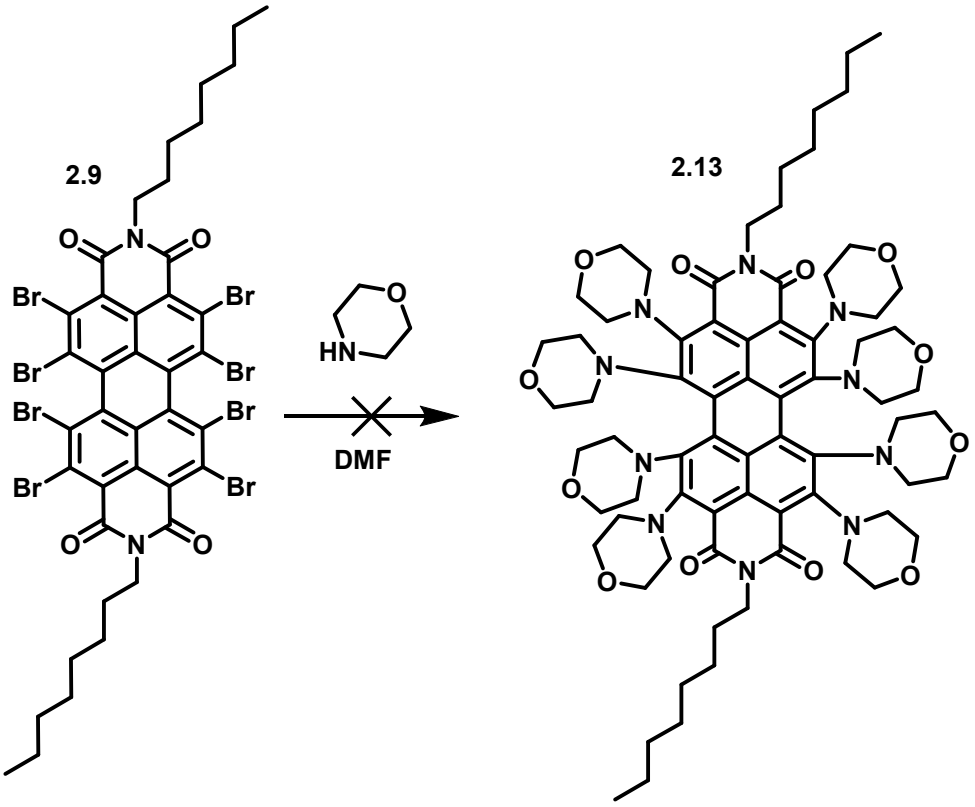


Scheme 2-20: attempted synthesis of **2.13**

## 2.2.2: Investigation of Optical and Electrochemical Properties

In order to investigate how optical and electronic properties of **2.10**, **2.11** and **2.12** had been modified CV, bulk electrolysis spectroelectrochemical and EPR experiments were undertaken. Also in an attempt to aid explanation of observed properties crystal structures were obtained and DFT calculations were performed for each of the molecules.

### *2.2.2.1: Optical Properties*

It is clear upon visual inspection of the morpholated NDIs that there has been a significant bathochromic shift. Typical NDIs have a slight beige colour while **2.10**-**2.12** are intensely coloured (Figure 2-6).

Figure 2-6: Solutions of NDIs in chloroform. From left to right **2.6, 2.10, 2.11** and **2.12**

This shift in absorption can be more qualitatively measured when examining the UV/vis spectra of these compounds (Figure 2-7). Single substitution with morpholine (**2.10**) causes an absorption

band to move to lower energy from the UV into the visible range at 525 nm. Di substitution (**2.11**) seems to follow the typically observed trend shifting the band to lower energy at 597 nm, an increase of 72 nm.

However unlike typical literature examples tetra substitution (**2.12**) leads to an absorption band at 545 nm, higher in energy than the disubstituted counterpart, in fact being closer in energy to the mono substituted analogue. This oddity is of particular interest which could be imposed by the tertiary amine substitution and so further work to discover the origin of this phenomenon was conducted.

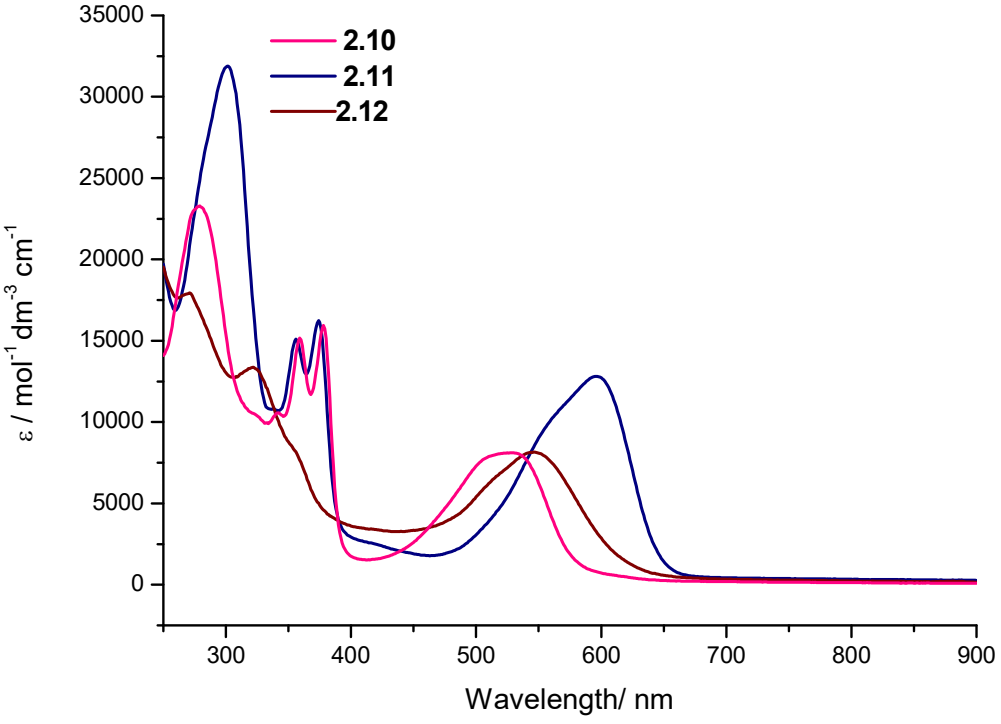


Figure 2-7: UV/vis absorbtion Spectra of **2.10**, **2.11** and **2.12** in DCM.

Both **2.10** and **2.11** retain the typically structured NDI band below 400 nm, with very little shift when comparing the two. Inspecting

**2.12** reveals that the overall landscape of the spectrum changed, most notability the depletion of the two peaks below 400 nm.

### *2.2.2.2: Cyclic voltammetry*

In order to explore the redox properties of **2.10**-**2.12** cyclic voltammetry was performed, this work would also give insight as to the energy of the LUMO orbital. All compounds within this series showed the typical two reversible reductions associated with NDIs, though at increasingly more negative potentials with increasing morpholation (Figure 2-8). This trend reflects previous reports for amine substituted NDIs, including the results found for **2.12** unlike in UV/vis spectra.

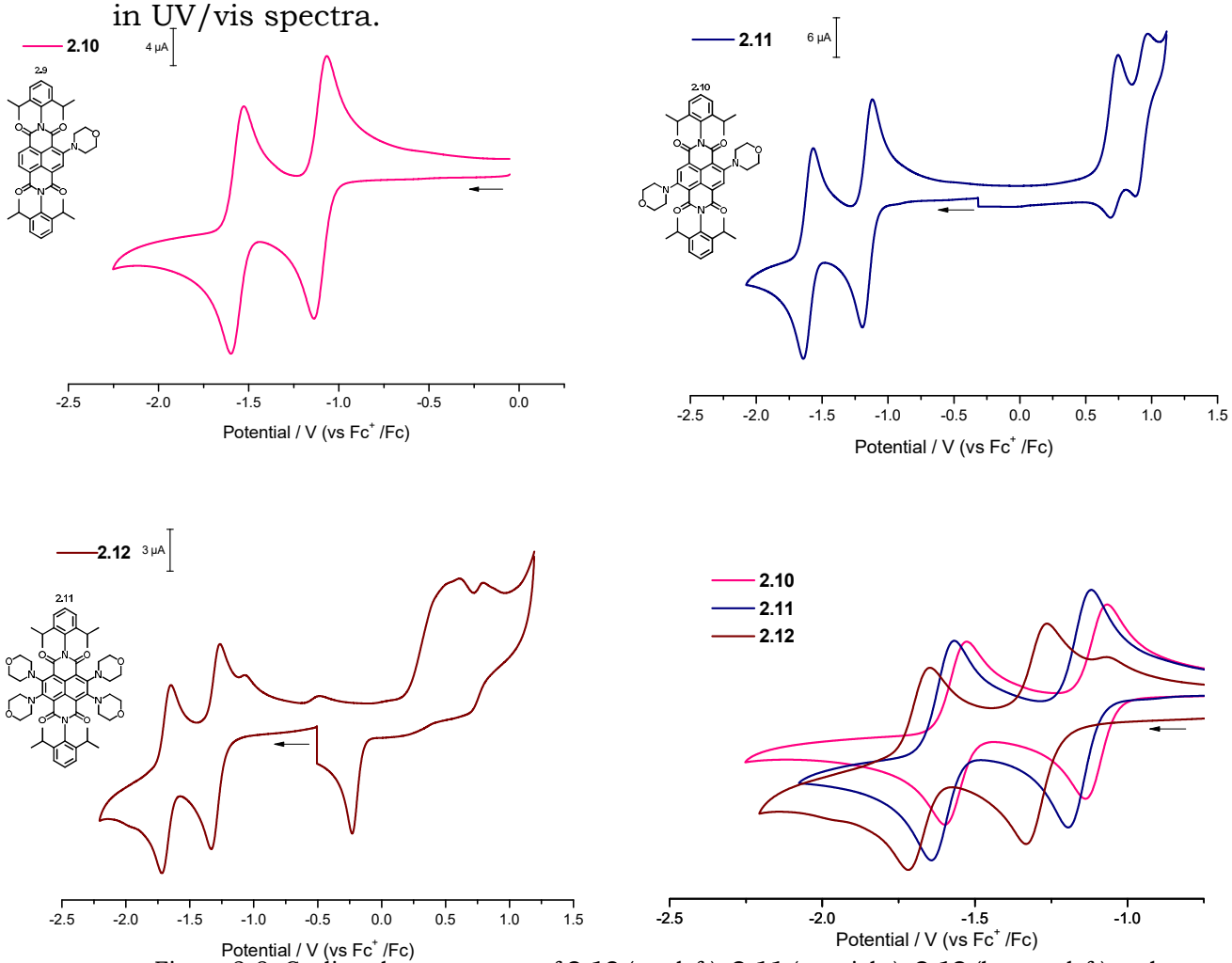


Figure 2-8: Cyclic voltammograms of **2.10** (top left), **2.11** (top right), **2.12** (bottom left) and a comparison of the reduction potentials (bottom right) in DCM with 0.4 M[$Bu_4N$][$BF_4$] supporting electrolyte, at a scan rate of 100 $mVs^{-1}$

**2.11** and **2.12** showed, in addition to these typical reversible reductions, some electronically non-reversible oxidative processes. Surprisingly the second reduction of **2.12** was not electrochemically reversible. Upon returning from the highly negative potential a new electroactive species can be assumed to be generated, producing a redox peak at – 1.15 V (vs $Fc^+/Fc$). This species is not observed when probing the first reduction at less negative potential, it is therefore reasonable to propose that is species has been generated by decomposition of $\mathbf{2.12^{2-}}$ (Figure 2-9). The electronic reversibility of these processes were assessed by examination at various scan rates in a range of 0.02 - 0.3 $Vs^{-1}$. The reductions were found to be one electron in nature *via* coulometry.

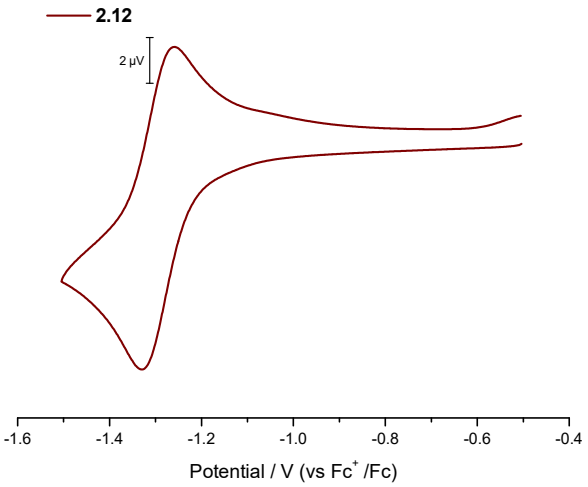


Figure 2-9: Cyclic voltammograms of **2.12**, when potential is only swept from -0.5 V to -1.5 V in DCM with 0.4 $M[Bu_4N][BF_4]$ supporting electrolyte, at a scan rate of 100 $mVs^{-1}$

| Molecule | 1st Reduction $E_{1/2}$ / V | 2nd Reduction $E_{1/2}$ / V |
|---|---|---|
| **2.10** | -1.10 | -1.56 |
| **2.11** | -1.15 | -1.61 |
| **2.12** | -1.30 | -1.68 |

Table 2-2: Reduction potentials of **2.10**, **2.11** and **2.12**. Potentials recorded relative to the internal standard $E_{1/2}$ $Fc^+/Fc$ at a scan rate of 100 $mVs^{-1}$ at room temperature

The trend in the shift of the reductions to more negative potentials (Table 0-12) can be easily explained. As more amines are substituted onto the aromatic core of the NDI, more electron density is donated onto it, increasing the energy of the LUMO. This makes it less favorable to put further electron density into this orbital lowering the reduction potentials.

This increase in LUMO energy may lead to the assumption that the HOMO-LUMO gap would be larger, with increasing substitution. This however is clearly not the case as clearly demonstrated by the UV-vis spectra, were it decreases from **2.10** to **2.11** then increases from **2.11** to **2.12**. It can therefore be inferred that the HOMO must also be increasing in energy. This increase in energy of the HOMO must be to a lesser extent from **2.11** to **2.12** compared to that of **2.10** to **2.11** as the HOMO-LUMO gap of **2.12** larger than that of **2.11**.

It can also be noted that the second reduction potential of **2.12** is less affected by its increased substitution. This causes the two

reductions to be closer together, 0.38 V apart, unlike **2.10** and **2.11** where the difference between the potentials remains the same, 0.46 V. This shows that upon successive substitution, the LUMO of the molecule is perturbed to a decreasing extent.

This increased electron density also explains the atypical oxidative processes; the increased amount of electron density on the core makes it easier to remove electrons. This increase in electron density increases the energy of the HOMO and the electrons within are more available and more easily removed. However the reduced chemical species is most likely chemically unstable in the experimental timescale and so decomposes, making the oxidations non reversible.

#### *2.2.2.3: Spectroelectrochemistry*

The optical behavior of **2.10**, **2.11** and **2.12** upon reduction was examined *via* spectroelectrochemical methods. In each case the progress of both one electron reductions of the molecules were followed utilizing UV/vis spectroscopy. These measurements were all carried out using DCM as the solvent. After undergoing the initial one electron reduction the main bands related to the neutral species can be seen to be reduced and new, red shifted, bands correlating to the monoanionic species are generated concurrently.

For both **2.10** (Figure 2-10) and **2.11** (Figure 2-11) the two peaks typical of NDIs, just below 400 nm, can be seen to deplete and a highly adsorbing band around 490 nm is generated. In addition to this a series of broadly absorbing lower energy bands are generated

located at 634 nm, 719 nm and 805 nm for **2.10**$^{1-}$ and at 664 nm and 836 nm for **2.11**$^{1-}$ (Table 2-3). These changes can be assigned tothe

Reduction of **2.12** (Figure 2-12) does not generate a new band at higher energy. In addition to this the absorbtion profile of **2.12**$^{1-}$ at lower energies (below 700 nm) becomes broad and does not give way to discrete bands as those observed in **2.10** and **2.11**. This broad absorbance causes **2.12**$^{1-}$ to absorb light across the entirity of the observed spectral range. Notable in all 3 monoanionic species is a highly absorbing band located at 495 nm for **2.10**$^{1-}$, 505 nm for **2.11**$^{1-}$and 526 nm for **2.12**$^{1-}$ is observed.

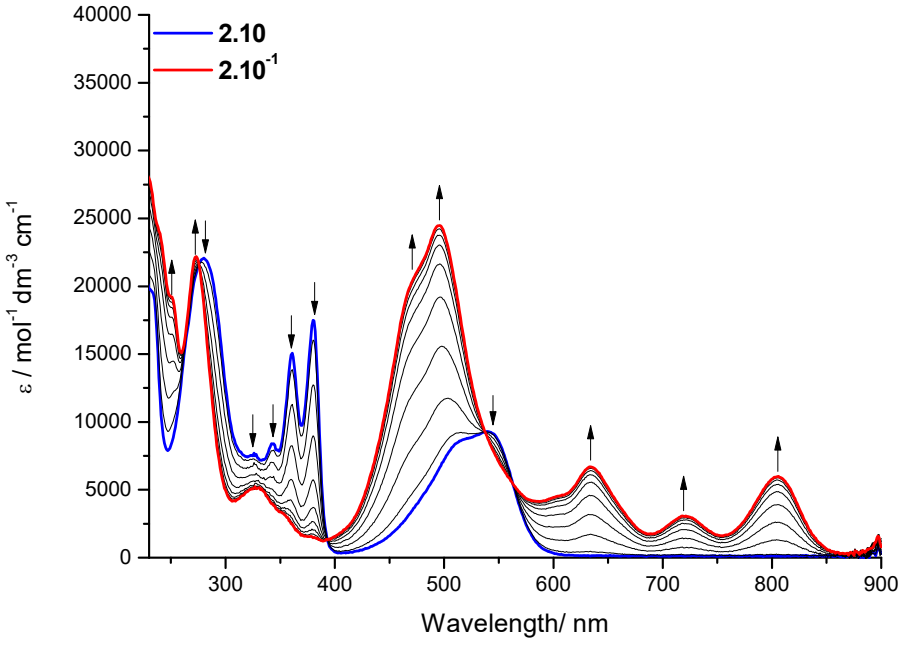


Figure 2-10: UV/vis absorption spectra recorded in DCM containing [Bu$_4$N][BF$_4$] (0.4 M) using spectroelectrochemical methods for **2.10** at 243 K showing the inter-conversion of **2.10** (blue) to **2.10**$^{1-}$ (red). Arrows show the progress of the reduction.

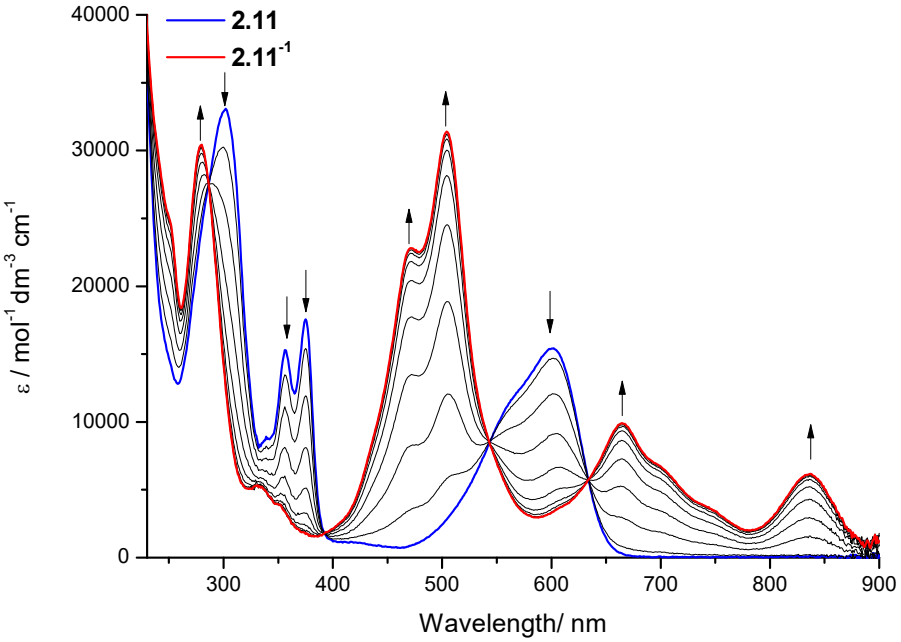


Figure 2-11: UV/vis absorption spectra recorded in DCM containing $[Bu_4N][BF_4]$ (0.4 M) using spectroelectrochemical methods for **2.11** at 243 K showing the inter-conversion of **2.11** (blue) to **2.11**$^{1-}$ (red). Arrows show the progress of the reduction.

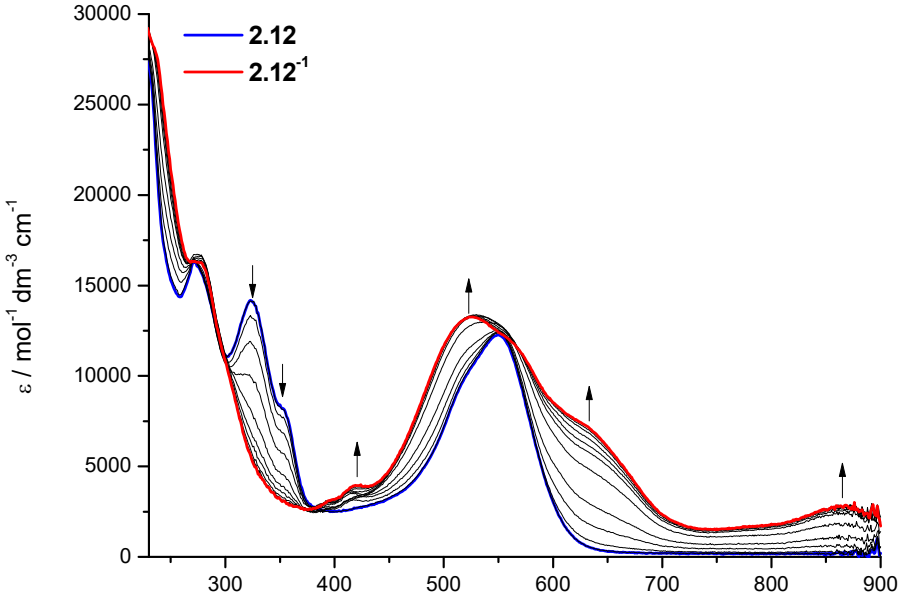


Figure 2-12: UV/vis absorption spectra recorded in DCM containing $[Bu_4N][BF_4]$ (0.4 M) using spectroelectrochemical methods for **2.12** at 243 K showing the inter-conversion of **2.12** (blue) to **2.12**$^{1-}$ (red). Arrows show the progress of the reduction

The dianionic states of these molecules were also probed using the same techniques. The generation of **2.10**$^{2-}$ (Figure 2-33) and **2.11**$^{2-}$ (Figure 2-44) from their monoanionic partners follows a similar pattern. The low energy bands, below 700 nm are seen to entirely deplete, as do the highly absorbing bands at around 500 nm. Each of the dianionic species generate a series of 3 bands, located at 535 nm, 579 nm and 631 nm for **2.10**$^{2-}$ and 547 nm, 592 nm and 646 nm for **2.11**$^{2-}$. In both dianionic species a pair of peaks at around 400 nm (Table 2-4) is also generated. The similarity in the spectra for each of the species implies that the orbitals involved in the transitions are not heavily affected by the contribution of the morpholines, as increasing morpholation has little affect upon their energies.

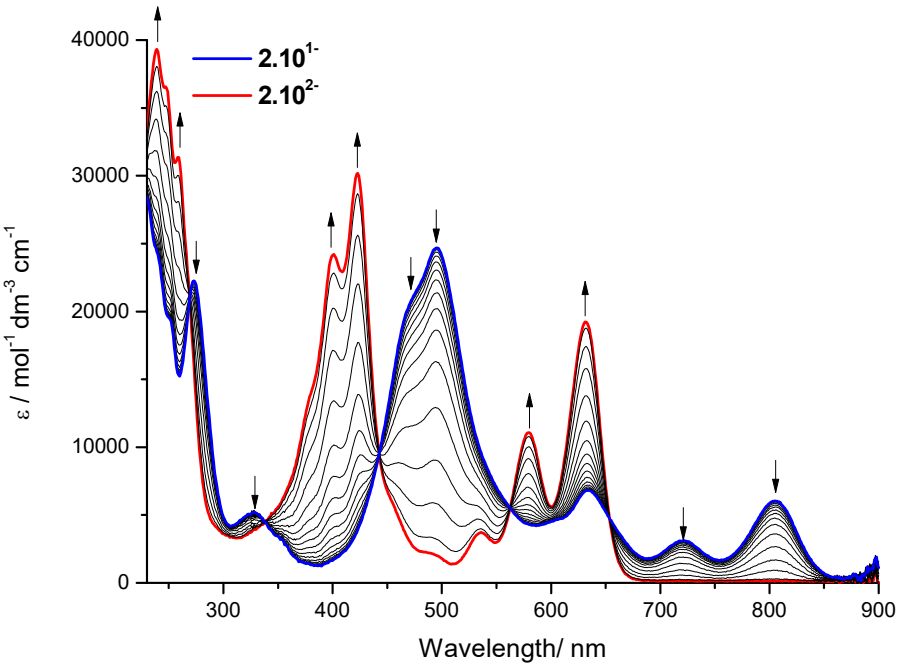


Figure 2-53: UV/vis absorption spectra recorded in DCM containing [Bu4N][BF4] (0.4 M) using spectroelectrochemical methods for **2.10** at 243 K showing the inter-conversion of **2.10**$^{1-}$ (blue) to **2.10**$^{2-}$ (red). Arrows show the progress of the reduction

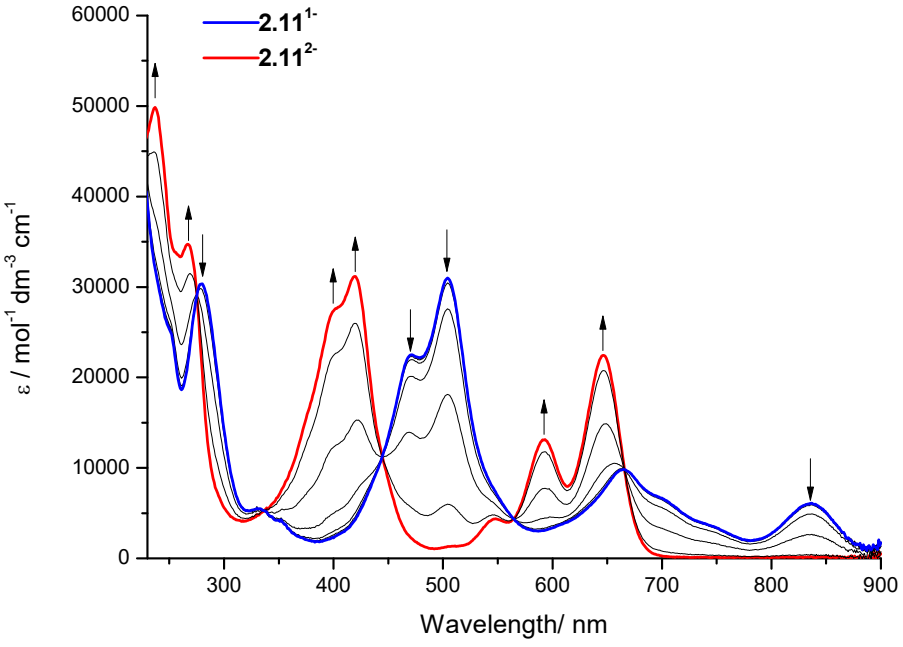


Figure 2-64: UV/vis absorption spectra recorded in DCM containing [Bu4N][BF4] (0.4 M) using spectroelectrochemical methods for **2.11** at 243 K showing the inter-conversion of **2.11**$^{1-}$ (blue) to **2.11**$^{2-}$ (red). Arrows show the progress of the reduction

While both **2.10**$^{2-}$ and **2.11**$^{2-}$ proved to be stable and undergo these electrochemical processes reversibly, **2.12**$^{2-}$ was found to behave differently from typical NDIs as its dianionic state was not chemically stable. Regeneration of **2.12**$^{1-}$ showed significant decrease of the original bands' intensity. This unfortunately meant that **2.12**$^{2-}$ could not be studied because assignment of bands to one species would not be possible. This instability could be related to the decreased reduction potential generating a higher energy species which is more likely to react chemically.

These measurements give a better understanding of the reduced forms of the morpholated NDIs. The particular bands associated with each of the species could be used to track the generation of these species in charge transfer studies. They also gave information towards the electrochemical stability of these species.

| | $\lambda_{abs}$ / nm (ε / $10^3$ $mol^{-1}dm^3cm^{-1}$) | | |
|---|---|---|---|
| **Molecule** | **Neutral** | **Monoanionic** | **Dianionic** |
| **2.10** | 280 (22.0), 326 (7.6), 342 (8.3), 361 (15.1), 380 (17.5), 519 (8.7), 541 (9.3) | 251 (19.1), 272 (22.1), 327 (5.1), 472 (20.8), 495 (24.5), 634 (6.6), 719 (3.0), 805 (5.9) | 239 (39.3), 247 (33.7) , 258 (31.4), 401 (24.2), 423 (30.1), 535 (3.6), 579 (11.1), 631 (19.2) |
| **2.11** | 301 (33.1), 338 (8.7), 356 (15.3), 374 (17.5), 567 (12.2), 602 (15.4) | 249 (25.0), 279 (30.4), 334 (5.1), 353 (3.9), 471 (22.7), 505 (31.6), 664 (9.9), 836 (6.1) | 236 (50.0), 267 (34.7), 399 (27.5), 419 (31.3), 547 (4.4), 592 (13.2), 646 (22.3) |
| **2.12** | 271 (16.2), 323 (14.1), 351 (8.4), 550 (12.2) | 277 (16.3), 421 (4.0), 526 (13.3), 633 (7.2), 865 (2.8) | N/A |

Table 2-5: Spectroelectrochemical data for **2.10**-**2.12** for neutral, monoanionic and dianionic states

### *2.2.2.4: Electron Paramagnetic Resonance*

The molecules were reduced chemically using [Co(Cp)$_2$] then EPR experiments were undertaken on the monoanionic molecules **2.10$^{1-}$**, **2.11$^{1-}$** and **2.12$^{1-}$** in order to confirm the presence of an unpaired electron and attempted to determine its location. All three anions proved to be active within EPR confirming the presence of an unpaired electron within each (Figure 2-15). While both **2.10$^{1-}$** and **2.11$^{1-}$** proved to have significant hyperfine coupling under these conditions **2.12$^{1-}$** was seen to show only very faint coupling.

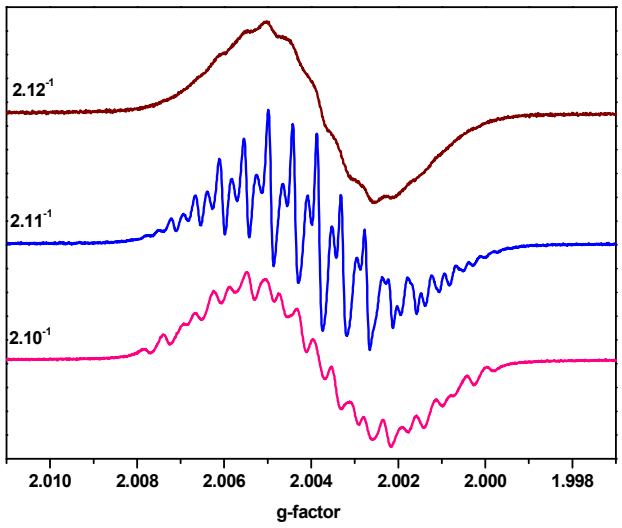


Figure 2-15: Fluid solution X-band EPR spectra for **2.10$^{-1}$**, **2.11$^{-1}$** and **2.12$^{-1}$** in DCM (0.5 mmol), generated by reduction of **2.10$^{-1}$**, **2.11$^{-1}$** and **2.12$^{-1}$**, respectively with [Co(Cp)2] (1:1) under an atmosphere of argon . The spectra were recorded at ambient temperature

The calculated $g_{iso}$ values for each of the molecules process to be the same (Table 2-6). This is interesting as it would imply that the lone electron is located in a similar environment in all three of the molecules. This would indicate that it is primarily located upon the aromatic core and imides of these species as they are the common components which they share.

| **Molecule** | $g_{iso}$ |
|---|---|
| **2.10**$^{1-}$ | 2.0037 |
| **2.11**$^{1-}$ | 2.0038 |
| **2.12**$^{1-}$ | 2.0038 |

Table 2-7: Experimentally determined $g_{iso}$ values for reduced morpholated NDIs

To gain further insight towards the environment of the lone electron the spectra were attempted to be simulated, this was not possible with **2.12**$^{1-}$ due to its lack of hyperfine coupling. It was also impractical to simulate **2.10**$^{1-}$ due to the lack of symmetry within the molecule. Simulation was attempted for **2.11**$^{1-}$ (Figure 2-16) this was done for a more concentrated sample of the anion which was generated *via* bulk electrolysis. This simulation represents the best attempt to reproduce the spectrum using hyperfine parameters broadly consistent with other NDI monoanions.

The agreement between the simulated and the experimental spectra reveal information about the location of the LUMO of **2.11**. The hyperfine coupling is a result of splitting from two sets of two equivalent nitrogens, one set of two equivalent hydrogens. This

shows that the LUMO of this species extends across the whole aromatic core and onto the morpholines, accounting for the two core hydrogens and the two nitrogens of the morpholines. The final set of equivalent nitrogens can be assigned to the two in the imides of the NDI.

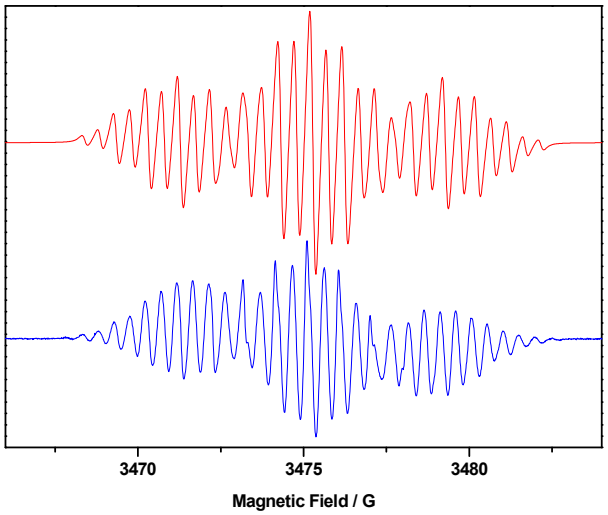


Simulation Parameters:

$g_{iso}$ 2.0037

$a_{2N}$: 0.91 x $10^{-4}$ $cm^{-1}$

$a_{2N}$: 0.43 x $10^{-4}$ $cm^{-1}$

$a_{2H}$: 3.74 x $10^{-4}$ $cm^{-1}$

linewidth: 0.19 G

Lineshape: Lorentzien

Figure 2-16: EPR spectra (left) of **2.11**$^{-1}$ (blue) and simulated spectra (red) and the parameters used to generate the simulated spectra (right).

### 2.2.3: X-ray crystallography

Single crystals of **2.10** – **2.12** were grown and the crystal structures were obtained. In all cases crystal growth was achieved *via* vapour diffusion using $CHCl_3$ as the solvent. Methanol was used as the anti-solvent for both **2.10** and **2.11**, while hexane was used for the more polar **2.12**. Disorder was commonly observed relating to the isopropyl groups and was modelled accordingly. Upon examination of

structures (Figure 2-17) a clear difference between the geometry of **2.12** compared to **2.10** and **2.11** is observed.

The first oddity on the geometry of **2.12** is the distortion of the naphthyl core of the molecule. While both **2.10** and **2.11** retain their planar structure, **2.12** can be seen to have a slight bend within the structure. This de*via*tion is caused by the extensive steric crowding imposed by the morpholines. The morpholine substituents are tertiary amines and therefore limited in the number of conformations that they can adopt and still pack around the core and so the core is forced to adopt this strain.

Closer inspection reveals a more pronounced difference between the different environments of the morpholine substituents relative to the naphthyl core. Both of the less sterically crowded molecules, **2.10** and **2.11**, share similar conformations of the morpholine appendages. In the case of **2.10** the angle formed by the plane of the morpholine group and the plane NDI core was found to be 45.3$^{o}$ or 50.9$^{o}$, while **2.11** the angle was found to be 50.6$^{o}$ or 57.9$^{o}$ (two angles are reported as two molecules are seen in the crystallographic asymmetric unit for both **2.10** and **2.11**). For the more sterically crowded **2.12,** the angle is found to be 43.3$^{o}$ for two of the appendages but 80.0$^{o}$ for the other two, almost perpendicular to the naphthalene plane.

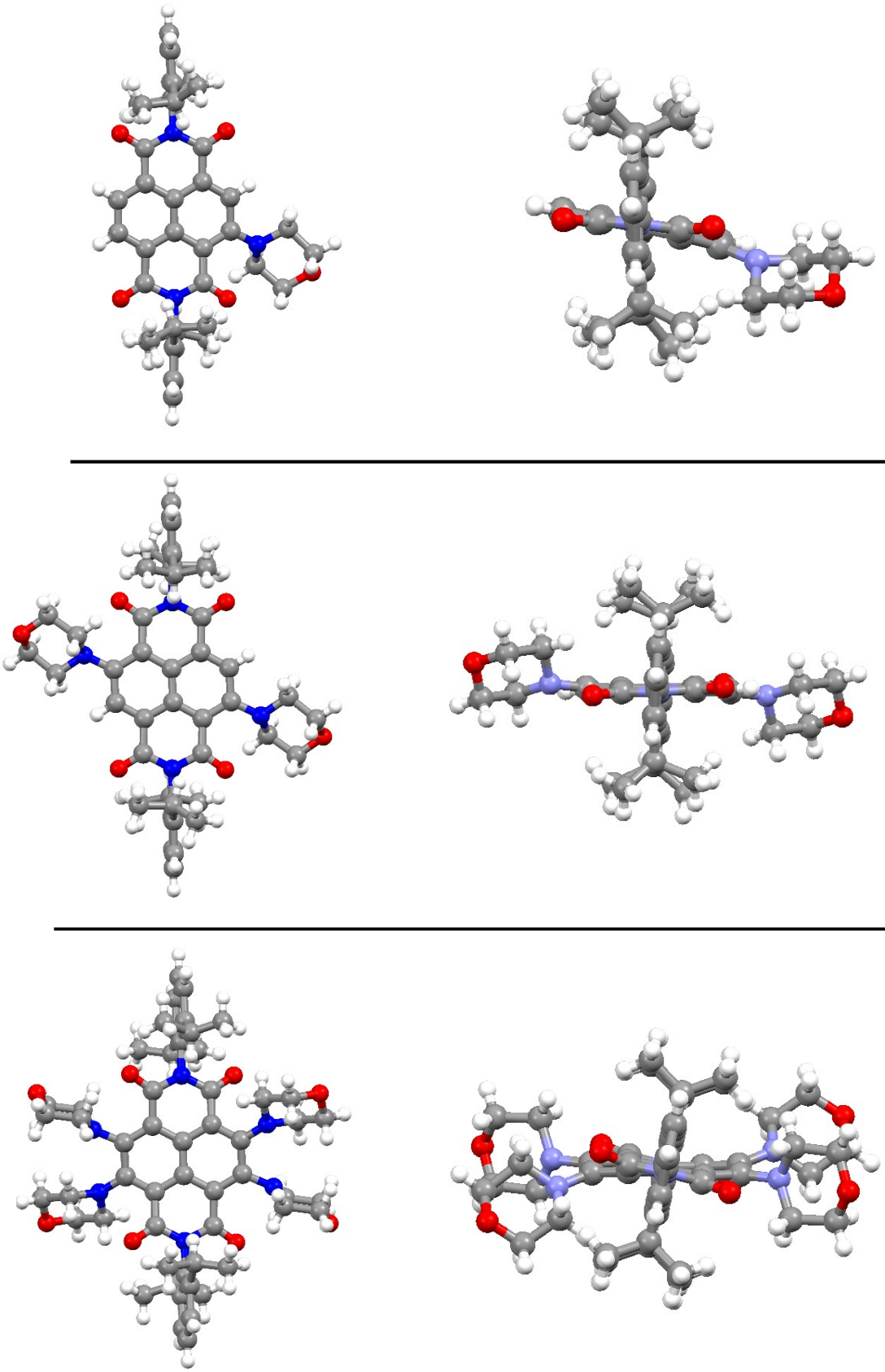

Figure 2-17: Crystal structures of **2.10**-**2.12** from top to bottom. The left shows a top down view and the right a perpendicular view to highlight the difference in the angles of the substituted morpholines. Crystallographically resolved solvent have been removed for clarity.

These differences in the conformations will change the extent to which the morpholines can contribute to the molecular π system of the molecules due to differing orbital overlap. It is most likely that the sterics of **2.12** are causing the morpholines to adopt a conformation where they are less able to contribute into the molecular orbitals of the chromophore. If the contribution of the amines is limited based upon conformation the peculiar optical properties of **2.12** could be a direct result.

### 2.2.4: DFT

In order to further examine if the frontier orbitals of the species DFT calculations were performed. The starting geometries of the molecules were obtained from the crystal structures of each system. These molecular geometries were optimized and the molecular orbitals and energies were generated using B3LYP/6-31G* basis set.

The geometries produced by the calculations showed similar differences in the planes of the morpholine relative to the naphthyl core as observed in the crystallographic data. As well as this the energies of the molecular orbitals agreed with the trend observed in the UV-Vis spectra of **2.10** – **2.12**, the electronic transitions between particular molecular orbitals being assigned to bands within the experimental spectra. As the calculations agreed well with experimental work they were used to gain further insight into the unexpected values obtained for lowest energy electronic transitions.

For **2.10** – **2.12** this lowest energy absorption band was assigned to the $S_0$ to $S_1$ transition, between the HOMO and the LUMO. Examining the calculated energy difference of these molecular orbitals showed the same trend as the experimental values, decreasing in energy from **2.10** to **2.11** then increasing in energy from **2.11** to **2.12** (Figure 2-19).

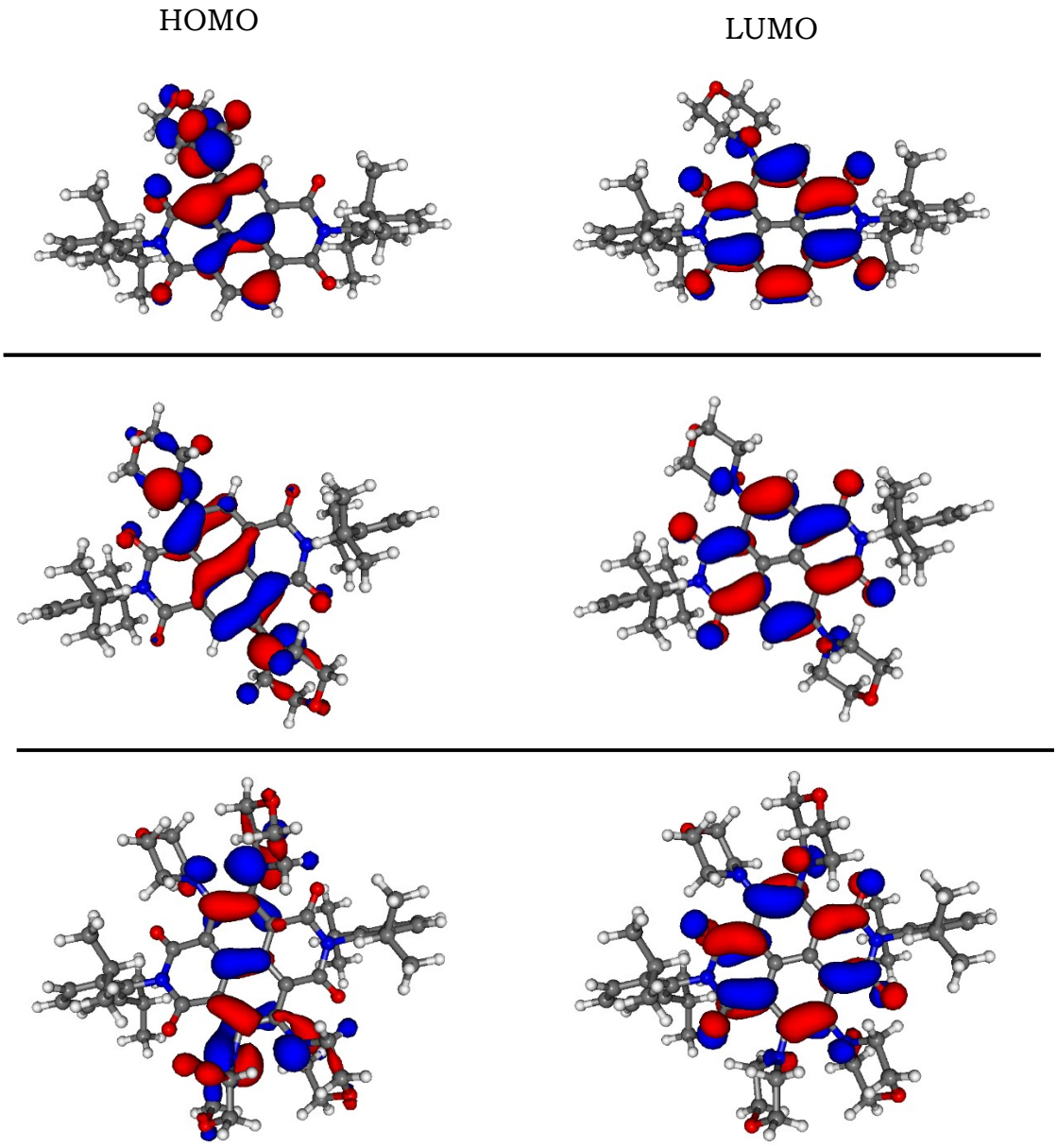


Figure 2-18: Calculated molecular orbital diagrams for **2.10** – **2.12** from top to bottom respectively

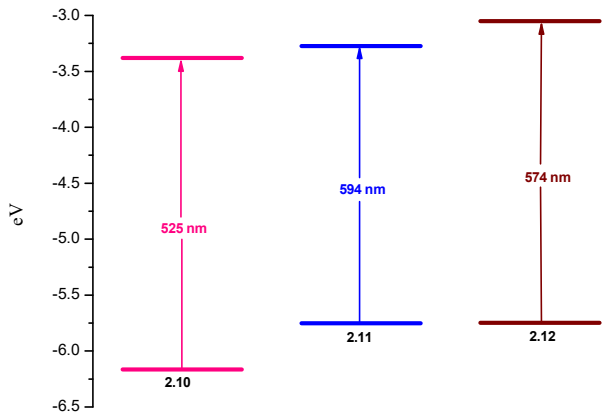


Figure 2-19: Calculated wavelengths for the transitions from the HOMO to the LUMO for **2.10** – **2.12**

The energies of the calculated LUMOs can be seen to increase with substitution, agreeing with the cyclic voltammetry. In addition the energies of the calculated HOMOs can be seen to increase from substantially from **2.10** to **2.11** (0.413 eV) and much less from **2.11** to **2.12** (0.004 eV).

To gain further insight into these phenomena the electron density of the HOMO and LUMO for each of the species was calculated and investigated. It can clearly be seen that the morpholine substituents contribute to the electronic orbitals to a significant degree. It was also observed that depending upon the orientation of the morpholines this contribution varied (Figure 2-18).

The contribution of the morpholine groups to the HOMO and LUMO increases with substitution (Table 2-8). However noticeably in the HOMO this contribution increases almost linearly with substitution,

increasing from 49.3 % for **2.10** to 66.9 % for **2.12**, averaging around ~5 % per morpholine.

| Molecule | HOMO | | LUMO | |
|---|---|---|---|---|
| | Morph | NDI | Morph | NDI |
| **2.10** | 49.3 % | 50.2 % | 5.3 % | 94.4 % |
| **2.11** | 54.0 % | 45.8 % | 7.6 % | 92.1 % |
| **2.12** | 66.9 % | 32.8 % | 12.5 % | 87.0 % |

Table 2-9: Showing the percentage contribution to the molecular orbitals of the morpholine and NDI components of **2.10** – **2.12**

The contribution of the individual morpholine groups to the frontier orbitals of **2.10**-**2.12** were calculated. For **2.10**, the single morpholine appendage is responsible for all of the morpholine contribution to each frontier orbital (Table 2-10). When considering **2.11** (Table 2-11) it can be seen that both morpholine moieties possess identical geometries and also contribute equally to the HOMO and LUMO.

**2.10**

| Orbital | Energy / eV | % Morph | % NDI |
|---|---|---|---|
| **HOMO** | -6.164 | 49.3 | 50.2 |
| **LUMO** | -3.379 | 5.3 | 94.4 |
| **Angle** | - | 40.47 | - |

Table 2-12: Showing the energy of the HOMO and LUMO, contribution of both the Morpholine and NDI to the orbital and angle between the plane of the morpholine and NDI for **2.10**

**2.11**

| Orbital | Energy / eV | % Morph 1 | % Morph 2 | % NDI |
|---|---|---|---|---|
| **HOMO** | -5.751 | 27.0 | 27.0 | 45.8 |
| **LUMO** | -3.270 | 3.8 | 3.8 | 92.1 |
| **Angle** | - | 43.25 | 43.25 | - |

Table 2-13: Showing the energy of the HOMO and LUMO, contribution of both the Morpholine and NDI to the orbital and angle between the plane of the morpholine and NDI for **2.11**

Inspecting these contributions for **2.12** reveals why the HOMOs energy is increased by such a small amount. Here, the morpholine contribution to the molecular orbitals varies with each morpholine substituent (Table 2-8). This is most likely due to the fact that they are forced to adopt different geometries by steric interactions with one another. These geometries perturb the electron donation capability of the most likely by lowering the availability of the lone pair on the morpholine nitrogen to the aromatic core.

**2.12**

| Orbital | Energy / eV | % Morph 1 | % Morph 2 | % Morph 3 | % Morph 4 | % NDI |
|---|---|---|---|---|---|---|
| **HOMO** | -5.747 | 21.1 | 5.5 | 14.8 | 25.5 | 32.8 |
| **LUMO** | -3.133 | 5.1 | 1.2 | 3.5 | 2.7 | 87.0 |
| **Angle** | - | 54.37 | 61.31 | 61.52 | 68.10 | - |

Table 2-14: Showing the energy of the HOMO and LUMO, contribution of both the Morpholine and NDI to the orbital and angle between the plane of the morpholine and NDI for **2.12**

## 2.3: Conclusions

A synthetic pathway which allows for the synthesis of cNDIs has been explored. This involved synthesizing an exploratory series of cNDIs from commercially available species. These cNDIS were substituted with morpholine as it is a readily available and highly electron donating secondary amine. This created a novel sterically crowded cNDI which had it properties altered due to this crowding.

The frontier orbitals of the series were thoroughly examined. This examination revealed that the series did not follow the typical trend for increase substitution onto the NDI core. Typically increasing amine substitution results in a smaller HOMO-LUMO gap, however in this case the tetra substituted species had a larger gap than the di.

Upon viewing the crystal structures of these species it was revealed that due to the steric crowing the tetra substituted species had been caused to adopt a stressed geometry. Utilizing the co-ordinates from the crystal structure DFT calculations were performed. These calculations agreed with the geometries enforced by the sterics. From these calculations the contributions of each morpholine to the frontier orbitals was assessed and it was found that the contribution was lessened for some of the substituents in the tetra substituted species. This lack of contribution resulted in a smaller shift in the frontier orbitals and the larger HOMO-LUMO gap was rationalized.

This body of work lends itself easily to expansion as the methodology for synthesizing cNDIs can be applied to create more complex cNDIs, which is to an extent discussing in Chapter 3. However the synthesis of the tetra brominated species **2.8** would require further optimization to allow for ready access to tetra substituted cNDIs. This work also extends the knowledge of how the frontier orbitals of cNDIs can be tuned to give a particular HOMO-LUMO gap energy, allowing to tailor species which absorb a particular wavelength of light. Finally this body of work gives an example of it is important to be mindful of the geometry of amines when considering their ability to donate electron density to molecular orbitals.

## 2.3: Experimental

### 2.3.1: General procedures

All starting materials were purchased form Sigma Aldrich or Fisher Scientific and used without further purification. Column chromatography was conducted using silica gel (merck silica gel 60, 0.2-0.5 mm, 50-130 mesh). The $^{1}H$ and $^{13}C$ NMR spectra were obtained on a Bruker 400 MHz spectrometer. MALDI MS spectra were collected with a Bruker Ultraflex III mass spectrometer using trans-2-[3-(4-tert-butylphenyl)-2-methyl-2-propenylidene]malononitrile as the matrix. FD MS spectra were measured with a JOEL AccuTOF GCX spectrometer. Single crystal X-ray diffraction experiments were performed on an Oxford Diffraction Supernova CCD area detector diffractometer at 120 K using monochromated Cu K α radiation (λ = 1.54184 Å); on Agilent GV1000 AtlasS2 and TitanS2 CCD area detector diffractometers at 120 K using monochromated Cu K α radiation (λ = 1.54184 Å). Absorption corrections were applied using analytical numerical methods using either ShelXS or ShelXT and refined with ShelXL using a least squares method. In all instances, Olex2 software was used as the solution refinement and analysis program. All hydrogen atoms were placed in geometrically calculated positions; non-hydrogen atoms were refined with anisotropic displacement.

### 2.3.2: Synthesis of 2.1

Cyanuric acid (1.61 g, 12.48 mmol), sodium hydroxide (1.50 g, 37.5 mmol), sodium carbonate (1.99 g, 18.8 mmol), and potassium bromide (4.46 g, 37.5 mmol) was dissolved in water (180 mL) and cooled to 0 $^{o}$C. To this, oxone (23.1 g, 152.0 mmol) in water (150 mL) was added slowly with stirring. This was left for 16 h and the precipitate then collected *via* filtration and washed with water. The solid was dried in a vacuum desiccator to give tribromocyanuric acid (**2.1**) (4.38 g, 12.11 mmol, 97%) as a white powder.

IR : $\tilde{\nu}$ = 1741, 1724, 1660, 1405, 1339, 1197, 1146, 1051, 737, 717 $cm^{-1}$.

### 2.3.3: Synthesis of 2.6 and 2.7

**2.1** (800 mg, 2.19 mmol) and 1,4,5,8-naphthalenetetracarboxylic dianhydride (670 mg, 2.5 mmol) were slurried in $H_2SO_4$ (8 ml, 95%) and stirred at room temperature for 24 h. The reaction mixture was poured onto ice, filtered and washed with water (2 x 50 ml) and methanol (10 ml) to give a yellow solid. Acetic acid (10 ml) and 2,6-diisopropylaniline (0.52 ml, 2.0 mmol) were added and the mixture heated to 80 $^{o}$C for 8 h. This was poured onto ice and the solid collected *via* filtration. The residue was purified *via* column chromatography (silica [$CHCl_3$:Hexane 9:1]) to give **2.5** (238mg, 0.36 mmol, 39 %) and **2.6** (172 mg, 0.231 mmol, 19 %) as beige powders.

**2.6**:$^{1}$H NMR (400 MHz, Chloroform-*d*) δ 9.07 (s, 1H), 8.97 – 8.87 (m, 2H), 7.51 (t, *J* = 7.7 Hz, 2H), 7.36 (dd, *J* = 7.8, 2.8 Hz, 4H), 2.68 (td, *J* = 6.9, 5.0 Hz, 4H), 1.20 – 1.14 (m, 23H).$^{13}$C NMR (101 MHz, Chloroform-*d*) δ 162.75, 162.06, 161.32, 145.62, 145.55, 139.15, 132.42, 131.49, 130.28, 130.14, 127.20, 126.57, 126.30, 124.45, 77.48, 77.16, 76.84, 29.51, 24.08. FD MS: 664.19327 [$M^+$] Calc: 664.19367

**2.7**:$^{1}$H NMR (400 MHz, Chloroform-*d*) δ 9.12 (s, 2H), 7.55 – 7.49 (m, 2H), 7.36 (d, *J* = 7.8 Hz, 4H), 2.72 – 2.58 (m, 4H), 1.17 (d, *J* = 6.9 Hz, 25H).$^{13}$C NMR (101 MHz, Chloroform-*d*) δ 161.05, 161.02, 145.50, 139.71, 130.29, 129.94, 129.17, 128.76, 125.78, 124.72, 124.50, 77.48, 77.16, 76.84, 29.55, 24.09. MS FD MS: 744.10232 [$M^+$] Calc: 744.10214

**Crystal Data** for $C_{23}H_{22}BrCl_6NO_2$ (*M* =637.02 g/mol): monoclinic, space group I2/a (no. 15), *a* = 13.4015(4) Å, *b* = 18.1628(4) Å, *c* = 16.6005(4) Å, *β* = 102.918(3)°, *V* = 3938.44(18) Å$^3$, *Z* = 8, *T* = 120(2) K, μ(CuKα) = 10.584 mm$^{-1}$, *Dcalc* = 2.149 g/cm$^3$, GooF = 1.079, 19775 reflections measured (7.318° ≤ 2Θ ≤ 148.952°), 3947 unique ($R_{int}$ = 0.0328, $R_{sigma}$ = 0.0160) which were used in all calculations. The final $R_1$ was 0.0310 (I > 2σ(I)) and $\omega R_2$ was 0.0809 (all data).

### 2.3.4: Synthesis of 2.9

A pressure tube was charged with 3,4,9,10-perylenetetracarboxylic dianhydride (500 mg, 1.28 mmol) **2.1** (2.0 g, 5.47 mmol) and $H_2SO_4$ (5 ml, 95%). This was sealed and heated to 110 $^oC$ for 4 days. An additional portion of **2.1** (1 g, 2.74 mmol) was added at the end of each day. The mixture was then cooled, poured onto ice, filtered and washed with water. MALDI MS showed the presence of only **2.5** and no lesser brominated species. A portion of this (500 mg) was added to octylamine (161 µL, 0.98 mmol) and DCM (20 mL). This mixture was heated to reflux for 2 h then phosphorous tribromide (95 uL, 0.98 mmol) was added and the mixture refluxed for 1 h. This was cooled and water (60 ml) was added, the product was extracted into DCM (2x 25 mL), dried over $MgSO_4$ filtered and the solvent removed *in vacuo*. The residue was purified *via* column chromatography (silica [$CHCl_3$:Hexane 3:1]) to give **2.9** ( 150 mg, 0.12 mmol, 25 %)

$^1H$ NMR (400 MHz, Chloroform-*d*) δ 4.23 (m, 2H), 4.14 (m, 2H), 1.70 (m, 4H), 1.49 (m, 4H), 1.38 (m, 4H), 1.31-1.22 (m, 12H), 0.81 (t, J = 7.5, 6H) $^{13}C$ NMR (101 MHz, Chloroform-*d*) δ 160.10, 133.53, 132.76, 132.04, 127.60, 125.81, 121.95, 42.52, 31.80, 29.71, 29.27, 28.06, 27.20, 22.71, 14.13. MALDI MS: m/*z*: 1245.61 [$M^+$] Calc: 1245.59

### 2.3.5: Synthesis of 2.10

**2.6** (60 mg, 0.09 mmol) was dissolved in DMF (1 mL) and morpholine (8.00 µl, 0.09 mmol) and stirred at room temperature for 3 h. The solvent was removed and the residue purified *via* column

chromatography (silica [$CHCl_3$:EtOAc 19:1] ) to give **2.10** as a pink powder (55 mg, 0.082 mmol, 91 %)

$^1$H NMR (400 MHz, Chloroform-*d*) δ 8.78 (d, *J* = 7.7 Hz, 1H), 8.57 (d, *J* = 7.7 Hz, 1H), 8.53 (s, 1H), 7.53-7.43 (m, 2H), 7.35 (dd, *J* = 7.8, 2.7 Hz, 5H), 3.94 (t, *J* = 4.6 Hz, 4H), 3.55 (t, *J* = 4.7 Hz, 4H), 2.74-2.66 (m, 4H), 1.20 – 1.14 (m, 24H). $^{13}$C NMR (101 MHz, Chloroform-*d*) δ 163.51, 163.26, 163.22, 162.01, 154.41, 145.67, 145.57, 131.76, 131.54, 130.25, 130.05, 129.82, 127.02, 126.37, 126.22, 125.74, 124.32, 122.32, 77.48, 77.16, 76.84, 66.85, 52.71, 29.42, 29.40, 24.22, 24.15, 24.10, 23.97. FD MS: 671.33488 [$M^+$] Calc: 671.33592.

**Crystal Data** for $C_{86}H_{95}N_6O_{11}Cl_3$ (*M* =1495.02 g/mol): monoclinic, space group $P2_1/n$ (no. 14), *a* = 24.3041(10) Å, *b* = 8.5699(2) Å, *c* = 38.5331(15) Å, *β* = 102.843(4)°, *V* = 7825.0(5) Å$^3$, *Z* = 4, *T* = 120(2) K, μ(CuKα) = 1.579 mm$^{-1}$, $D_{calc}$ = 1.269 g/cm$^3$, Goof = 1.043, 39965 reflections measured (7.214° ≤ 2Θ ≤ 147.084°), 15388 unique ($R_{int}$ = 0.0327, $R_{sigma}$ = 0.0400) which were used in all calculations. The final $R_1$ was 0.0904 (I > 2σ(I)) and $\omega R_2$ was 0.2645 (all data)

## 2.3.6: Synthesis of 2.11

**2.7** (75 mg, 0.1 mmol) was dissolved in DMF (1 mL) and morpholine (17.2 uL, 0.2 mmol) then heated to 135 °C for 3 h. The solvent removed and the residue purified *via* column chromatography (silica [$CHCl_3$:EtOAc 19:1]) to give **2.11** as a blue powder ( 61 mg, 0.081 mmol, 81%).

$^{1}$H NMR (400 MHz, Chloroform-*d*) δ 8.50 (s, 2H), 7.50 (t, *J* = 7.8 Hz, 2H), 7.34 (d, *J* = 7.4 Hz, 4H), 3.92 (t, *J* = 4.5 Hz, 8H), 3.43 (t, *J* = 4.5 Hz, 8H), 2.69 (hept, *J* = 7.0 Hz, 4H), 1.20 – 1.13 (m, 24H).$^{13}$C NMR (101 MHz, Chloroform-*d*) δ 162.75, 161.75, 152.02, 145.26, 130.82, 129.48, 126.13, 125.41, 125.07, 123.97, 77.16, 76.84, 76.53, 66.60, 52.32, 29.08, 23.95, 23.69. FD MS: 756.38323 [M$^{+}$] Calc: 756.38869.

**Crystal Data** for $C_{24}H_{27}Cl_3N_2O_3$ (*M* =497.82 g/mol): triclinic, space group P-1 (no. 2), *a* = 10.4980(3) Å, *b* = 15.6200(4) Å, *c* = 16.6076(5) Å, *α* = 96.329(2)°, *β* = 106.564(3)°, *γ* = 107.664(3)°, *V* = 2428.82(13) Å$^3$, *Z* = 4, *T* = 120(2) K, μ(CuKα) = 3.648 mm$^{-1}$, $D_{calc}$ = 1.361 g/cm$^3$, GooF = 1.027 18176 reflections measured (7.378° ≤ 2Θ ≤ 147.376°), 9512 unique ($R_{int}$ = 0.0477, $R_{sigma}$ = 0.0433) which were used in all calculations. The final $R_1$ was 0.0473 (I > 2σ(I)) and $wR_2$ was 0.1320 (all data).

## 2.3.7: Synthesis of 2.12

**2.1** (2.00 g, 5.48 mmol) and 1,4,5,8-naphthalenetetracarboxylic (500 mg, 1.87 mmol) were combined in $H_2SO_4$ (10 ml) and heated to 100 $^{o}$C for 24 h and a second portion of **2.1** (1.00 g, 2.74 mmol) is added and the mixture heated for another 24 h. The mixture was cooled, neutralised with $NaHCO_3$ saturated aqueous solution (50 mL), poured onto ice and filtered. The solid was washed with water (2 x 50 mL and methanol (10 mL). This was then added to acetic acid (10 mL) and 2,6-diisopropylaniline (2.11 mL, 11.22 mmol) and heated to 100 $^{o}$C for 6 h. This was cooled to RT, and $NaHCO_3$ saturated

aqueous solution (50 mL), extracted into $CHCl_3$ (2 x 20 mL), dried over $MgSO_4$, filtered and the solvent removed. The residue was then dissolved in DMF (5 mL) and morpholine (2 mL, 23.19 mmol) and heated to 135 $^oC$ for 16 h. The solvent was then removed and the residue purified *via* column chromatography (silica [$CHCl_3$:EtOAc 9:1] ) to yield **2.12** as a a purple powder (52 mg, 0.056 mmol, 3 %).

$^1H$ NMR (400 MHz, Chloroform-*d*) δ 7.54 – 7.49 (m, 2H), 7.35 (d, *J* = 7.8 Hz, 4H), 3.88 (t, *J* = 4.7 Hz, 16H), 3.35 (d, *J* = 4.7 Hz, 16H), 2.83 – 2.70 (m, 4H), 1.20 (d, *J* = 6.8 Hz, 24H).$^{13}C$ NMR (101 MHz, Chloroform-*d*) δ 163.11, 154.05, 146.08, 131.13, 130.03, 124.46, 124.05, 122.81, 77.48, 77.16, 76.84, 67.38, 49.59, 29.66, 24.42. FD MS: 926.49348 [$M^+$] Calc: 926.49421.

**Crystal Data** for $C_{29}H_{35}Cl_6N_3O_4$ (M =702.30 g/mol): monoclinic, space group P21/c (no. 14), a = 13.7970(3) Å, b = 15.6969(3) Å, c = 15.2455(2) Å, β = 98.979(2)°, V = 3261.26(11) Å3, Z = 4, T = 120(2) K, μ(CuKα) = 5.127 mm-1, $D_{calc}$ = 1.430 g/cm3, GooF = 1.027, 32698 reflections measured (6.486° ≤ 2Θ ≤ 147.292°), 6487 unique (Rint = 0.0689, Rsigma = 0.0374) which were used in all calculations. The final $R_1$ was 0.0638 (I > 2σ(I)) and $\omega R_2$ was 0.1833 (all data).

## 2.3.8: Electrochemical and Optical Investigations

UV/visible absorption spectra were recorded on Perkin-Elmer Lambda 25 spectrometer. Cyclic voltammetric and coulometric studies were conducted using an Autolab PGSTAT20 potentiostat. DCM was dried *via* distillation under nitrogen on calcium hydride.

Standard cyclic voltammetry was carried out under an atmosphere of argon using a three electrode arrangement in a single compartment cell. Electrodes used in the cell were as follows; A glassy carbon working electrode, a Pt wire secondary electrode and a calomel reference electrode, chemically isolated from the test solution *via* a bridge tube containing electrolyte solution and fitted with a porous vycor frit. The solutions were $10^{-3}$ M in molecule of interest and 0.4 M in $[Bu_4N][BF_4]$ as the supporting electrolyte. Redox potentials are quoted versus the ferrocenium-ferrocene couple used as an internal reference. Compensation for internal resistance was not applied.

The UV/vis spectroelectrochemical experiments were carried out with and optically transparent electrochemical cell (modified quartz cuvette, optical pathlength: 0.5 mm). A three electrode configuration, consisting of Pt/Rh gauze working electrode, a Pt wire secondary electrode (in a fritted PTFE sleeve) and a saturated calomel electrode, as reference, chemically isolated from the test solution *via* a bridge tube containing electrolyte solution and terminated in a porous frit, was used in the cell. The potential at the working electrode was controlled by a Sycopel scientific Ltd DD10M potentiostat. The UV/vis spectra were recorded on a Perkin Elmer Lambda 16 spectrophotometer. The cavity was purged with dinitrogen and temperature control at the sample was achieved by flowing cooled dinitrogen across the surface of the cell.

Bulk electrolysis was performed under an argon atmosphere at 0 $^{o}$C in a two-component cell: a platinum/rhodium gauze working electrode and a secondary electrode separated by a glass frit. A silver/silver chloride reference electrode reference electrode was bridged to the test solution through a vycor frit, orientated at the centre of the working electrode. The working electrode compartment, containing analyte (1mM), was stirred rapidly with a magnetic stirred bar during electrolysis. $[Bu_4N][BF_4]$ (400 mM) was used as the supporting electrolyte for the experiments.

## 2.4: References


(1) R.E. Bird, L.J. Lewis, *Solar Energy* **1983**, *30*.
(2) T.Earmme, Y.-J.Hwang, N. M Murari, S.Subramaniyan, S. A.Jenekhe, *JACS,* **2013**, *135*, 14960.
(3) A.Sharenko, C. M.Proctor, T. S van der Poll, Z. B.Henson, T.-Q.Nguyen, G. C.Bazan, *Adv Mat,* **2013**, *25*, 4403.
(4) C.Röger, F. Würthner, *J. Org. Chem,* **2007**, *72*, 8070.
(5) D.Buckland, S. V.Bhosale, S. J.Langford, *Tetrahedron Lett,* **2011**, *52*, 1990.
(6) J. E.Anthony, A.Facchetti, M.Heeney, S. R.Marder, X.Zhan, *Adv. Mater,* **2010**, *22*, 3876.
(7) B. A.Jones, M. J.Ahrens, M.-H.Yoon, A.Facchetti, T. J.Marks, M. R.Wasielewski, *Angew. Chem. Int. Ed,* **2004**, *43*, 6363.
(8) X.Zhan, A.Facchetti, S.Barlow, T. J.Marks, M. A.Ratner, M. R.Wasielewski, S. R.Marder, *Adv.Mater,* **2011**, *23*, 268.
(9) D.Shukla, S. F.Nelson, D. C.Freeman, M.Rajeswaran, W. G.Ahearn, D. M.Meyer, J. T.Carey, *Chem. Mater,* **2008**, *20*, 7486.
(10) P. A. Paula, *Physical Chemistry*; 8 ed.; W.H.Freeman, 2006.
(11) N. G.Pschirer, C.Kohl, F.Nolde, J.Qu, K.Müllen, *Angew. Chem. Int. Ed,* **2006**, *45*, 1401.
(12) F. O.Holtrup, G.R. J. Müller, H.Quante, S.De Feyter, F. C.De Schryver, K.Müllen, *Chem. Eur. J,* **1997**, *3*, 219.
(13) Z.Yuan, S.-L.Lee, L.Chen, C.Li, K. S.Mali, S.De Feyter, K. Müllen, *Chem. Eur. J,* **2013**, *19*, 11842.
(14) J.Quinn, Y.Zheng, Z.Chen, H.Usta, C.Newman, H.Yan, A.Facchetti, Google Patents: 2011.
(15) L. M.Kozycz, C.Guo, J. G.Manion, A. J.Tilley, A. J.Lough, Y.Li, D. S. Seferos, *J. Mater. Chem,* **2015**, *3*, 11505.
(16) B. A.Llewellyn, E. S.Davies, C. R.Pfeiffer, M.Cooper, W.Lewis, N. R.Champness, *Chem Commun,* **2016**, *52*, 2099.
(17) A. J.Tilley, R. D.Pensack, T. S.Lee, B.Djukic, G. D.Scholes, D. S.Seferos, *J. Phys. Chem,* **2014**, *118*, 9996.
(18) H. Vollmann, H. M. Corell, Streeck *Liebigs Ann,* **1937**, *531*, 1.
(19) R. S. K. Kishore, O. Kel, N.Banerji, D.Emery, G.Bollot, J.Mareda, A.Gomez-Casado, P.Jonkheijm, J.Huskens, P.Maroni, M.Borkovec, E.Vauthey, N.Sakai, S.Matile, *JACS,* **2009**, *131*, 11106.
(20) S.Bhosale, A. L.Sisson, P.Talukdar, A.Fürstenberg, N.Banerji, E.Vauthey, G.Bollot, J.Mareda, C.Röger, F.Würthner, N.Sakai, S.Matile, *Science,* **2006**, *313*, 84.
(21) S.Chopin, F.Chaignon, E.Blart, F.Odobel, *J. Mater. Chem,* **2007**, *17*, 4139.

(22) A.Błaszczyk, M.Fischer, C.von Hänisch, M.Mayor, *Helv. Chim. Acta*, **2006**, *89*, 1986.
(23) M. C. R.Delgado, E.-G.Kim, D. A. S.Filho, J.-L.Bredas, *JACS,* **2010**, *132*, 3375.
(24) R. E.Dawson, A.Hennig, D. P.Weimann, D.Emery, V.Ravikumar, M J.ontenegro, T.Takeuchi, S.Gabutti, M.Mayor, J.Mareda, C. A.Schalley, S.Matile, *Nat. Chem,* **2010**, *2*, 533.
(25) F.Wurthner, *Chem.Commun,* **2004**, 1564.
(26) F.Würthner, S.Ahmed, C.Thalacker, T.Debaerdemaeker, *Chem. Eur. J,* **2002**, *8*, 4742.
(27) C.Thalacker, C.Röger, F.Würthner, *J Org Chem,* **2006**, *71*, 8098.
(28) R. S. K.Kishore, V.Ravikumar, G.Bernardinelli, N.Sakai, S.Matile, *J. Org. Chem,***2008**, *73*, 738.
(29) K.Canto, R.da Silva Ribeiro, A. F. P.Biajoli, C. R. D.Correia, *Eur.J. Org. Chem,* **2013**, *2013*, 8004.
(30) Y.Kim, J.Hong, J. H.Oh, C.Yang, *Chem.Mater,* **2013**, *25*, 3251.
(31) Y.Kumar, S.Kumar, S.K. Keshri, J.Shukla, S. S.Singh, T. S.Thakur, M.Denti, A.Facchetti, P.Mukhopadhyay, *Org. Lett,* **2016**, *18*, 472.
(32) X.Lu, W.Zhu, Y.Xie, X. Li, Y.Gao, F.Li, H.Tian, *Chem. Eur. J,* **2010**, *16*, 8355.

# Chapter 3 : cNDIs as Electron Donor Acceptor Candidates

# 3.1: Introduction

## 3.1.1: Organic Electronics

Organic electronics[1,2] is a rapidly growing field of material science. The primary advantages of utilising organic materials over inorganic systems is the potential for reduced cost due to the more ready availability of carbon based starting material. On top of this, many organic materials have increased mechanical flexibility compared to metals allowing them to create organic based analogues of electronic devices such as transistors.[3] As organic materials can be tailored at the molecular level they offer potential to create complex devices.

Organic electronics are beginning to be integrated into our everyday lives; the most ubiquitous example being Organic LEDs[4] (OLEDs) which can be found in many devices today. Electroluminescence of organic materials was first reported by Bernanose[5] in 1953, with the first working device being reported in 1987[6] and are now found in many modern electronic devices. This example shows how these materials can revolutionise electronics.

Organic electronic materials are thought to have the potential to be extremely useful in the generation of photovoltaic systems. This typically involves highly absorbing dye molecules acting as light harvesters to generate a charge separated state from which the high energy electron can be used to generate a photocurrent, similar to the photosystems seen in chlorophyll.

### 3.1.2: Electron donor acceptor systems

Chemical systems which are able to form long lived charge separated states are considered highly useful to several applications including the conversion of solar energy into chemical potential, molecular optoelectronics and artificial photosynthetic systems. Electron donor acceptor systems fit this purpose as they are species which are capable of undergoing electron charge transfer, from an electron rich donor species to an electron poor acceptor species.[7-10]

These components can either be separate molecular entities, or can both be included within one molecule. In the case of the latter, species composed of one donor and acceptor are named dyads, while those with three components are considered triads. The first donor acceptor dyad was created in 1973[11] utilising tetrathiafulvalene as a donor and tetracyanoquinodimethane as an acceptor. This example sparked interest in these systems as the donor-acceptor system showed conductivity comparable to that of metals. Since then these systems have found multiple uses in as ambipolar semiconductors for organic field effect transistors[12] and as solar energy harvesters for photovoltaic devices.[4]

The application of donor-acceptor systems within photovoltaic systems is due to their ability to be tuned to undergo photoinduced electron transfer (PET). This phenomenon involves a photon of light being absorbed by the system causing the donor molecule to donate an electron to the acceptor molecule. There are two mechanisms by

which this generally occurs, photoinduced reduction (PIR) and photoinduced oxidation (PIO). Which mechanism is observed depends upon which of the two species, donor or acceptor, is excited by the incoming photon (**Error! Reference source not found.**).

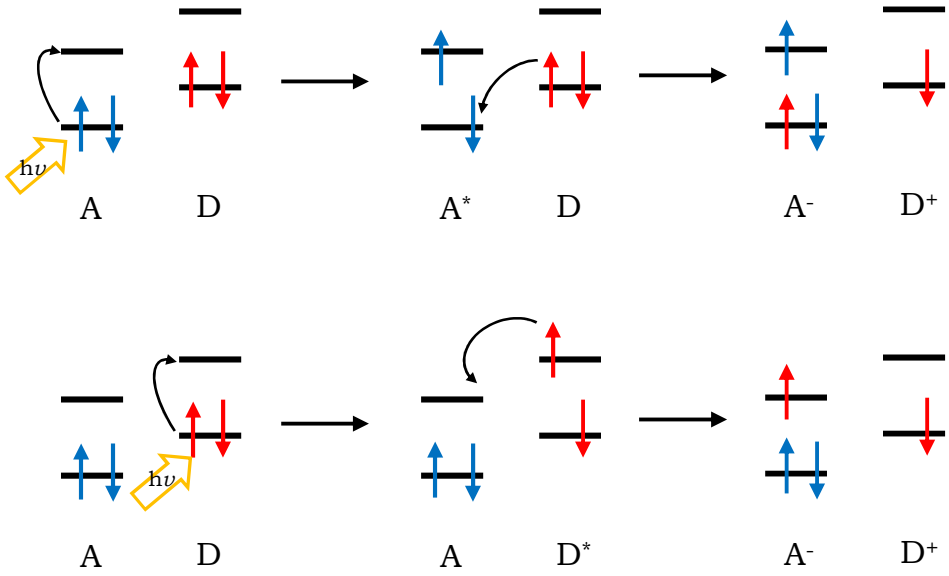


Figure 3-1: Diagram describing the two mechanisms for the generation of charge separated acceptor (A) donor (D) pairs.

In the case of PIR the donor is excited and the high energy electron enters the lower energy LUMO of the acceptor. PIO works in the opposite way; exciting the acceptor to generate an electron hole in the HOMO to which an electron from the donor can occupy. In both instances a charge separated state is generated with a positively charged donor species and a negatively charged acceptor. This charge separated state can then recombine into the original neutral species.

The efficiency of this transfer is dependent on a number of factors, but is mainly down to the energies of the frontier orbitals involved and their energy separation. It is typical within dyads to have the two molecular components chemically linked by a bridge. This bridge acts to physically hold the donor and acceptor together. However it can act as a node within the molecular orbital of the species so that the acceptor and donor orbitals are kept separate and are more capable of generating longer lived charge separated states. Alternatively, these bridges can be designed to act as molecular wires creating a pathway through which the electron can be transferred.[13-15] Bridges can also have an effect on the rate of and nature of the electron transfer, with some species suited to acting as molecular wires to shuttle electrons.

Manipulation of the charge recombination pathway is how such species are utilised to generate photocurrents *via* a form of artificial photosynthesis. Since the recombination is thermodynamically favoured the high energy electron can be utilised to propagate a current within a dye sensitised solar cell.

### 3.1.3: Electron donor acceptor systems incorporating NDIs

There are several properties of NDIs which make them an attractive candidate as the acceptor in a donor acceptor system. This is due to their chemical and physical robustness, with NDIs able to undergo reduction multiple times without chemical degradation owing to the

stability of their anions. On top of this their initial reduction is at quite an achievable potential, due to their electron deficient nature, typically being around -1.1 V (vs. $Fc^{+}/Fc$). There are many examples of different donor-acceptor systems incorporating NDIs as electron acceptors.

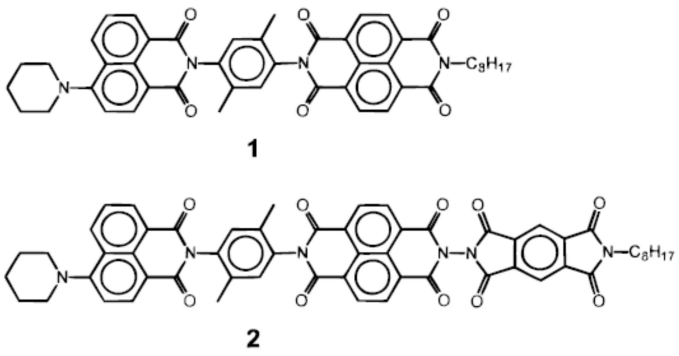


Figure 3-2: Examples of the triads prepared by the Wasielewski group[12]

The Wasielewski group synthesised and investigated a series of triads which were composed of NDI linked to aminonaphthalic subunits (Figure 3-3).[16-18] These species were found to be capable of storing ~2 eV of energy for over 300 ms in non-polar solvents following photoexcitation. The recombination of this state led to a radical pair triple state, seen with EPR spectroscopy. An example of a more complex species is the pentad composed of two NDI-fullerene units linked by a central silicon-phthalocyanine (Figure 3-4), which showed fast charge separation through the singlet excited state of the NDI and then recombination into triplet states of the fullerenes and phthalocyanine.[19]

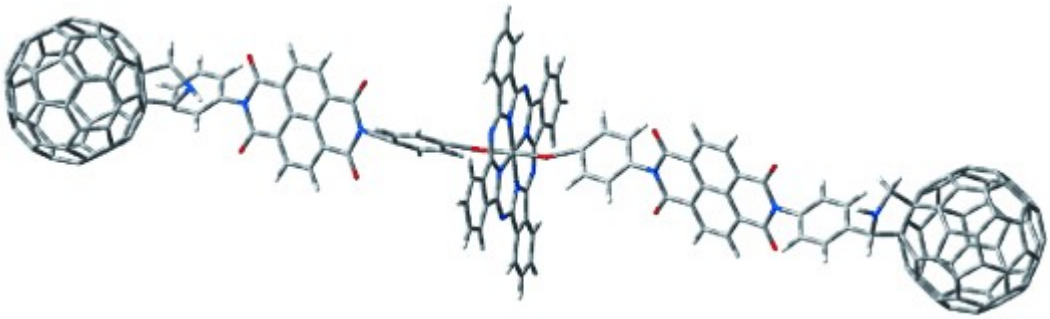

Figure 3-5: Structure of NDI-fullerene-phthalocyanine pentad[18]

Other donor-acceptor species have been made utilising donors linked to the acceptor cNDIs, including several based on porphyrin-cNDI architectures[20,21] and a tetrasubstituted porphyrin-NDI pentad (Figure 3-6).[22] This pentad was shown to absorb across the entire visible range, acting as an antenna, this absorption could then induce the formation of a charge separated state. However due to the size of the molecule this state was particularly short lived, indicating smaller molecules with fewer degrees of freedom would be more successful.

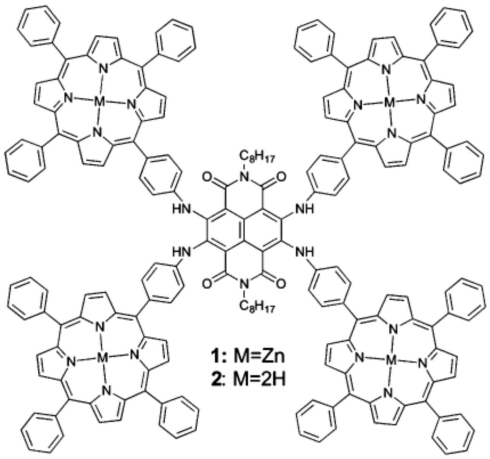


Figure 3-7: Porphyrin-cNDI donor acceptor pentad[22]

### 3.1.4: Aims and Objectives

The aim of this work was to build upon the synthetic work of Chapter 2. This involves synthesising more complex species to substitute onto the NDIs core. This would allow for production of large complex species through relatively simple and reliable substitution chemistry.

As discussed in the introduction to this chapter NDIs are electron accepting species, pairing this with electron rich donor species would create an electron donor-acceptor system. The donor species selected for substitution where the two electron rich species phenothiazine (**3.6**) and phenoxazine (**3.7**). While phenothiazine has been incorporated into these systems prior, little work has been done exploring phenoxazine. This is perhaps owing to the lack of synthetic president for substitution of the amine in phenoxazine. In order to compare and contrast the two donor species a series of target molecules where suggested (Figure 3-8 and Figure 3-9).

By core substituting onto the NDI the light it absorbs will be shifted to lower energy, into the visible range, allowing for the NDI to be excited by visible light. In a donor-acceptor system this excitation has the potential to cause electron transfer creating a charge separated state, this could then be utilised to generate a current creating a photovoltaic device.

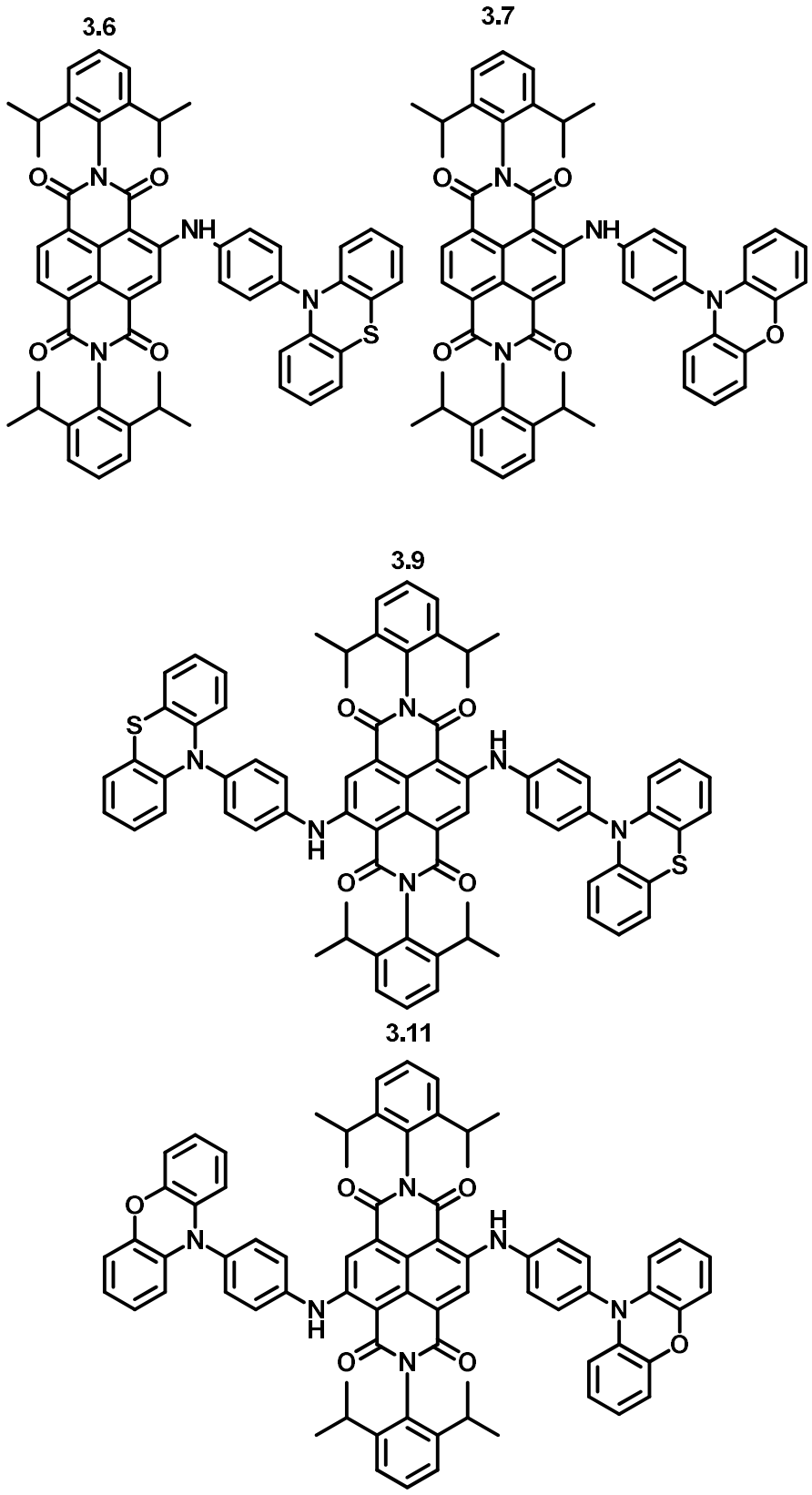


Figure 3-10: Target molecules of Chapter 3

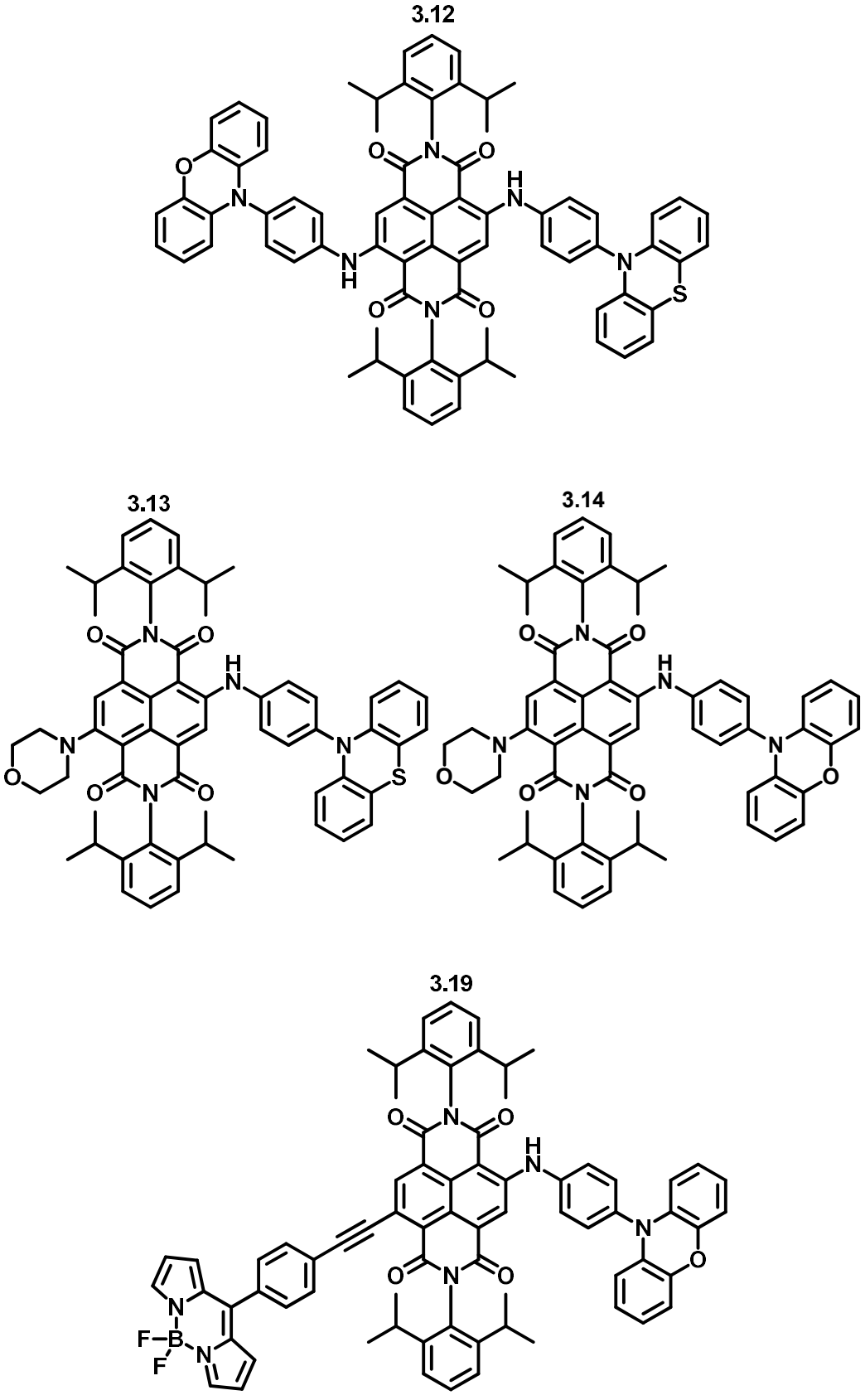


Figure 3-11: Target molecules of Chapter 3

## 3.2: Results and Discussion

Herein is reported the complete synthesis of a series of cNDI based electron donor-acceptor systems. These systems are composed of a cNDI acceptor species furnished with phenothiozine or phenoxazine donor species. The electronic and optical properties of these species were probed using cyclic voltammetry and spectroelectrochemistry.

### 3.2.1: Synthesis

As the NDI is already sufficiently electron deficient to act as an electron acceptor, suitable donor molecules are needed to be selected and created. For this purpose phenothiazine, an electron rich donor species was selected. In order to attach the phenothiazine to the NDI core we decided to furnish this donor species with an amine. This was initially carried out following a literature procedure[13] (Scheme 3-1) generating the nitro species **3.1** *via* a Buchwald-Hartwig coupling at 90 °C.

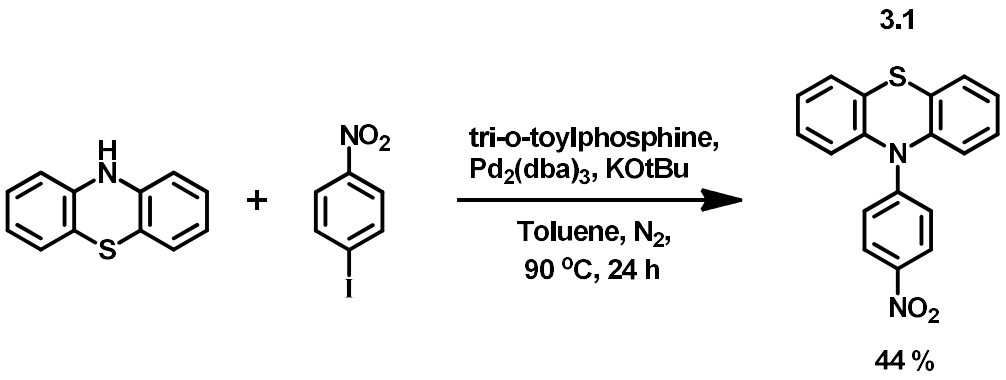


Scheme 3-2: Synthesis of **3.1**

The nitro group was then reduced by heating in acidic conditions with a tin chloride catalyst. However the elevated temperature was found to cause some decomposition of the desired product **3.2**. Alternative conditions using Pd/C under an atmosphere of $H_2$ at RT (Scheme 3-3), was found to give a higher yield and provided a simpler, faster work up. **3.2** slowly decomposed in light at room temperature and so was stored in the dark below -4 $^oC$.

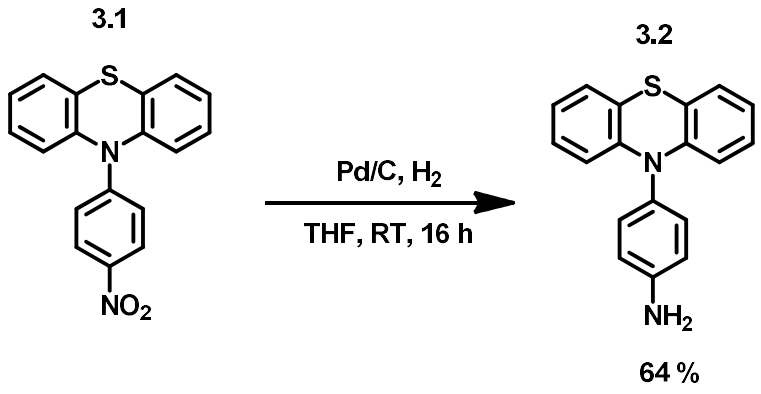


Scheme 3-4: Synthesis of **3.2**

It was noticed that despite their similarities there was very little literature precedent referring to the sister molecule to phenothiazine, phenoxazine. The two species share similar electron donor properties so a phenoxazine analogue of **3.2** was proposed, **3.5**. The same Buchwald-Hartwig coupling conditions, using phenoxazine in place of phenothiazine, were attempted (Scheme 3-5). Unfortunately this did not lead to the generation of **3.3** and instead led to the decomposition of the phenoxazine, due to the elevated temperature and the less stable nature of phenoxazine. The lack of reaction is

also not unexpected; the secondary amine in phenoxazine is a poor nucleophile as its lone pair of electrons are incorporated into the aromatic system and so are not as available for reactions.

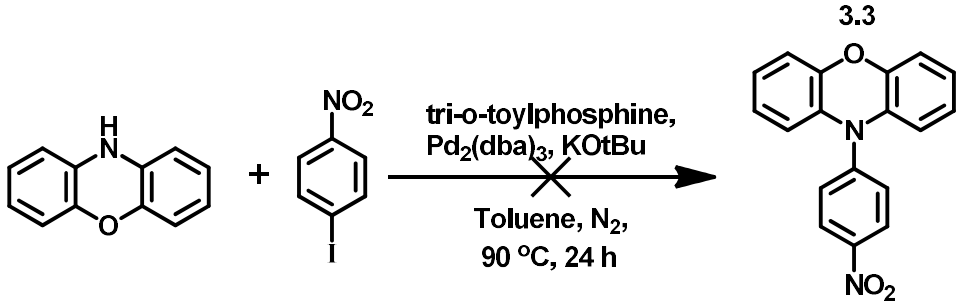


Scheme 3-6: Attempted Synthesis of **3.3**

Another synthetic route was required to create **3.3** that would overcome the lower reactivity of the phenoxazine amine. To this end the copper catalysed Chan-Lam coupling was proposed, which typically progresses well with secondary amines at RT. These coupling conditions require first the copper precatalyst to be generated under dry anaerobic conditions. After this the mixture is exposed to the atmosphere to allow oxygen into the system to complete the catalytic cycle. As the copper catalyst is cheap a high catalytic loading can be used.

The Chan-Lam coupling occurs between a secondary amine and a boronic acid (**3.4**). **3.4** was generated from 1-iodo-4-nitrobenzene using a standard literature preparation[23] (Scheme 3-7) involving a Suzuki coupling with bis(pinacolato)diboron to generate the boronic

ester, followed by hydrolysis using sodium periodate followed by hydrochloric acid to generate **3.4**.

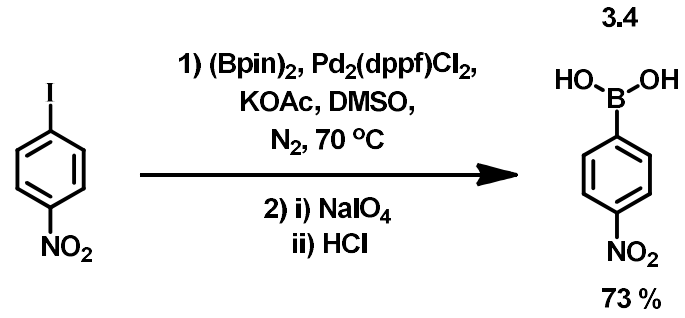


Scheme 3-8: Synthesis of **3.4**

The Chan-Lam Coupling conditions were tested using phenothiazine due to its ready availability (Scheme 3-9). These conditions were found to work resulting in a higher yield of **3.1**, at 83%, representing a 39 % increase compared to the previous preparation, described above, and giving higher yield than reported in the literature.[24]

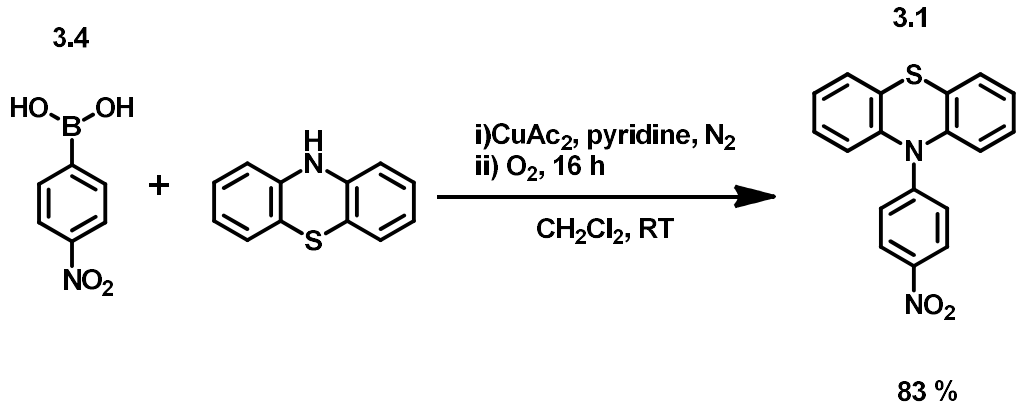


Scheme 3-10: Alternate Synthesis of **3.1**

Once these conditions had been proved to work well with phenothiazine they were applied to phenoxazine (Scheme 3-11), and these conditions successfully generated **3.3**, though in a noticeably

lower yield than **3.1**. As there was no phenoxazine remaining the lower yield was attributed to the less stable nature of phenoxazine, which decomposed even under these comparatively mild conditions.

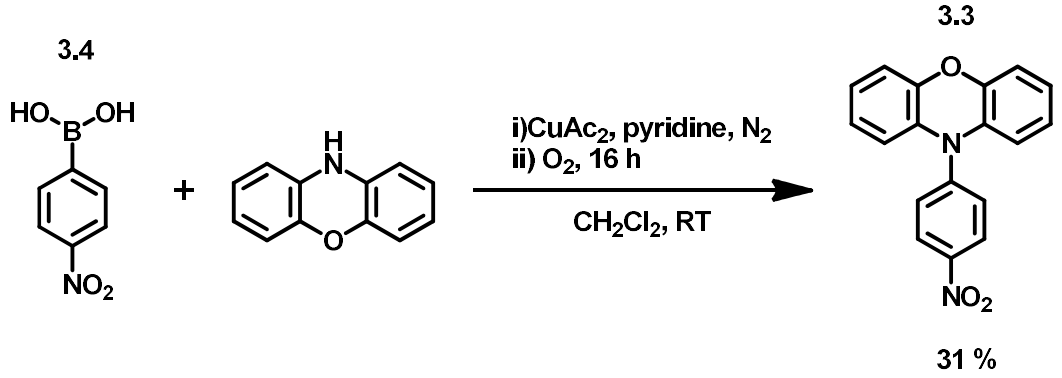


Scheme 3-12: Synthesis of **3.3**

**3.3** was then reduced, once again using Pd/C and a $H_2$ atmosphere (Scheme 3-13) to generate **3.5**. This reaction progressed as expected however, much like **3.2**, **3.5** was found to slowly decompose at RT in light and so was stored in the dark at -14 °C.

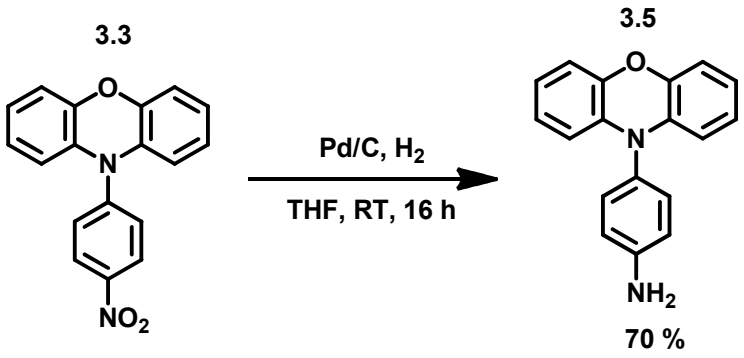


Scheme 3-14: Synthesis of **3.5**

Now that suitable donor species had been synthesised a suitable NDI acceptor molecule needed to be selected. For this purpose **2.5** and **2.6** were selected due to their stability and their reliable reactivity. **2.5** or **2.6** were reacted with **3.2** or **3.5** using simple SNAR chemistry

similar to the morpholine substitution in Chapter 2. This involved heating the reaction mixture of **2.5** or **2.6** with **3.2** or **3.5** to 135 $^{o}$C in DMF in the presence of the desired amine (Scheme 3-15).This was initially preformed using **2.5** and the donor acceptor dyads **3.6** and **3.7** were produced. A slight excess of the amines **3.2** and **3.5** were used in order to mitigate their decomposition. As in Chapter 2 this caused a very noticeable change in the physical appearance of the compounds from beige to pink.

In an attempt to generate the triad **3.9**, **2.6** was reacted with **3.2** (Scheme 3-16), this interestingly led to a mixture of two products **3.8** and **3.9.** This type of reactivity was to be expected as in Chapter 2 the addition of amines lowers the reactivity of the remaining bromo-substituents allowing for partially substituted species to be isolated. **3.8** was further selected as the major product as the amine **3.2** decomposes under these harsh conditions. After substitution the products were far more stable than **3.2**, perhaps indicating that decomposition route involves nucleophilic attack of the amino nitrogen upon another molecule of **3.2.** The partial substitution of **3.8** can be exploited further to generate asymmetric cNDIs.

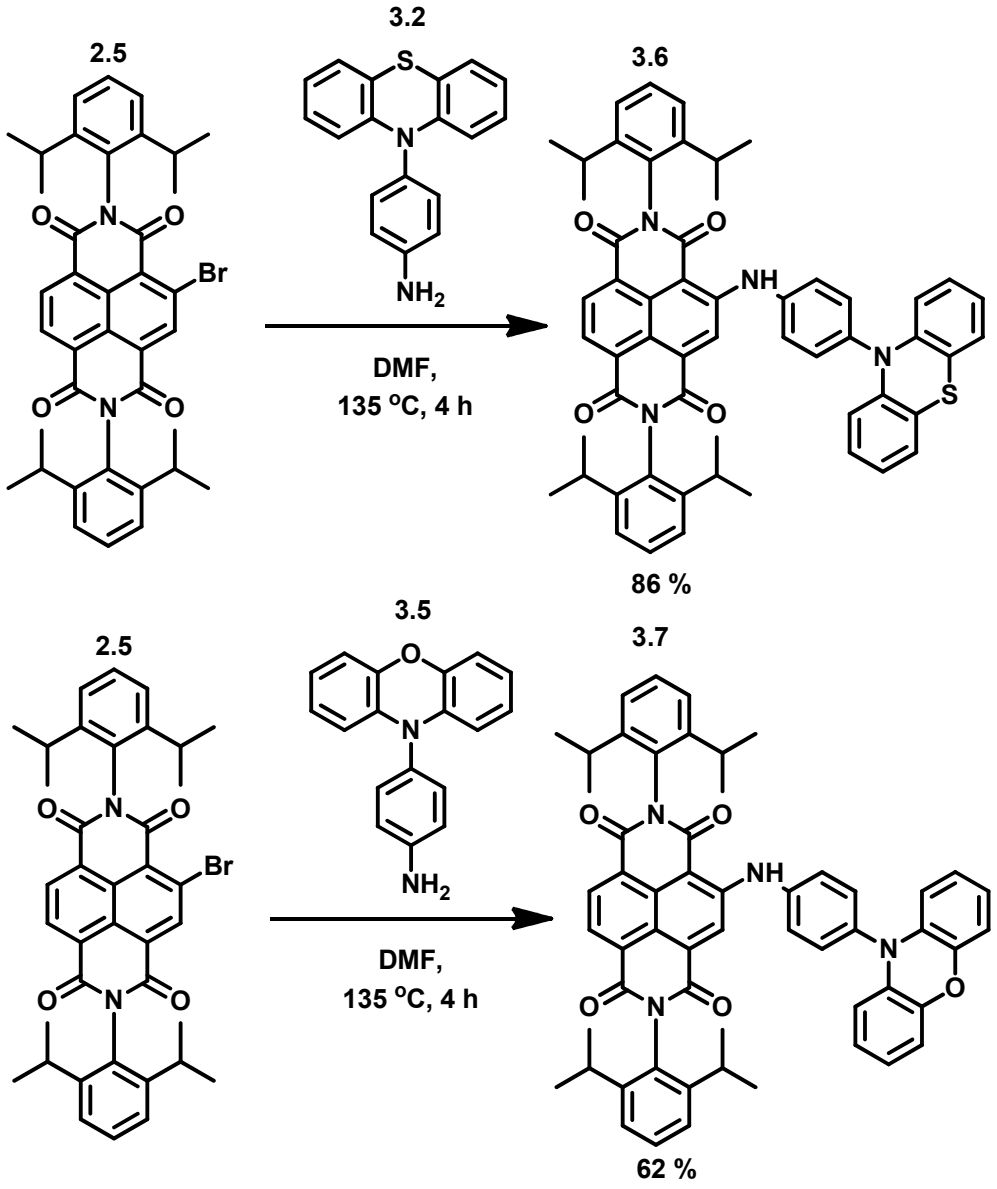


Scheme 3-17: Synthesis of **3.6** and **3.7**

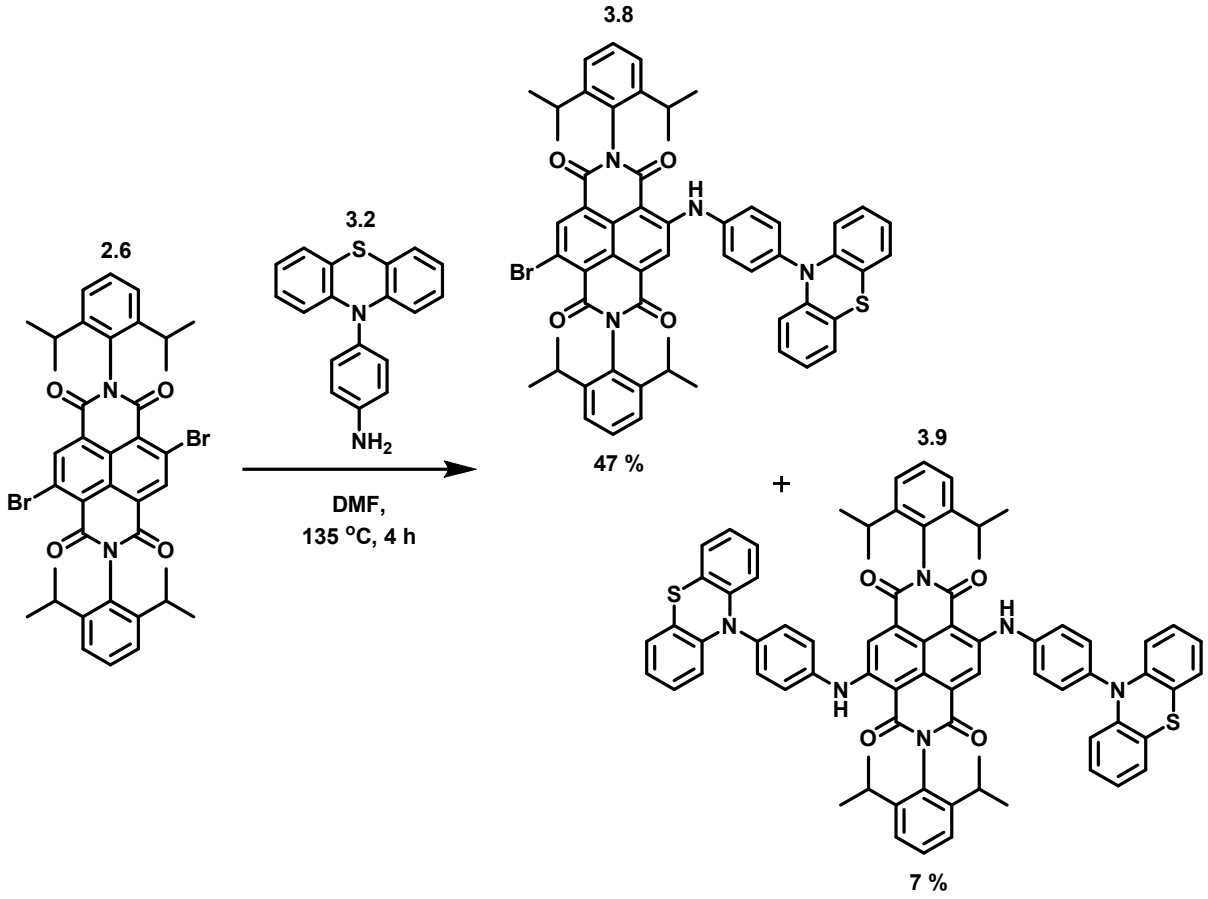


Scheme 3-18: Synthesis of **3.8** and **3.9**

An analogous reaction was attempted with phenoxazine species **3.5** (Scheme 3-19) and it was found that under the same conditions mono-substituted **3.10** was selectively generated without any evidence for the formation of di-substituted **3.11.** This selectivity is most likely due to the decreased stability of **3.5** effectively lowering the proportion of **3.5** within the reaction.

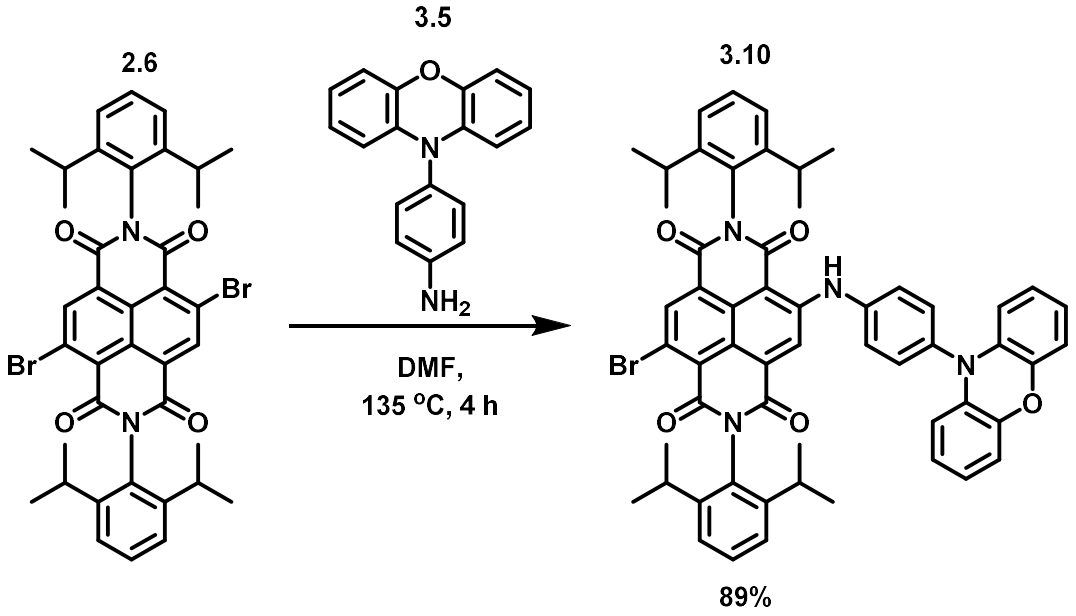


Scheme 3-20: Synthesis of **3.10**

In order to generate the di-substituted species in appreciable yield **3.10** was reacted again with a large excess of **3.5** to generate **3.11** (Scheme 3-21). Even with several equivalents of **3.5**, the yield of **3.11** was still low due to **3.5** preferentially undergoing intermolecular reactions with itself.

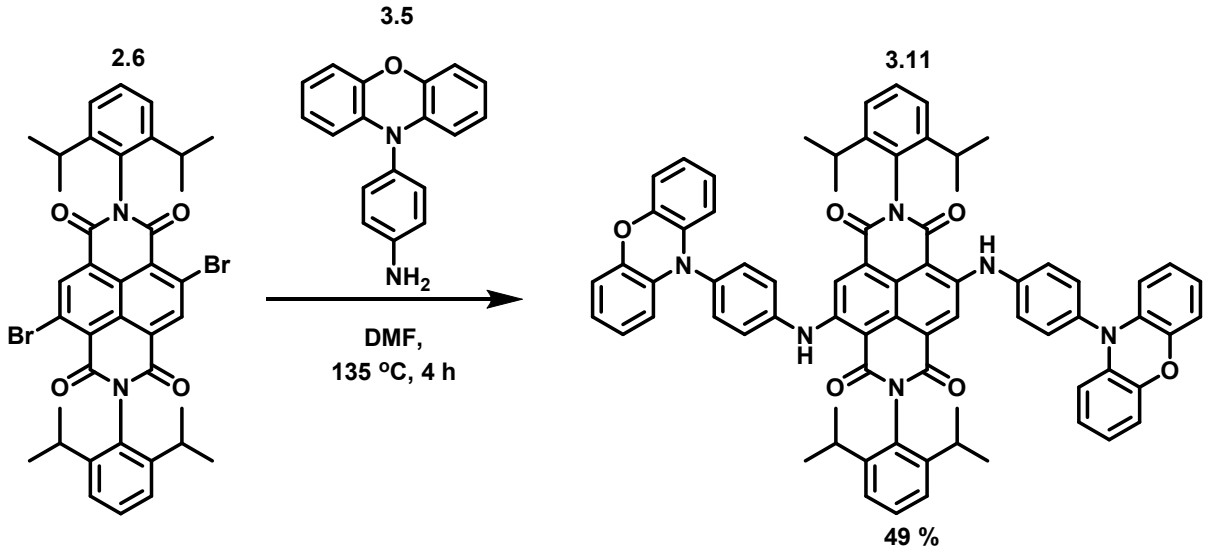


Scheme 3-22: Synthesis of **3.11**

A triad with mixed donor molecules was generated by reacting **3.8** with **3.5** (Scheme 3-23) to generate **3.12.** Characterisation of **3.9**, **3.11** and **3.12** by NMR proved to be something of a challenge owing to the poor solubility of these species, a suitably concentrated sample could only be achieved using toluene as solvent. This unfortunately led to a large overlap between the aromatic environments of the sample and the solvent. This is also troublesome due to the broad multiplets generated by **3.2** and **3.5** in the aromatic region.

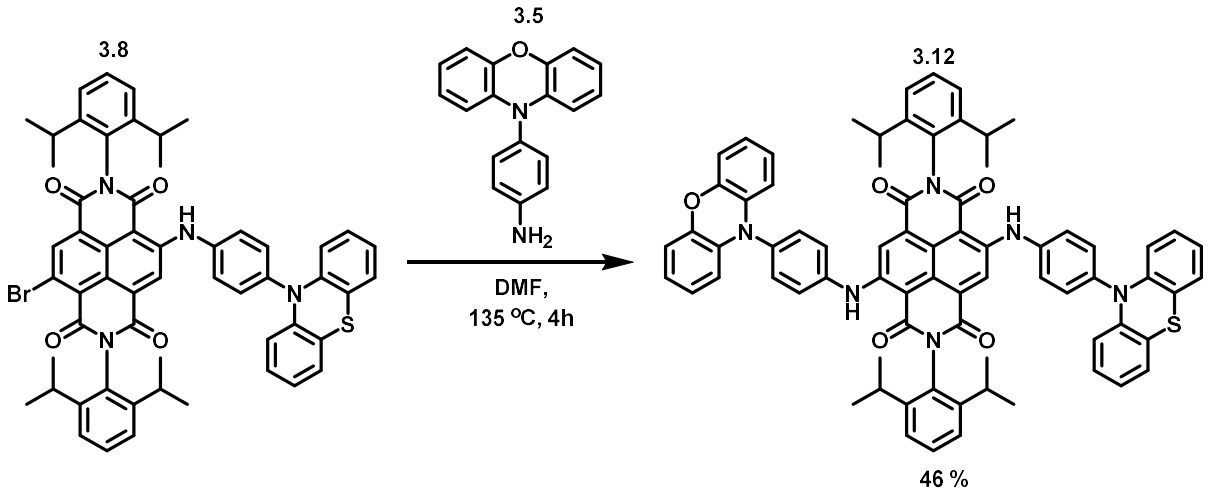


Scheme 3-24: Synthesis of **3.12**

In order to investigate how modulation of the electronic properties of the chromophore affected the properties of both **3.8** and **3.10** were reacted with morpholine (Scheme 3-25). The reaction with morpholine progressed as expected giving excellent yields of **3.13** and **3.14**, using only a slight excess of morpholine. The decreased reaction time is indicative of the higher reactivity of morpholine when compared to the aromatic species **3.2** and **3.5**.

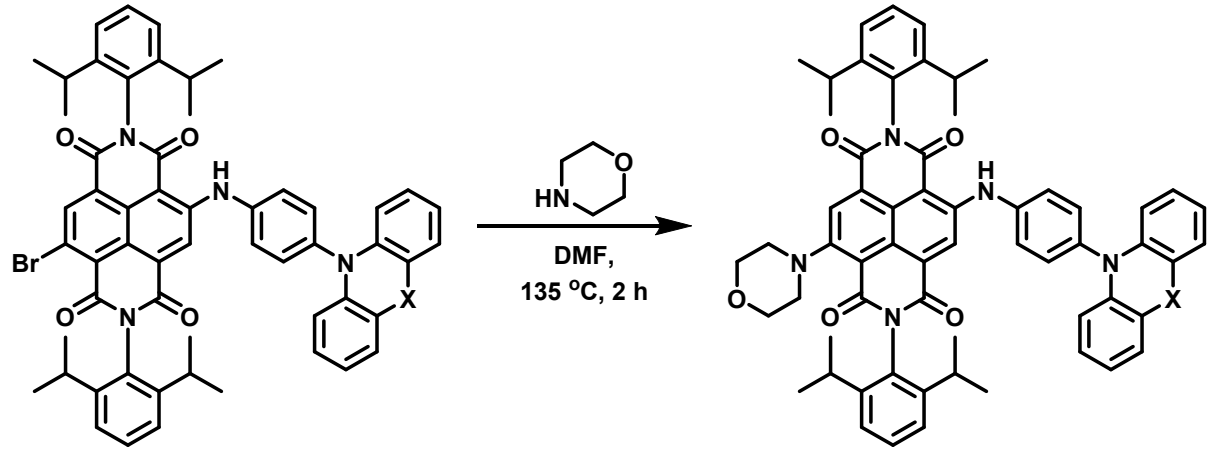


Scheme 3-26: Synthesis of **3.13** and **3.14**

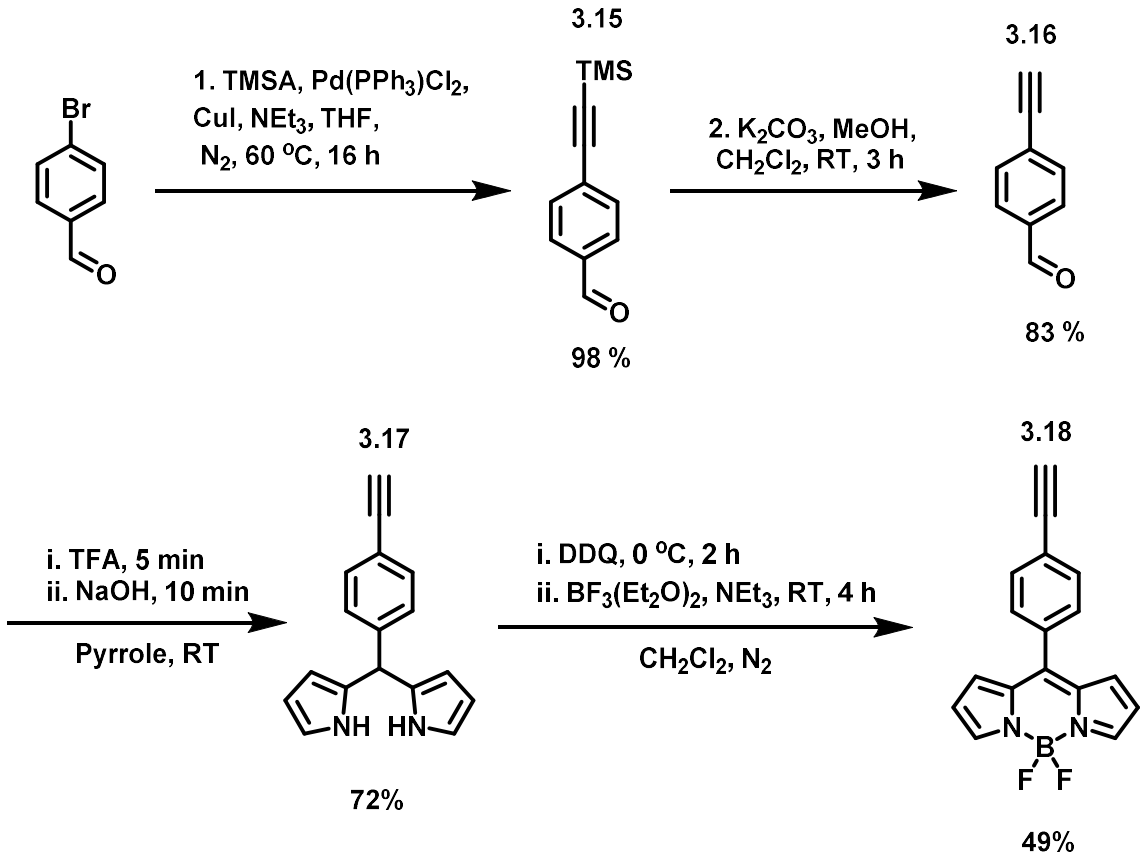


Scheme 3-27: Synthesis of **3.15**, **3.16**, **3.17** and **3.18**

In order to further extend the potential properties of these molecules it was thought that their visible light harvesting efficiency could be further increased by addition of an additional chromophore. For this

purpose a BODIPY chromophore was selected (**3.18**). Synthesis of **3.18** (Scheme 3-28) involved first the generation of a suitable aldehyde **3.16**. This was achieved by preforming a Sonogashira coupling on bromobenzaldehyde with trimethylsilylacetylene to generate **3.15**. This was followed by deprotection, removing the TMS group, using $K_2CO_3$ and MeOH to generate **3.16**. The aldehyde was employed in an acid catalysed condensation with pyrrole to generate the corresponding dipyrromethane **3.17**. This was oxidised using DDQ, generating a dipyrromethene and finally reacted with $BF_3.OEt_2$ under basic conditions, to generate the **3.18** as a red fluorescent solid.

In order to link **3.18** to **3.8** Sonogashira coupling conditions were utilised (Scheme 3-29). These reactions gave poor yields perhaps due to unwanted side reactions with the large molecular system. **3.19** was successfully isolated as a red solid which didn't show any visible signs of fluorescence. Synthesis of the phenoxazine analogue of **3.19** was not attempted due to the low overall yields of the various steps of the synthetic pathway and the anticipated lower stability of the phenoxazine moiety.

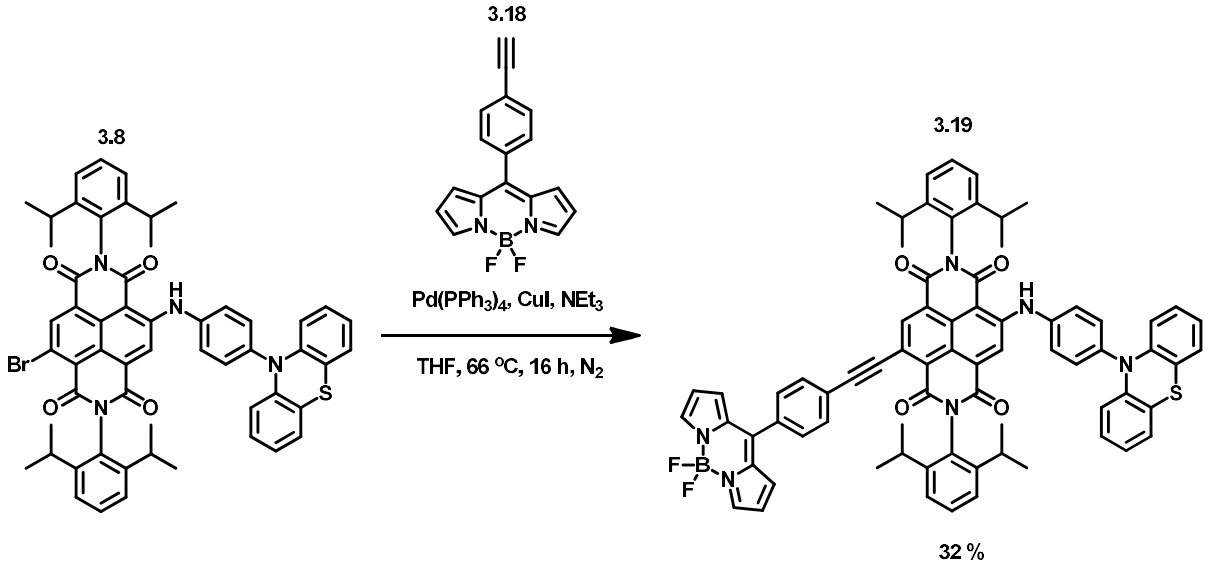


Scheme 3-30: Synthesis of **3.19**

## 3.2.2: Investigation of Optical and Electrochemical Properties

In order to investigate the optical and electronic properties of dyads and triads CV, bulk electrolysis and spectroelectrochemical experiments were undertaken. These measurements allow for closer inspection of the energies of the frontier orbitals and reveal the spectroscopic features of the neutral and ionized species.

### *3.2.2.1: Cyclic voltammetry*

Initially the redox properties of the new donor species **3.5** were investigated (Figure 3-12). It was found to reversibly undergo a single electron oxidation 0.25 V (vs $Fc^+/Fc$), which was not a large perturbation from **3.2** at 0.21 V (vs $Fc^+/Fc$). As oxygen is more electronegative than sulphur the oxidation of **3.5** occurring at a higher potential is not unexpected.

While these perturbations may not be large it does allow for fine tuning of electron donor acceptor systems. By precisely selecting the donor and acceptor species with complimentary frontier orbital energies it should be possible to create species which more readily enter a charge separated state upon photoexcitation.

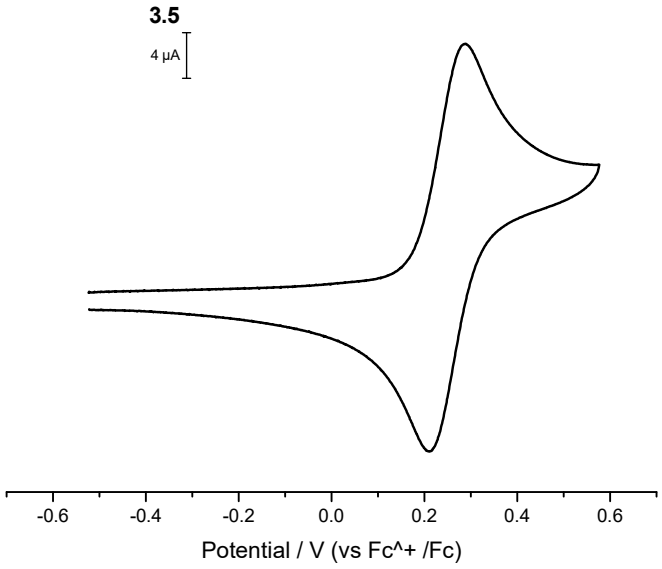


Figure 3-13: Cyclic voltammogram of **3.5** in DCM with 0.4 M $[Bu_4N][BF_4]$ supporting electrolyte, at a scan rate of 100 $mVs^{-1}$

The redox properties of the first donor acceptor dyads, **3.6** and **3.7**, were then probed (Figure 3-14). Two reversible one electron reductions, associated with the NDI, and a reversible one electron oxidation, associated with the phenothiazine and phenoxazine respectively, were observed.

In both cases the reductions occurred at –1.06 V vs $Fc^+/Fc$ and –1.48 V vs $Fc^+/Fc$. The fact that the reduction potentials are identical for each species shows that the NDIs orbitals are only being affected by the contribution from the aniline amine. This is lack of communication through the amine could allow for a wider range of species to be added to NDI in a similar manner and the LUMO of the NDI be predicted relatively securely.

The oxidation related to the **3.6** occurred at 0.33 V vs $Fc^+/Fc$ and the oxidation of **3.7** occurred at 0.35 V vs $Fc^+/Fc$. The two donor species still have a small difference between them, with a shift of 20 mV between the two oxidations. In addition these higher potential oxidations indicate that the energy of the HOMO of the donor species has been decreased. This decrease is most likely caused by some of the amines electron density being donated to the NDI rather than the donor.

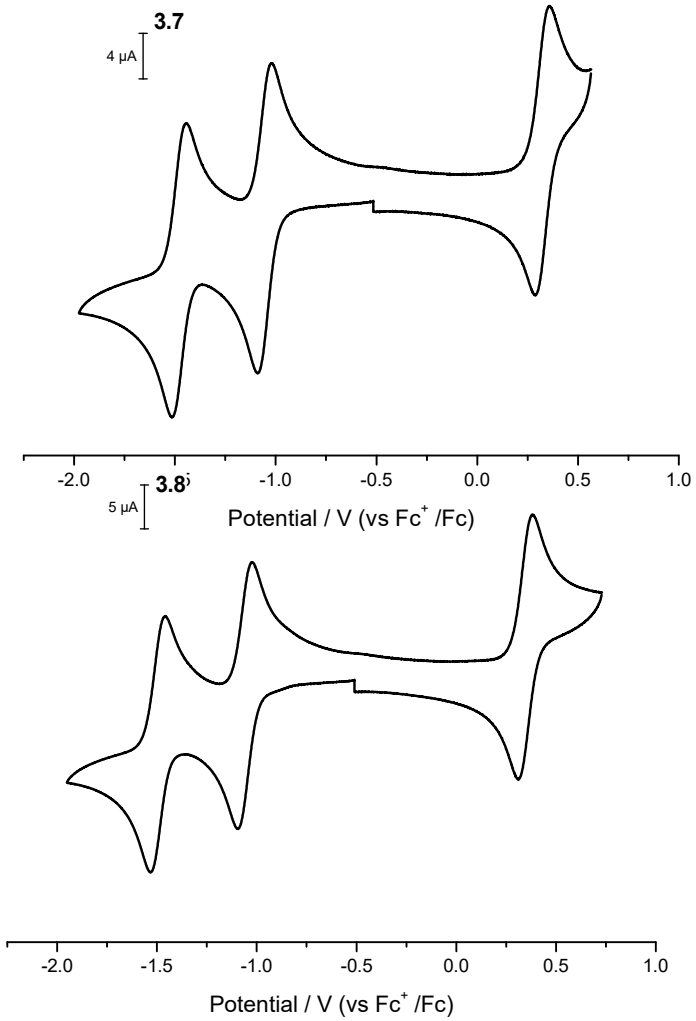


Figure 3-14: Cyclic voltammograms of **3.6** (top) and **3.7** (bottom) in DCM with 0.4 M $[Bu_4N][BF_4]$ supporting electrolyte, at a scan rate of 100 $mVs^{-1}$

From here the three triad species, **3.9**, **3.11** and **3.12** were investigated (Figure 3-15). Each once again retains the typical two, reversible, one electron reductions associated with the NDI and a single reversible two electron oxidation of the donor species.

The reductions are once again observed at the same potentials the first at -1.13 V vs $Fc^+/Fc$ and the second at -1.50 V vs $Fc^+/Fc$. This reinforces the idea that the residues attached to the aniline has little affect upon the reduction potentials of the NDI.

The two electron oxidations of **3.9** and **3.11**, which occur at 0.35 V vs $Fc^+/Fc$ and 0.30 V vs $Fc^+/Fc$, can be easily explained as both identical donor species oxidising at the same potential. Once again a small difference of 30 mV can be seen between the oxidation potentials of the two species. Both oxidations occur at lower potentials than those observed in **3.7** and **3.8** as each amine has more electron density to donate to the donor, increasing the energy of their HOMOs and making the electron more available for ionisation.

The oxidation of the mixed donor system **3.12** occurs at 0.33 V vs $Fc^+/Fc$. This potential sits in between the oxidations of **3.9** and **3.11**. As the two donor species oxidise at such similar potentials it was not possible to identify the oxidations separately and instead one two electron oxidation was detected with a potential resulting from this shared oxidation.

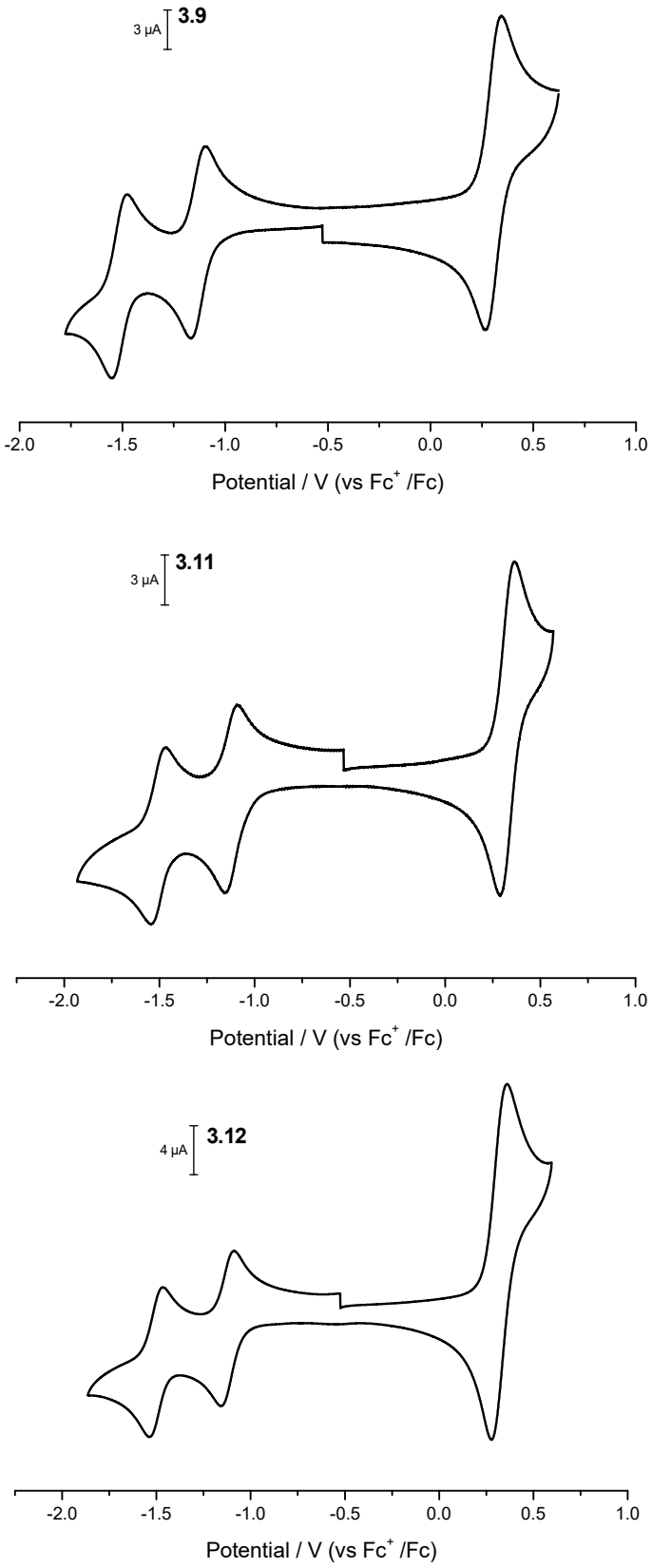


Figure 3-15: Cyclic voltammograms of **3.9** (top), **3.11** (middle) and **3.12** (bottom) in DCM with 0.4 M $[Bu_4N][BF_4]$supporting electrolyte, at a scan rate of 100 $mVs^{-1}$

While the oxidations of the different donors of **3.12** cannot viewed separately using this method it would be expected that the phenothiazine species would be more readily oxidised. If these species could be photo induced to enter a charge separated state the lifetimes and identities of these estates could be identified via time resolved spectroscopy experiments and more the suitable donor species could be determined.

The analogous morpholine substituted species were redox properties were also investigated. The intention of these species was to prove that the NDIs redox properties could still be perturbed and tuned to gain control over the LUMO of the acceptor molecule. This control allows for a greater ability to pair the energy of the LUMO of the acceptor with that of the HOMO of the donor. Morpholine was selected as a commercially available, electron donating amine that fit well into the confines of this thesis.

The redox chemistry of **3.13** and **3.14** (Figure 3-16) can be seen to be very similar to that of **3.7** and **3.8** (Figure 3-14). That is two reversible one electron reductions on the NDI and a reversible one electron oxidation of the donor species.

The reduction potentials of **3.13** and **3.14** are shared again, the first reduction occurring -1.15 V vs $Fc^{+}/Fc$ and the second at -1.56 V vs $Fc^{+}/Fc$. Both of the reduction potentials of these species are more negative than those of any of the other species in this chapter. This

shows clearly that by having a second site that can be independently substituted on the NDI allows for tuning of the LUMO of the NDI.

Interestingly however the oxidation potentials of **3.13** and **3.14** are also seen to shift to lower potentials when compared to the other dyad species, a shift of 10 mV comparing **3.7** and **3.13** and a shift of 15 mV comparing **3.8** and **3.14**.

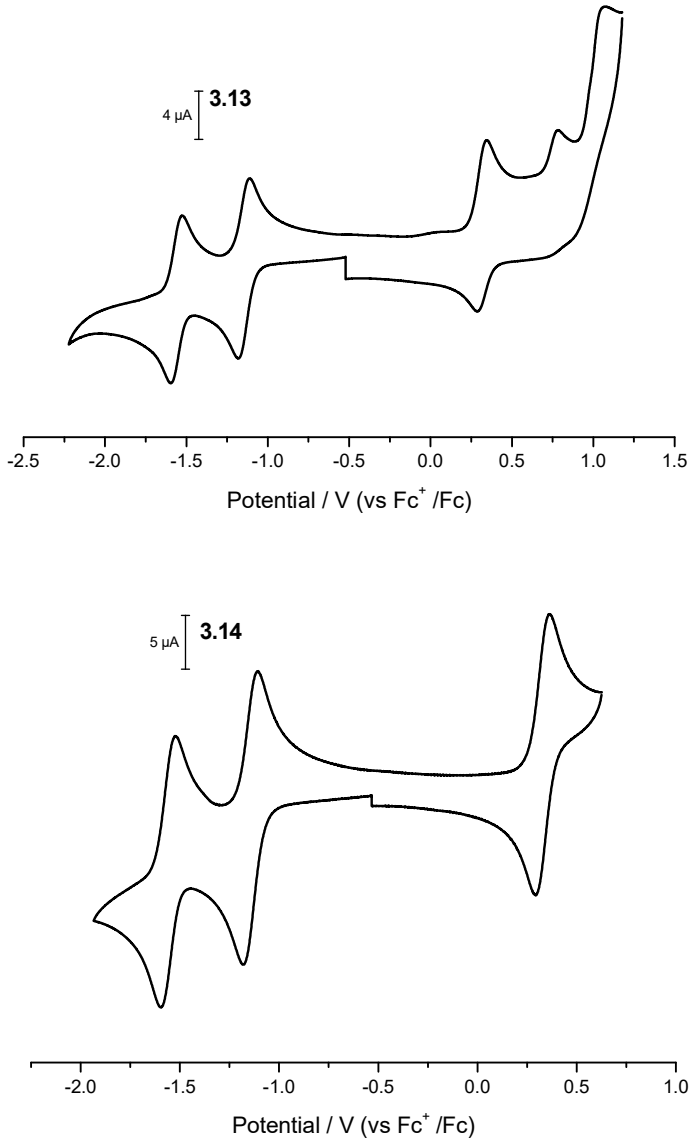


Figure 3-16: Cyclic voltammograms of **3.13** (top) and **3.14** (bottom) in DCM with 0.4 M $[Bu_4N][BF_4]$ supporting electrolyte, at a scan rate of 100 $mVs^{-1}$

Finally inspecting **3.19** (Figure 3-17) reveals a more complex series 3 one electron reversible reductions, the first and third being associated with the NDI and the second one being associated with the BODIPY species, there is also a one electron reversible oxidation relating to phenothiazine (Figure 3-12). It can clearly be seen that there is some small overlap between the first and second reduction though the two can easily be resolved.

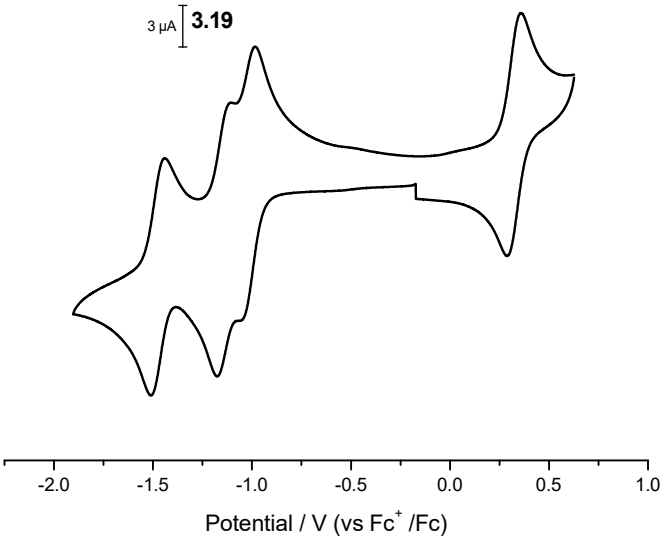


Figure 3-17: Cyclic voltammogram of **3.19** in DCM with 0.4 M [$Bu_4N$][$BF_4$] supporting electrolyte, at a scan rate of 100 $mVs^{-1}$

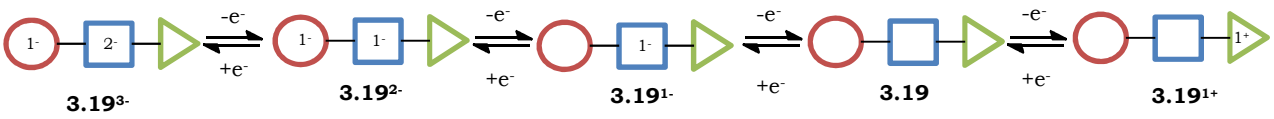


Figure 3-18: A schematic depicting the oxidation and reduction pathway of **3.19**. The BODIPY component depicted as a red circle, the NDI component as a blue square and the phenothiazine a green triangle.

When comparing the reduction potentials of **3.19** to other species it is found that they are most similar to the singly substituted species **3.6** and **3.7**, they are however seen to come at an even higher potential (Table 3-1). The initial reduction of the NDI occurs at -1.02 V vs $Fc^+/Fc$, this is 40 mV higher than that of the mono substituted species. This with the example of **3.13** and **3.14** form an example of how the LUMO energy of the NDI can be pushed and pulled to higher and lower energies via core substitution. This in turn gives the ability to tune the orbitals to be complementary to those of the donor species.

More pronounced, however, is the effect upon the oxidation potential. Here an increase of 70 mV when compared to **3.6** is observed, which shows the extent to which the nature of the NDI substituents can affect the potential of the donor species. This shift is assumed to be due to the alkyne being a poor electron donor, increasing electron density donation to the NDI core. In addition this result demonstrates that the potential of the donor can be shifted to higher potentials by utilising substituents.

| Molecule | 1st Oxidation $E_{1/2}$ / V | 1st Reduction $E_{1/2}$ / V | 2nd Reduction $E_{1/2}$ / V | 3rd Reduction $E_{1/2}$ / V |
|---|---|---|---|---|
| **3.6** | 0.33 | -1.06 | -1.48 | - |
| **3.7** | 0.35 | -1.06 | -1.48 | - |
| **3.9** | 0.30 | -1.13 | -1.50 | - |
| **3.11** | 0.33 | -1.13 | -1.50 | - |
| **3.12** | 0.32 | -1.13 | -1.50 | - |
| **3.13** | 0.32 | -1.15 | -1.56 | - |
| **3.14** | 0.33 | -1.15 | -1.56 | - |
| **3.19** | 0.40 | -1.02 | -1.14 | -1.48 |

Table 3-1: Reduction and oxidation potentials of **3.6, 3.7, 3.11, 3.12, 3.13, 3.14** and **3.19**. Potentials recorded relative to the internal standard $E_{1/2}$ $Fc^{+}/Fc$ at a scan rate of 100 $mVs^{-1}$ at room temperature

### *3.2.2.2: Spectroelectrochemistry*

The optical behavior of dyads and triads prepared upon oxidation and reduction was examined *via* spectroelectrochemical methods. In each case the progress of the oxidations and reductions of the molecules were followed utilizing UV/vis spectroscopy. This data confirms which components of the molecules are undergoing oxidation and reduction. In addition this measurements show what the spectra of the oxidized and reduced species look like and so could be used to inform time resolved spectroscopy experiments looking to identify photo induced charge transfer.

First the novel phenoxazine species **3.5** was examined (Figure 3-19), as the oxidation progresses, the high energy band at 242 nm is seen to deplete and new lower energy bands form, with two bands within the visible range at 412 nm and 532 nm and a broad poorly absorbing band above 700 nm and into the near IR. These bands can be used to identify the production of the oxidised phenoxazine species.

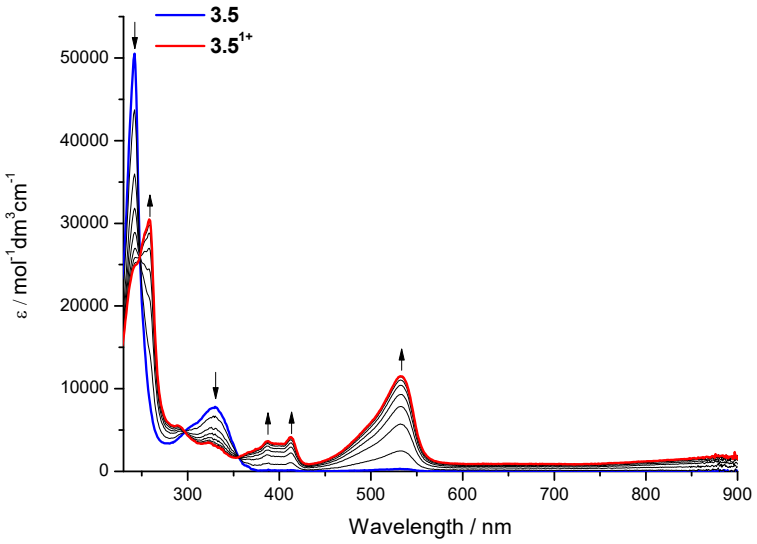


Figure 3-19: UV/vis absorption spectra recorded in DCM containing $[Bu_4N][BF_4]$ (0.4 M) using spectroelectrochemical methods for **3.5** at 243 K showing the inter-conversion of **3.5** (blue) to **3.5**$^{1+}$ (red). Arrows show the progress of the oxidation.

With the knowledge of the oxidized donor's absorption profile, the oxidations of the dyads **3.6** (Figure 3-20) and **3.7** (Figure 3-21) were investigated. The oxidation of these species yielded similar spectra, with a band at high energy depleting and new bands at lower energy being generated. The band within the visible region can be seen to gain intensity as well as a very broad absorption of both oxidized molecules above 700 nm, these changes are consistent with the oxidation of the donor species. This confirms that the oxidation is occurring upon the phenothiazine and phenoxazine species.

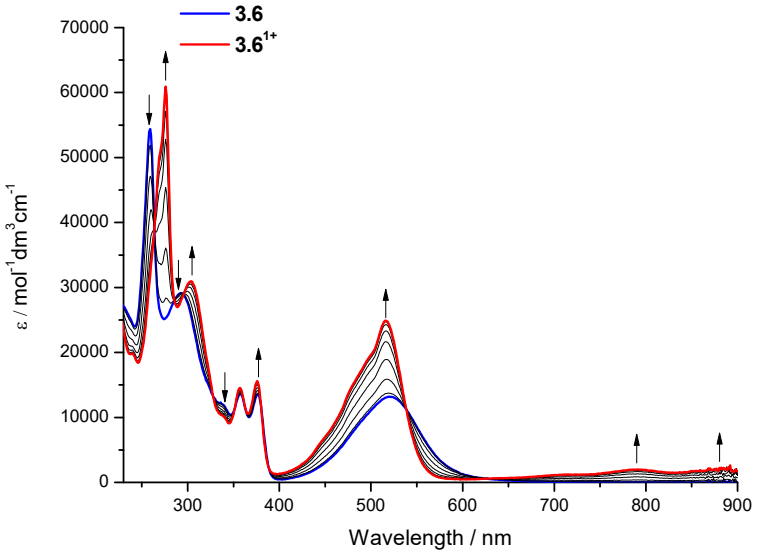


Figure 3-20: UV/vis absorption spectra recorded in DCM containing $[Bu_4N][BF_4]$ (0.4 M) using spectroelectrochemical methods for **3.6** at 243 K showing the inter-conversion of **3.6** (blue) to **3.6**$^{1+}$ (red). Arrows show the progress of the oxidation.

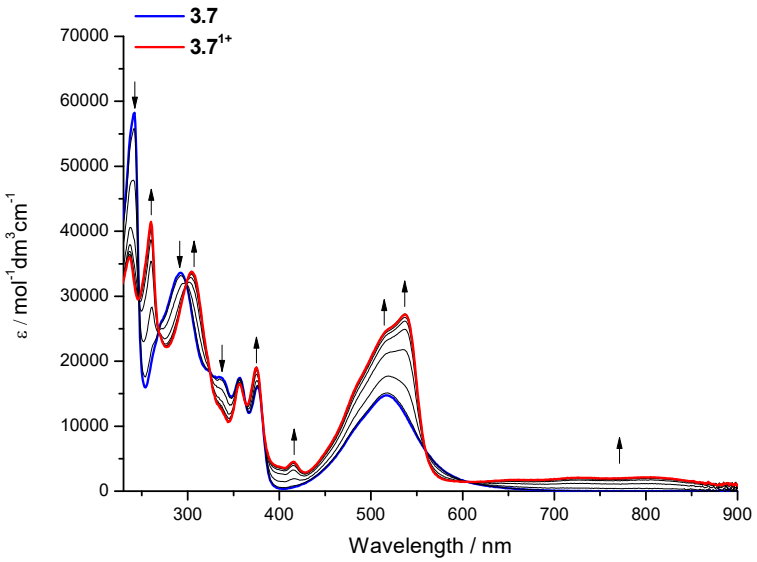


Figure 3-21: UV/vis absorption spectra recorded in DCM containing $[Bu_4N][BF_4]$ (0.4 M) using spectroelectrochemical methods for **3.7** at 243 K showing the inter-conversion of **3.7** (blue) to **3.7**$^{1+}$ (red). Arrows show the progress of the oxidation.

When viewing the initial reduction of **3.6** (Figure 3-22) and **3.7** (Figure 3-23) they can be seen to mirror each other. In the case of each compound, the two bands at around 350 nm associated with the NDI are seen to deplete and new bands are produced throughout the visible range, associated with the monoanionic NDI.

Both spectra of the monoanionic species share a similar landscape. The band observed at around 500 nm is seen to increase in intensity and develop an additional shoulder. In addition three bands at around 635 nm, 740 nm and 830 nm (Table 3-2) are seen to be produced. The similarity between these spectra shows that the reduction of these species is confined to the NDI and that the change in donor species has little effect upon its frontier orbitals.

Upon regeneration of the neutral species the bands associated with **3.7** can be seen to be less intense. It is proposed that under these conditions a portion of these species had chemically decomposed, once again highlighting the instability of phenoxazine when compared to phenothiazine. This however is only indicative of how the species acts under bulk reduction on these time scales, on shorter time scales it maybe more stable and so is still a candidate for photovoltaic devices. This instability however made it impractical to view spectra of dianionic **3.7**

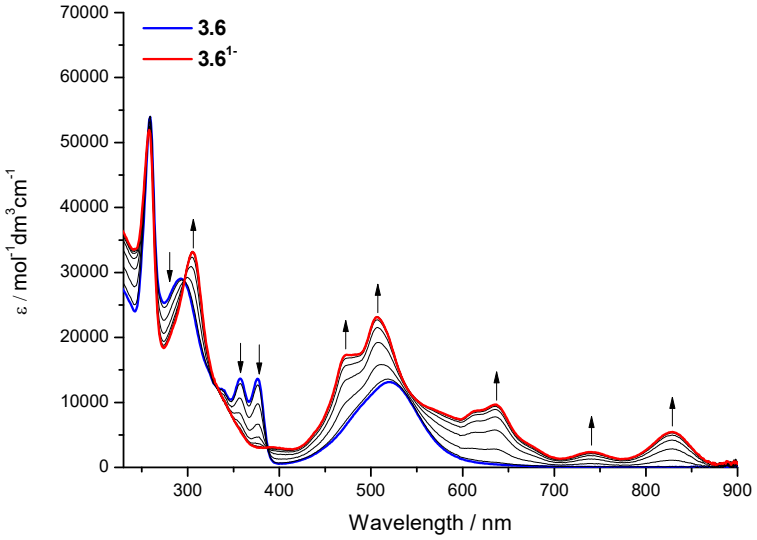


Figure 3-22: UV/vis absorption spectra recorded in DCM containing $[Bu_4N][BF_4]$ (0.4 M) using spectroelectrochemical methods for **3.6** at 243 K showing the inter-conversion of **3.6** (blue) to **3.6$^{1-}$** (red). Arrows show the progress of the reduction.

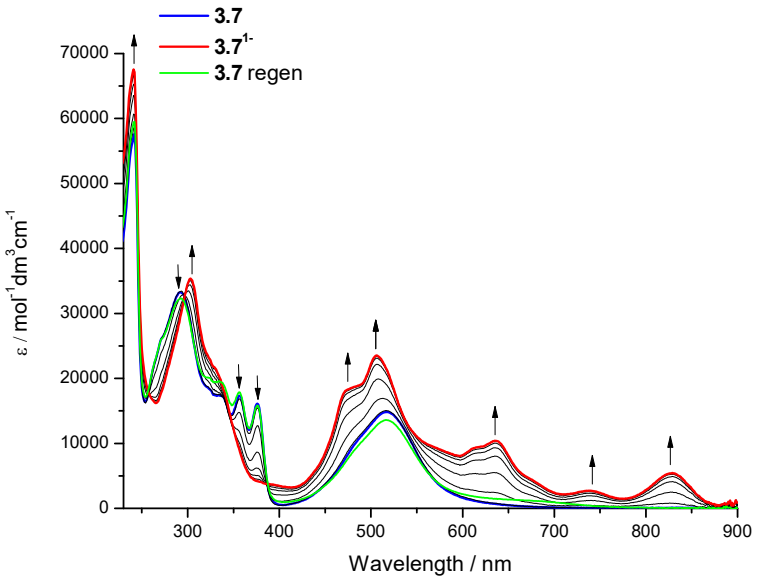


Figure 3-23: UV/vis absorption spectra recorded in DCM containing $[Bu_4N][BF_4]$ (0.4 M) using spectroelectrochemical methods for **3.7** at 243 K showing the inter-conversion of **3.7** (blue) to **3.7$^{1-}$** (red) to the regenerated species (green). Arrows show the progress of the reduction.

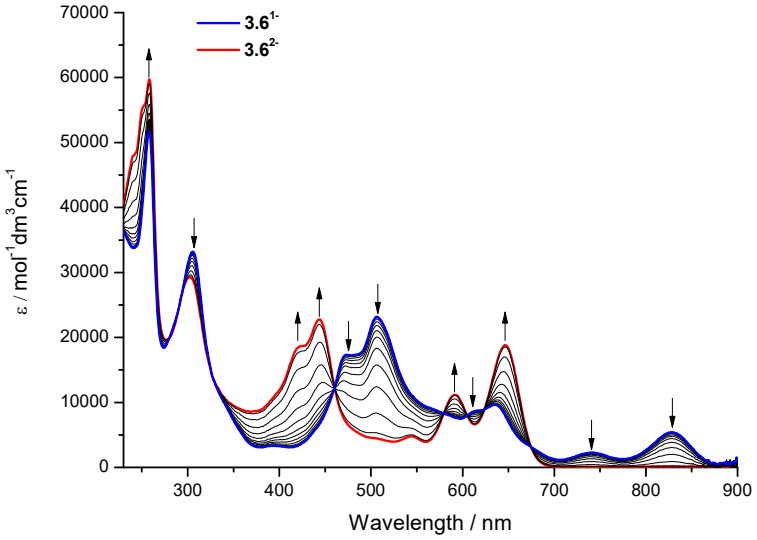


Figure 3-24: UV/vis absorption spectra recorded in DCM containing $[Bu_4N][BF_4]$ (0.4 M) using spectroelectrochemical methods for **3.6** at 243 K showing the inter-conversion of **3.6**$^{1-}$ (blue) to **3.6**$^{2-}$ (red). Arrows show the progress of the reduction.

Production of the dianionic **3.6**$^{2-}$ (Figure 3-24) shared similar features with the dianions reported in Chapter 2. Namely the depletion of the bands at lower energy and the generation of lower wavelength bands, with the species no longer absorbing above 700 nm. The monoanion's absorbance bands are then replaced by bands at 646 nm, 590 nm, 443 nm and 422 nm (Table 3-2), showing that in many of these systems the NDI continues to have similar properties. This similarity also confirms that the phenothiazine substituent is still not participating in this reduction.

| | $\lambda_{abs}$ / nm (ε /$10^3$ $mol^{-1}dm^3cm^{-1}$) | | | |
|---|---|---|---|---|
| **Molecule** | **Neutral** | **Cationic** | **Monoanionic** | **Dianionic** |
| **3.5** | 242 (50.5), 330 (7.9) | 243 (253.2), 258 (30.5), 291 (5.6), 324 (3.5), 387 (3.7), 412 (4.2), 532 (11.6) | - | - |
| **3.6** | 259 (54.3), 293 (29.3), 340 (11.9), 357 (13.7), 376 (13.6), 520 (13.2) | 239 (19.9), 276 (61.2), 304 (31.0), 357 (14.6), 376 (15.7), 516 (25.1), 790 (2.0), 881 (2.3) | 258 (52.0), 305 (33.3), 471 (17.4), 507 (23.4) 613 (8.8), 637 (9.9), 740 (2.5), 829 (5.7) | 240 (48.1), 250 (55.4), 258 (59.8), 303 (29.4), 422 (18.8), 443 (22.8), 544 (50.0), 590 (11.3), 646 (19.0) |
| **3.7** | 241 (58.3), 292 (33.8), 337 (17.6), 357 (17.6), 376 (15.9), 517 (14.8) | 237 (36.1), 260 (41.7), 305 (34.0), 357 (16.6), 375 (19.0), 515 (24.7), 537 (27.3), 784 (2.3) | 240 (67.6), 303 (35.5), 475 (18.3), 506 (23.7), 612 (9.4), 635 (10.7), 741 (2.9), 827 (5.6) | - |

Table 3-2: Spectroelectrochemical data for **3.5-3.7** for neutral, cationic, monoanionic and dianionic states

Next the triad species **3.9** and **3.11** were inspected. The oxidation of the triad species **3.9** (Figure 3-25) and **3.11** (Figure 3-26) causes the depletion of high energy bands at 258 nm and 242 nm respectively, but also interestingly partial depletion of the band in the visible range. This depletion shows that the donor species are at least partially responsible for the neutral species absorbing in the visible range. This visible band in the neutral species maybe in part a charge transfer band, as the donor species alone do not absorb in the visible range.

The new bands generated by the oxidised species have finer structure to them. This is most like due to the fact that since there twice the amount of donor species being oxidised the contribution that is made to the spectra is larger and so more of the structure of the band can be seen. Upon regeneration of the neutral species **3.9** the intensity of the spectra had depleted indicating that the oxidized species is not chemically stable under these conditions and decomposed.

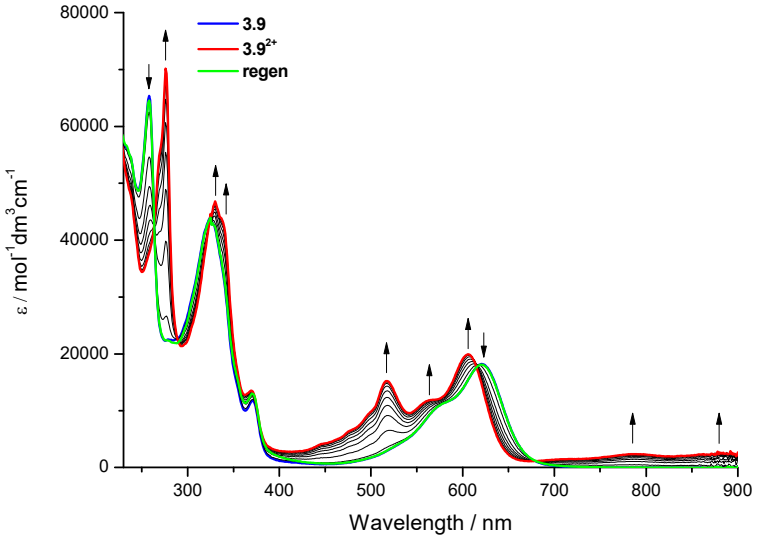


Figure 3-25: UV/vis absorption spectra recorded in DCM containing $[Bu_4N][BF_4]$ (0.4 M) using spectroelectrochemical methods for **3.9** at 243 K showing the inter-conversion of **3.9** (blue) to **3.9**$^{2+}$ (red). Arrows show the progress of the oxidation.

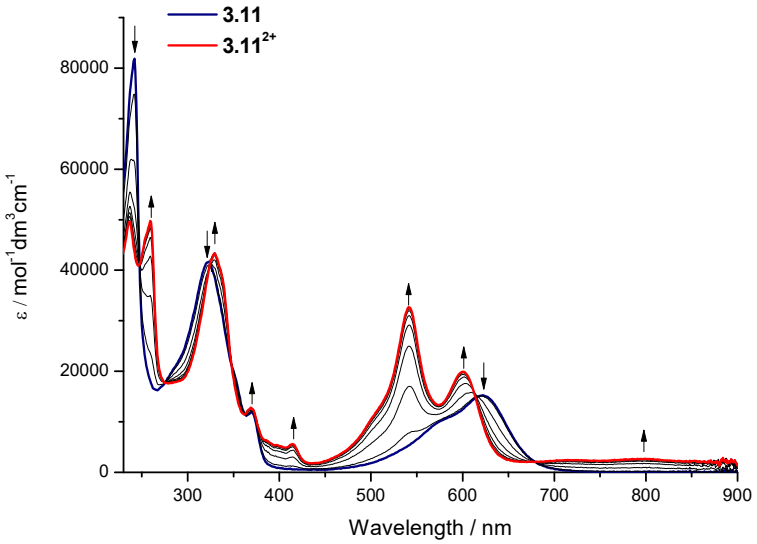


Figure 3-26 UV/vis absorption spectra recorded in DCM containing $[Bu_4N][BF_4]$ (0.4 M) using spectroelectrochemical methods for **3.11** at 243 K showing the inter-conversion of **3.11** (blue) to **3.11**$^{2+}$ (red). Arrows show the progress of the oxidation.

Reducing **3.9** (Figure 3-27) and **3.11** (Figure 3-28) the band in the visible range can be seen to deplete. This is indicative of the NDI being reduced as it is similar to the spectral changes seen in the molecules in Chapter 2. New bands across the entire visible range are seen to be produced in a similar to the reduction of **2.10**. The similarity between these species and **2.10**$^{1-}$ allows for the confirmation that the reduction is occurring upon the NDI core.

Surprisingly both species proved to be chemically unstable to reduction under these conditions and upon regeneration of the neutral species the corresponding absorption bands showed depletion. This is unexpected behaviour as NDIs typically form very stable anions, indicating that the addition of the second donor species causes this instability. As diamine substituted NDIs have been seen to still give stable anions the decomposition must be related to the donor species and not the amine substituted NDI. This however meant that the dianionic species could not be viewed using this technique.

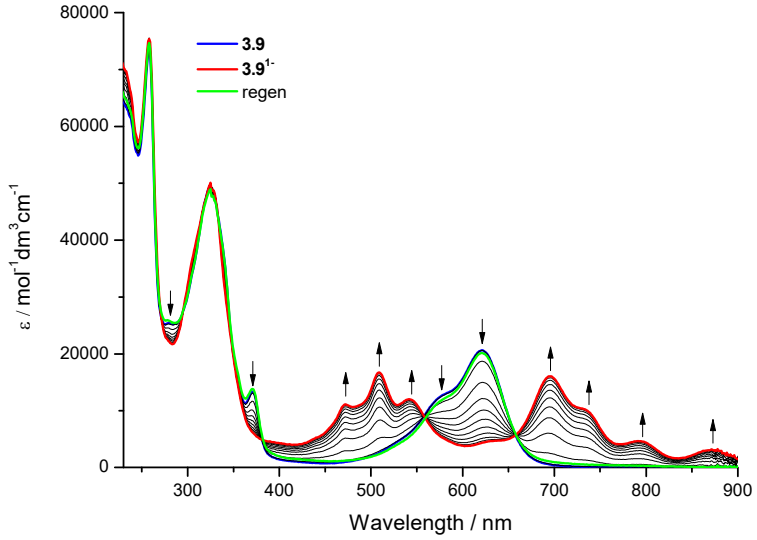


Figure 3-27: UV/vis absorption spectra recorded in DCM containing $[Bu_4N][BF_4]$ (0.4 M) using spectroelectrochemical methods for **3.9** at 243 K showing the inter-conversion of **3.9** (blue) to **3.9**$^{1-}$ (red). Arrows show the progress of the reduction.

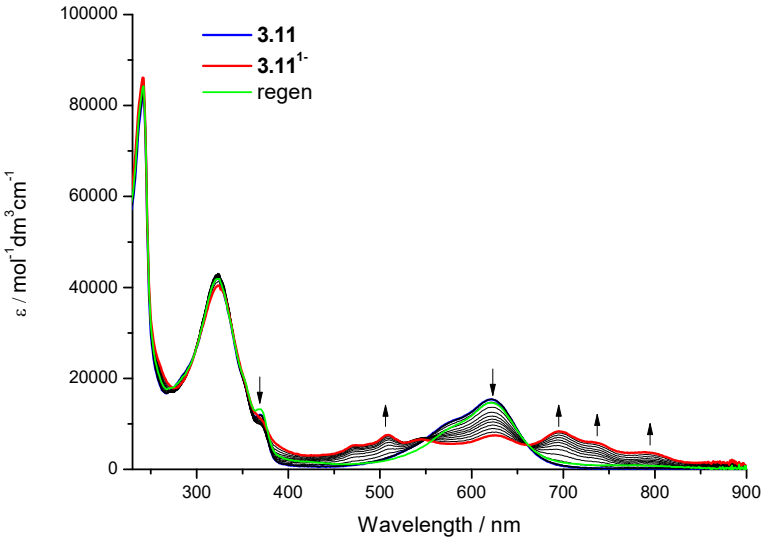


Figure 3-28: UV/vis absorption spectra recorded in DCM containing $[Bu_4N][BF_4]$ (0.4 M) using spectroelectrochemical methods for **3.11** at 243 K showing the inter-conversion of **3.11** (blue) to **3.11**$^{1-}$ (red) to the regenerated species (green). Arrows show the progress of the reduction.

Following the oxidation of the mixed triad system **3.12** (Figure 3-293) band at 242 nm and part of the band in the visible range are depleted (Table 3-5). The high energy band depletion is once again jus associated with the oxidation of the donor species. However once again the depletion of the visible band is observed this is a typical as the lone donor species do not absorb in the visible range. In order to firmly assign why the donor species in all of the triad species are contributing to the visible absorbtion band further examination would be required.

Two bands at 541 nm and 603 nm are generated of similar to that of **3.9**$^{1+}$ and **3.11**$^{1+}$ and are attributed the combined oxidised phenothiazine and phenoxazine. This species appears to be more stable than its **3.9**, and the neutral species can be completely regenerated. This indicates the decomposition pathway of **3.9**$^{1+}$ is related to the two same donor species being oxidised on the same molecule.

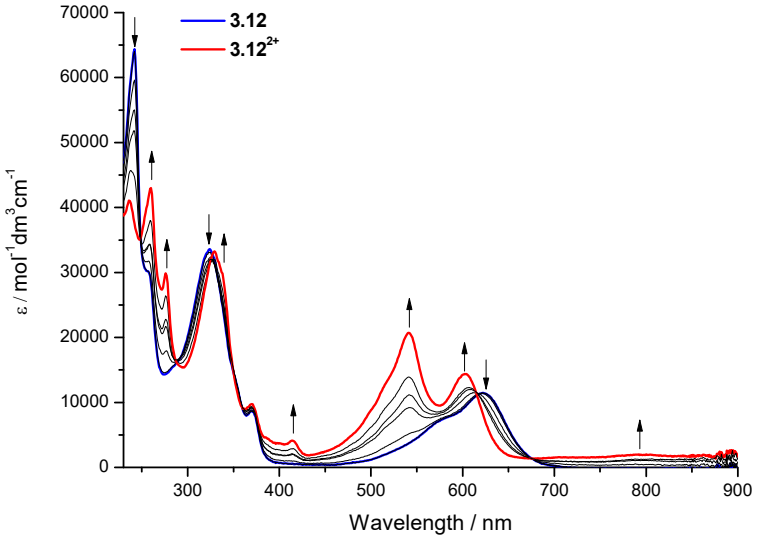


Figure 3-29: UV/vis absorption spectra recorded in DCM containing $[Bu_4N][BF_4]$ (0.4 M) using spectroelectrochemical methods for **3.12** at 243 K showing the inter-conversion of **3.12** (blue) to **3.12²⁺** (red). Arrows show the progress of the oxidation.

Upon probing the initial reduction of **3.12** (Figure 3-30) it can be seen to follow similar changes as **3.9** and **3.11**, depletion of the band around 600 nm related to the NDIs absorption as in Chapter 2. Growth of bands across the whole visible range are observed, this is the typical spectra of a reduced NDI and can be assign as such. Once again however **3.12** proved to be more chemically stable under these conditions and the neutral species was fully regenerated unlike both **3.9** and **3.11** which decomposed when reduced.

Given the stability shown by **3.12** its second reduction was also probed (Figure 3-31). The bands associated with the monoanionic species were seen to deplete and new bands associated with the dianionic species at around 610 nm and 670 nm are produced (Table

3-5). These spectral changes are similar to those observed in the **2.11**$^{-2}$, the broad spectra crossing the majority of the visible range being depleted and replaced with a $\lambda_{max}$ of 668 nm (Table 3-3). This clearly assigns the reduction to NDI core. Throughout these investigations **3.12** proved to be stable under these electrochemical conditions.

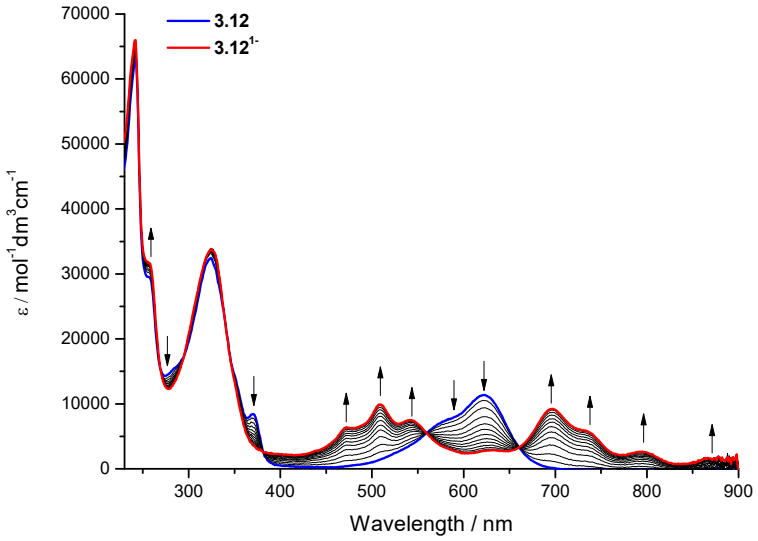


Figure 3-30: UV/vis absorption spectra recorded in DCM containing [Bu$_4$N][BF$_4$] (0.4 M) using spectroelectrochemical methods for **3.12** at 243 K showing the inter-conversion of **3.12** (blue) to **3.12**$^{-1}$ (red). Arrows show the progress of the reduction.

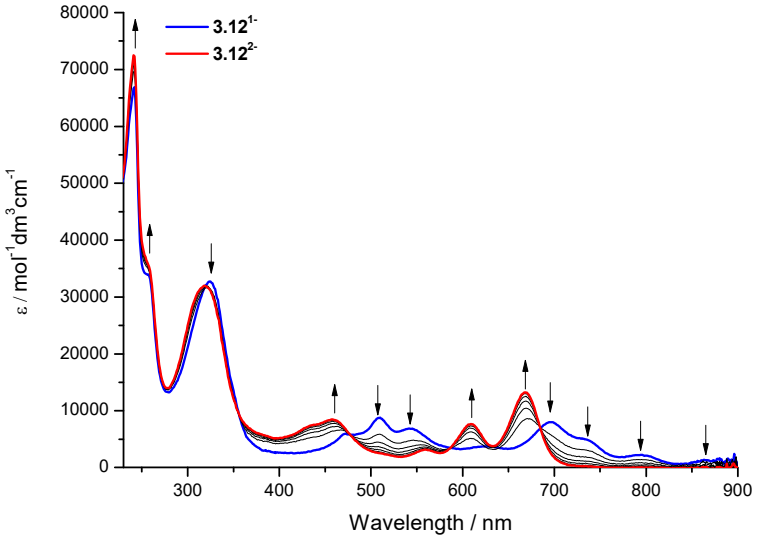


Figure 3-31: UV/vis absorption spectra recorded in DCM containing $[Bu_4N][BF_4]$ (0.4 M) using spectroelectrochemical methods for **3.12** at 243 K showing the inter-conversion of **3.12**$^{-1}$ (blue) to **3.12**$^{-2}$ (red). Arrows show the progress of the reduction.

Initial inspection of the UV-Vis spectra of the neutral morpholine substituted species **3.13** and **3.14** reveal that the morpholine substitution has had an effect on the $\lambda_{max}$ of these species (Table 3-4). In both cases this is seen to decrease by ~10 nm when compared to the di substituted triad species (**3.9**, **3.11** and **3.12**). This shows that the HOMO-LUMO gap of the NDI can be further controlled by additional substitution onto the aromatic core.

| | $\lambda_{abs}$ / nm (ε /$10^3$ $mol^{-1}dm^3cm^{-1}$) | | | |
|---|---|---|---|---|
| **Molecule** | **Neutral** | **Cationic** | **Monoanionic** | **Dianionic** |
| **3.9** | 258 (65.3), 325 (43.9), 371 (11.7), 574 (11.0), 621 (18.3) | 276 (70.1), 330 (46.9), 339 (43.7), 369 (13.6), 517 (15.5), 563 (12.1), 606 (20.2), 786 (2.6), 879 (2.7) | 258 (75.5), 325 (50.1), 472 (11.2), 509 (17.0), 543 (12.3), 627 (4.8), 695 (16.2), 736 (10.2), 795 (4.8), 873 (3.2) | - |
| **3.11** | 242 (81.6), 323 (42.0), 372 (12.1), 578 (10.4), 623 (15.4) | 235 (49.6), 260 (49.9), 330 (43.5), 369 (12.7), 415 (5.7), 541 (33.0), 601 (20.2), 799 (2.8) | 241 (86.1), 323 (40.4), 470 (5.5), 508 (7.7), 546 (6.9), 626 (7.7), 695 (8.5), 737 (6.0), 794 (3.9) | - |
| **3.12** | 242 (64.3), 256 (30.2), 324 (33.6), 371 (8.8), 579 (7.6), 624 (11.6) | 237 (41.2), 260 (43.1), 276 (30.1), 329 (33.5), 370 (9.9), 415 (4.1), 541 (20.9), 603 (14.5), 793 (2.1) | 242 (65.9), 258 (31.7), 325 (33.8), 472 (6.4), 509 (10.0), 542 (7.5), 628 (3.0), 696 (9.4), 737 (5.9), 795 (2.9), 869 (1.8) | 241 (72.5), 256 (36.1), 318 (32.0), 436 (7.7), 460 (8.8), 560 (3.3), 609 (7.7), 668 (13.6) |

Table 3-5: Spectroelectrochemical data for **3.9, 3.11 and 3.12** for neutral, cationic, monoanionic and dianionic states

Following oxidation of both **3.13** (Figure 3-32) and **3.14** (Figure 3-33) the spectral changes can be seen to be comparable to that of **3.6** and **3.7**. High energy bands can be seen to deplete and be replaced by red shifted absorptions related to the oxidised species. This is very similar to what is observed in the free donor species and so the oxidation can be assigned to the donor species. The most diagnostic of the generated bands being large is observed at around 515 nm (Table 3-6).

Viewing the initial reductions of both **3.13** (Figure 3-34) and **3.14** (Figure 3-35), similarly to **3.6** and **3.7** the band around 610 nm is seen to deplete and new bands across the entire visible range are generated. The landscape of the anion's spectra has become distinct throughout this investigation as the spectral of a reduced NDI, so the reduction can be assigned there. Unfortunately once again the phenoxazine species is proved to be chemically unstable under these conditions, similar to **3.7**, as the neutral species could not be fully regenerated upon re-oxidation.

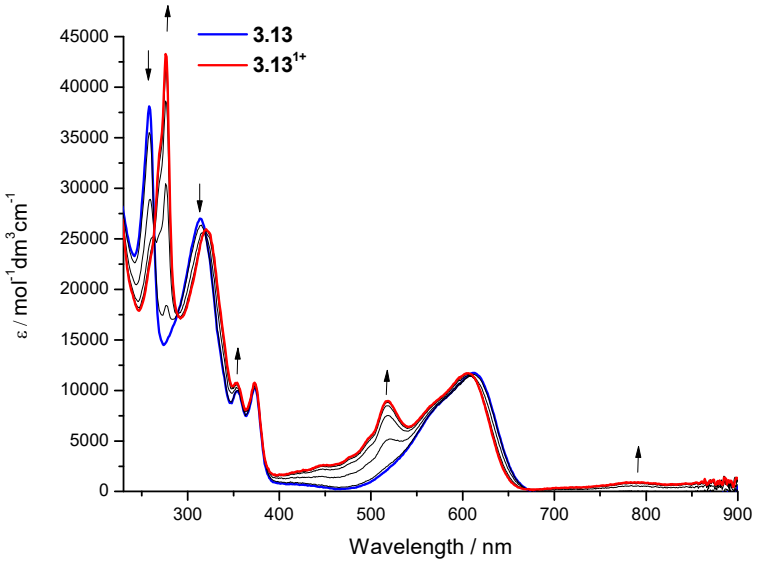


Figure 3-36: : UV/vis absorption spectra recorded in DCM containing $[Bu_4N][BF_4]$ (0.4 M) using spectroelectrochemical methods for **3.13** at 243 K showing the inter-conversion of **3.13** (blue) to **3.13**$^{1+}$ (red) to the regenerated species (green). Arrows show the progress of the oxidation.

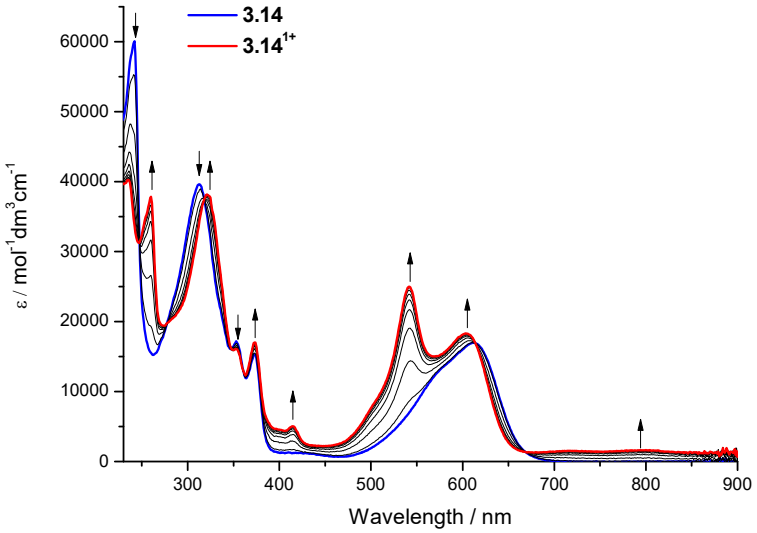


Figure 3-37: UV/vis absorption spectra recorded in DCM containing $[Bu_4N][BF_4]$ (0.4 M) using spectroelectrochemical methods for **3.14** at 243 K showing the inter-conversion of **3.14** (blue) to **3.14**$^{1+}$ (red). Arrows show the progress of the oxidation.

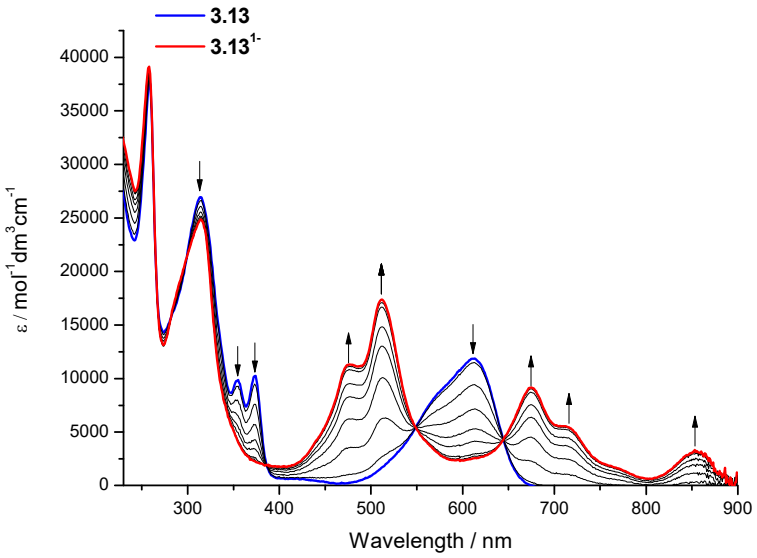


Figure 3-38: UV/vis absorption spectra recorded in DCM containing $[Bu_4N][BF_4]$ (0.4 M) using spectroelectrochemical methods for **3.13** at 243 K showing the inter-conversion of **3.13** (blue) to **3.13**$^{1-}$ (red). Arrows show the progress of the reduction.

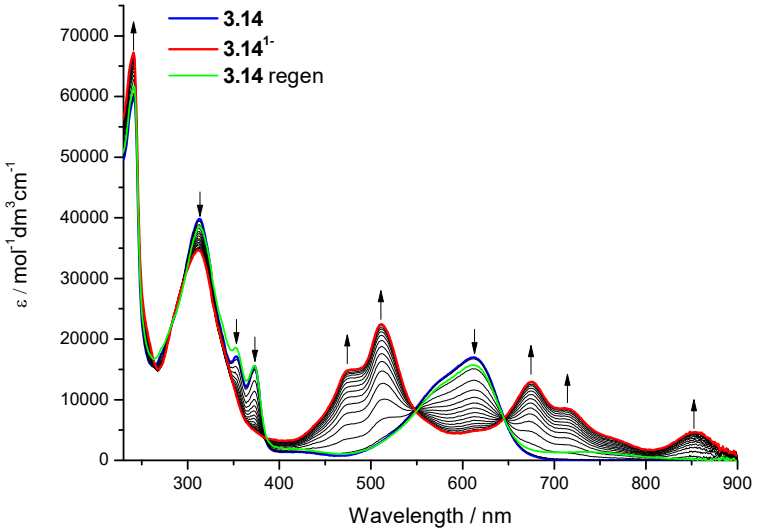


Figure 3-39: UV/vis absorption spectra recorded in DCM containing $[Bu_4N][BF_4]$ (0.4 M) using spectroelectrochemical methods for **3.14** at 243 K showing the inter-conversion of **3.14** (blue) to **3.14**$^{1-}$ (red) to the regenerated species (green). Arrows show the progress of the reduction.

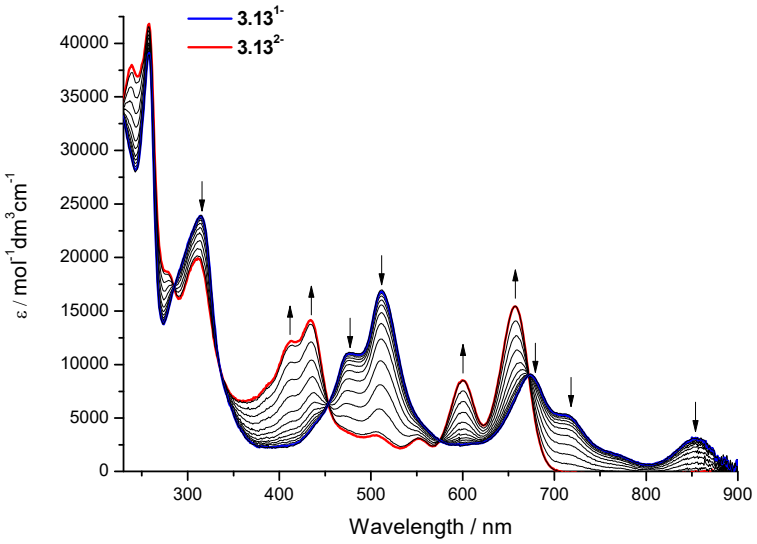


Figure 3-40: UV/vis absorption spectra recorded in DCM containing $[Bu_4N][BF_4]$ (0.4 M) using spectroelectrochemical methods for **3.13** at 243 K showing the inter-conversion of **3.13**$^{1-}$ (blue) to **3.13**$^{2-}$ (red). Arrows show the progress of the reduction.

The second reduction of **3.13** (Figure 3-41) is seen to be similar to that of **3.6**. The broad absorbtion profile being depleted and a new profile which does not extend above 700 nm. This can there for be easily assigned to the second reduction of the NDI core.

Finally the light harvesting BODIPY species **3.19** was examined. Viewing the spectra of the neutral species the presence of the BODIPY unit can be clearly be seen in the highly absorbing narrow band at 507 nm (Table 3-7). It clearly is causing the species to absorb more visible light as was intention of the addition of this species. Further study would be required to see if this energy was being transferred to the NDI centre. In addition the effect it has on the HOMO-LUMO gap of the NDI can be seen, $\lambda_{max}$ = 552 nm. This shows that the substitution has caused less of a decrease in the energy gap between the frontier orbitals when compared to the other

di substituted species in this chapter. This is a good example of the extent this gap depends upon the nature of the substituents.

The oxidation of **3.19** (Figure 3-42) was examined first as BODIPYs have a tendency to be unstable under bulk electrolysis. As with other phenothiazine species the high energy band at around 250 nm (Table 3-8) is depleted and bands at lower energy are generated, allowing this oxidation to be assigned to the phenothiazine species. As with **3.9** the oxidation of the species also showed a depletion of the band in the visible range, at ~ 600 nm. To firmly assign why the phenothiazine species is contribution to the visible absorbance band further study would be required. This oxidative process is seen to be entirely reversible under these conditions.

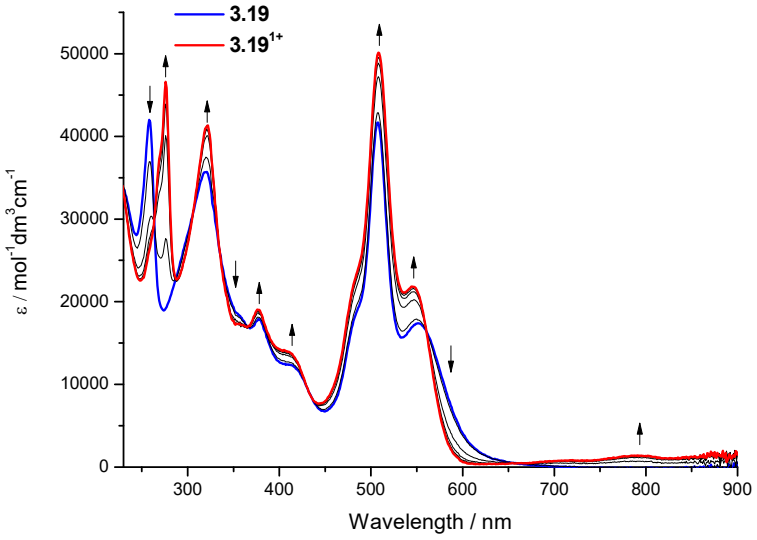


Figure 3-43: UV/vis absorption spectra recorded in DCM containing [Bu4N][BF4] (0.4 M) using spectroelectrochemical methods for 3.19 at 243 K showing the inter-conversion of 3.19 (blue) to 3.191+ (red). Arrows show the progress of the oxidation.

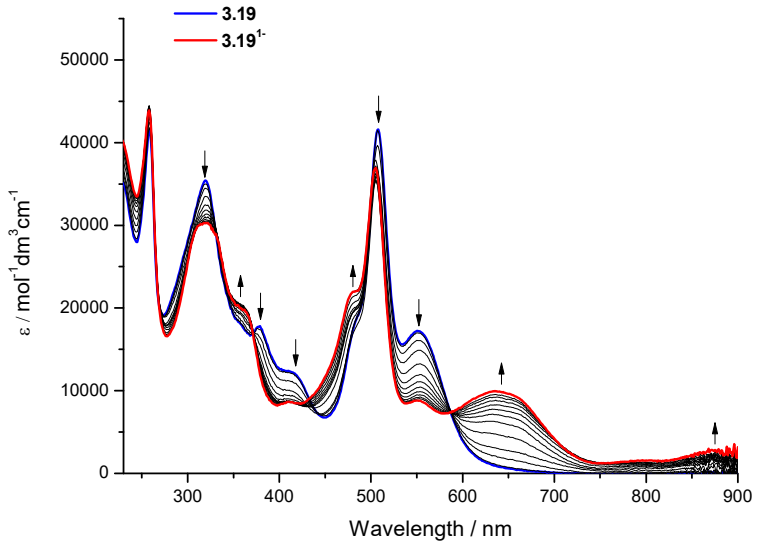


Figure 3-44: UV/vis absorption spectra recorded in DCM containing $[Bu_4N][BF_4]$ (0.4 M) using spectroelectrochemical methods for **3.19** at 243 K showing the inter-conversion of **3.19** (blue) to **3.19**$^{1-}$ (red). Arrows show the progress of the reduction.

The first reduction of **3.19** (Figure 3-45) causes clear depletion of the bands at 378 nm, 412 nm, 507 nm and 552 nm (Table 3-9) and the growth of new red-shifted band at 642 nm and a broad absorbance over the low energy region above 750 nm. These changes can be assigned to the reduction of an NDI, the broad absorbance profile being particularly diagnostic.

Inspecting the second reduction of **3.19** (Figure 3-46), shows depletion of the narrow band at 507 nm. This band is characteristic of BODIPY so the reduction is assigned to this component. In its place the spectra red shifts absorbtion in the low energy region into the near IR beyond what the spectrometer could detect. Unfortunately upon regeneration of the neutral species after the sample had undergone the second reduction a substantial reduction

in the intensity of the spectra was observed, due to the species decomposing which is typical for reduced BODIPY species.[25] This not only makes it impractical to observe the third reduction of the species but also draws into question the validity of the spectra of **3.19**$^{2-}$ as it maybe the spectra of these species and the decomposition product.

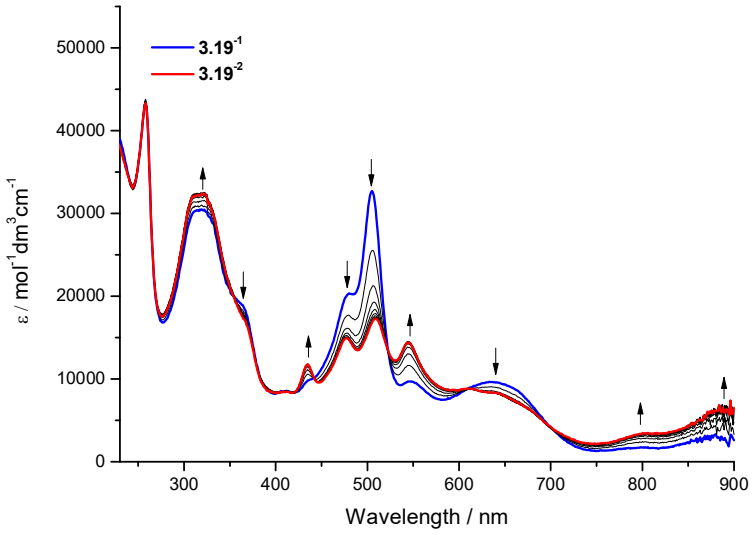


Figure 3-47: UV/vis absorption spectra recorded in DCM containing [Bu$_4$N][BF$_4$] (0.4 M) using spectroelectrochemical methods for **3.19** at 243 K showing the inter-conversion of **3.19**$^{1-}$ (blue) to **3.19**$^{2-}$ (red). Arrows show the progress of the reduction.

| | $\lambda_{abs}$ / nm (ε /$10^3$ $mol^{-1}dm^3cm^{-1}$) | | | |
|---|---|---|---|---|
| **Molecule** | **Neutral** | **Cationic** | **Monoanionic** | **Dianionic** |
| **3.13** | 258 (38.1), 314 (27.1), 354 (10.0), 373 (10.4), 612 (11.8) | 276 (43.3), 319 (26.0), 353 (10.8), 373 (10.8), 518 (9.1), 606 (11.8), 790 (1.0) | 258 (39.1), 314 (24.9), 475 (11.3), 512 (17.6), 674 (9.1), 716 (5.6), 853 (3.3) | 239 (38.1), 258 (41.9), 279 (18.7), 311 (20.0), 412 (12.2), 435 (14.1), 506 (3.4), 552 (3.0), 600 (8.6), 657 (15.5) |
| **3.14** | 242 (60.1), 313 (39.9), 353 (17.2), 373 (15.3), 614 (16.9) | 235 (40.2), 260 (37.9), 322 (38.3), 354 (16.1), 373 (17.1), 415 (5.2), 542 (25.1), 605 (18.5), 795 (1.6) | 241 (67.2), 311 (34.8), 474 (14.9), 512 (22.7), 675 (13.0), 715 (8.7), 853 (4.8) | - |
| **3.19** | 259 (42.1), 319 (35.8), 378 (17.9), 412 (12.3), 507 (41.6), 552 (17.4) | 276 (46.7), 322 (41.3), 378 (19.0), 412 (13.8), 508 (50.1), 546 (22.0), 792 (1.6), 873 (1.7) | 258 (43.9), 320 (30.4), 362 (19.8), 411 (8.7), 480 (22.0), 505 (37.1), 551 (8.9), 642 (10.0), 800 (1.7), 875 (2.9) | 258 (43.3), 318 (32.3), 435 (11.7), 478 (14.9), 509 (17.3), 545 (14.5), 640 (8.4), 798 (3.5), 889 (6.4) |

Table 3-10: Spectroelectrochemical data for **3.13, 3.14** and **3.19** for neutral, cationic, monoanionic and dianionic states

## 3.3: Conclusions

Throughout this chapter the work from Chapter 2 has been expanded upon and used to synthesis a series of cNDI electron donor-acceptor molecules. In order to achieve this a novel synthetic method for the N-substitution of the donor species phenothiazine and phenoxazine has been developed. This method allows for the simple synthesis of these species and could be utilized to prepare differently substituted species allowing for a larger amount of phenothiazine and phenoxazine compounds to be accessed.

By substitution onto the aromatic core of the NDI the frontier orbitals of the NDI are shifted in energy. This causes the HOMO-LUMO gap to decrease in energy to the point that the species can absorb visible light. This HOMO-LUMO gap can be tailored by the amount and nature of the substitution. By causing the NDI acceptor to be excited by visible light there is potential for this excitation to in turn cause the generation of a charge separated state, allowing an electron to move from the donor species onto the electron poor NDI acceptor. This charge separated state could then be utilized in a photovoltaic device to generate a current.

In order to assess how readily these states are being accessed the next step would be to analyze them using transient absorbtion studies. Here the NDI could be excited and then the absorbance of the species could be followed to assess the presence and lifetime of the charge separated state.

From this it could be assessed if which combination of, donor species and substitution accessed the charge separated state most efficiently. In addition to this the contribution of the donor species to the visible light absorbance of the triad species could be explored using this technique. In addition DFT calculations could be ran to help gain insight as to the molecules molecular orbitals. This would help to assign transitions observed in the UV-vis spectra.

Ultimately it would be hoped that this work would lead to the ability to create NDI donor-acceptor species with highly tunable HOMO-LUMO gaps. This would allow for tuning of the light absorbed by the acceptor species and allow for matching to the correct donor species. This in turn would make them excellent candidates for a new generation of photovoltaic devices.

## 3.4: Experimental

### 3.4.1: General procedures

All starting materials were purchased form Sigma Aldrich or Fisher Scientific and used without further purification. Column chromatography was conducted using silica gel (merck silica gel 60, 0.2-0.5 mm, 50-130 mesh). The $^{1}H$ and $^{13}C$ NMR spectra were obtained on a Bruker 400 MHz spectrometer, except **3.9**, **3.11** and **3.12** which were collected on a Bruker 500 MHz spectrometer. MALDI MS spectra were collected with a Bruker Ultraflex III mass spectrometer using trans-2-[3-(4-tert-butylphenyl)-2-methyl-2-propenylidene]malononitrile as the matrix. FD MS spectra were measured with a JOEL AccuTOF GCX spectrometer. Single crystal X-ray diffraction experiments were performed on an Oxford Diffraction Supernova CCD area detector diffractometer at 120 K using monochromated Cu K α radiation (λ = 1.54184 Å); on Agilent GV1000 AtlasS2 and TitanS2 CCD area detector diffractometers at 120 K using monochromated Cu K α radiation (λ = 1.54184 Å). Absorption corrections were applied using analytical numerical methods using either ShelXS or ShelXT and refined with ShelXL using a least squares method. In all instances, Olex2 software was used as the solution refinement and analysis program. All hydrogen atoms were placed in geometrically calculated positions; non-hydrogen atoms were refined with anisotropic displacement.

### 3.4.2: Synthesis of 3.1 (method 1)

To a $N_2$ degassed solution of toluene (150 mL), phenothiazine (1.01 g, 5.07 mmol), tri-o-tolylphosphine (0.744g, 2.44 mmol), tris(dibenzylideneacetone)dipalladium (0.225g, 0.246 mmol) and potassium t-butoxide (0.568 g, 5.07mmol) was added 4-nitro-iodobenzene (1.355 g, 5.44 mmol). The mixture was heated to 90 $^oC$ for 24 h, cooled washed with 2 M HCl (2 x 25 mL) and water (2 x 25 mL), and then sent through a silica plug ($CHCl_3$). Solvent was removed and the residue purified *via* column chromatography (silica [$CHCl_3$:Hexane 3:1]) to give **3.1** (0.711 g, 2.208 mmol, 44 %) as a yellow powder.

$^1H$ NMR (400 MHz, Chloroform-*d*) δ 8.74 – 8.68 (m, 2H), 8.17 (dd, *J* = 7.9, 1.4 Hz, 2H), 8.12 (dd, *J* = 7.9, 1.4 Hz, 2H), 8.05 (td, *J* = 7.7, 1.5 Hz, 2H), 7.95 (d, *J* = 1.4 Hz, 1H), 7.94 (s, 2H), 7.93 (s, 1H), 7.71 – 7.63 (m, 2H) ppm. $^{13}C$ NMR (101 MHz, Chloroform-*d*) δ 151.24, 141.13, 140.63, 134.80, 129.34, 127.66, 127.16, 126.92, 125.75, 114.05 ppm. ESI MS: 320.0619 [$M^+$] Calc: 320.0619

### 3.4.3: Synthesis of 3.1 (method 2)

Phenothiazine (100 mg, 0.5 mmol), **3.4** (207 mg, 1.25 mmol) and copper acetate (136 mg, 0.75 mmol) were dissloved in dry degassed dichloromethane (5 mL). To this pyridine (80 µL, 1 mmol) was added. The solution was then exposed to air and left to stir at RT for 18 h.

This was filtered through kieselguhr ($CHCl_3$) and washed with HCl (2 M, 100 mL) and brine (100 mL), then dried over $MgSO_4$ and filtered and the solvent removed. The residue was purified *via* column chromatography (silica [CHCl3]) to give nitro pheniothiazine (134 mg, 0.42 mmol, 83 %) as a yellow powder.

$^1$H NMR (400 MHz, Chloroform-*d*) δ 8.74 – 8.68 (m, 2H), 8.17 (dd, *J* = 7.8, 1.4 Hz, 2H), 8.12 (dd, *J* = 7.9, 1.4 Hz, 2H), 8.05 (td, *J* = 7.7, 1.5 Hz, 2H), 7.95 (d, *J* = 1.4 Hz, 1H), 7.94 (s, 2H), 7.93 (s, 1H), 7.71 – 7.63 (m, 2H) ppm.$^{13}$C NMR (101 MHz, Chloroform-*d*) δ 151.24, 141.13, 140.63, 134.80, 129.34, 127.66, 127.16, 126.92, 125.75, 114.05, 77.48, 77.16, 76.84 ppm. ESI MS: 320.0619 [$M^+$] Calc: 320.0619

### 3.4.4: Synthesis of 3.2

**3.1** (700 mg, 2.17 mmol) dissolved in THF (25 mL) and Pd/C 10 % (245 mg, 0.22 mmol) added. The mixture was stirred under an atmosphere of $H_2$ at RT, in the dark for 16h. The resulting solution was filtered through kieselguhr ($CHCl_3$), the solvent removed and the residue purified *via* column chromatography (silica [$CHCl_3$:Hexane 3:1]) to give **3.1** (402 mg, 1.39 mmol, 64 %) as a white powder.

$^1$H NMR (400 MHz, Chloroform-*d*) δ 7.18 (d, J = 8.6 Hz, 2H), 7.01 (dd, J = 7.4, 1.7 Hz, 2H), 6.93 – 6.77 (m, 6H), 6.29 (dd, J = 8.1, 1.4 Hz, 2H), 3.87 (s, 2H) ppm. $^{13}$C NMR (101 MHz, Chloroform-*d*) δ 146.31, 144.84, 132.04, 131.19, 126.78, 126.53, 122.08, 119.51, 116.73, 115.64 ppm. ESI MS: 290.103 [$M^+$] Calc: 290.088

### 3.4.5: Synthesis of 3.4

To dry $N_2$ degassed DMF (90 mL) was added 4-iodo-nitrobenzene (3.81 g, 15.3 mmol), bis(pinacolato)diboron (5.45 g, 21.5 mmol), [1,1'-Bis(diphenylphosphino)ferrocene]palladium(II) dichloride (330 mg, 0.451 mmol) and potassium acetate (4.51 g, 46 mmol). The solution was heated to 70 $^oC$ for 2 h, then cooled and water (200 mL) was added. The aqueous layer was extracted with diethyl ether (4 x 100 mL) and the ethereal phase was washed with water (100 mL), brine (100 mL) and dried over $MgSO_4$ and filtered. The solvent was removed and the residue was dissolved in THF (12 mL) and water (12 mL). Sodium periodate (9.85 g, 46.2 mmol) was added and the solution stirred at room temperature for 1.5 h. HCl was added (1 M, 35 mL) and the solution stirred for 3 h, then extracted into EtOAc (4 x 50 mL) and the organic washed with brine and dried over $MgSO_4$ and filtered. The solvent was removed and the residue was dissolved in sodium hydroxide solution (0.5 M, 50 mL), filtered and stirred over activated charcoal for 30 min. The resulting solution was filtered, cooled in an ice bath and acidified with conc. HCl (10 mL). The precipitate was collected to give **3.4** (1.87 g, 11.2 mmol, 73%) as a white powder.

$^1H$ NMR (400 MHz, Chloroform-*d*) δ 8.23 (d, *J* = 8.6 Hz, 2H), 7.94 (d, *J* = 8.6 Hz, 2H), 5.02 (brs, 1H) ppm. $^{13}C$ NMR (101 MHz, *DMSO-d*$^6$) δ data: 149.2, 135.4, 122.5. ESI MS:167.057 [$M^+$] Calc: 167.039

### 3.4.6: Synthesis of 3.3

Phenoxazine (100 mg, 0.55 mmol), **3.4** (230 mg, 1.38 mmol) and copper acetate (150 mg, 0.83 mmol) were combined in dry degassed $CH_2Cl_2$ (5 mL). To this pyridine (90 µL, 1.1 mmol) was added. The solution was exposed to air and left to stir at RT for 18 h. The solution was filtered through kieselguhr ($CHCl_3$) and washed with HCl (2 M, 100 ml) and brine (100 ml), then dried over $MgSO_4$ and filtered and the solvent removed. The residue was purified *via* column chromatography (silica [$CHCl_3$:EtOAc 19:1] ) to give **3.4** (59 mg, 0.197 mmol, 31 %) as an orange powder.

$^1$H NMR (400 MHz, Chloroform-*d*) δ 8.45 (d, *J* = 8.7 Hz, 2H), 7.57 (d, *J* = 8.7 Hz, 2H), 6.79 – 6.72 (m, 4H), 6.65 (m, *J* = 7.5, 2.1 Hz, 2H), 6.01 (d, *J* = 7.9 Hz, 2H) ppm. $^{13}$C NMR (101 MHz, Chloroform-*d*) δ 145.90, 144.53, 133.25, 131.41, 126.54, 123.53, 122.73, 122.72, 116.24, 113.93, 77.16 ppm. ESI MS:304.068 [$M^+$] Calc: 304.085

### 3.4.7: Synthesis of 3.5

**3.4** (100 mg, 0.33 mmol), Pd/C 10 % (7 mg, 0.0.066 mmol) were added to THF (5 mL) and stirred under an atmosphere of $H_2$ at RT, in the dark for 16h. The resulting solution was filtered through kieselguhr, the solvent removed and the residue purified *via* column chromatography (silica [$CHCl_3$:Hexane 3:1]) to give amino phenothiazine (63 mg, 0.230 mmol, 70 %) as a grey powder.

$^{1}$H NMR (300 MHz, Chloroform-*d*) δ 7.12 – 7.04 (m, 2H), 6.88 – 6.81 (m, 2H), 6.68 – 6.54 (m, 6H), 6.02 – 5.93 (m, 2H), 3.83 (s, 2H) ppm. $^{13}$C NMR (75 MHz, Chloroform-*d*) δ 146.56, 144.14, 135.11, 131.65, 129.26, 123.32, 121.03, 117.13, 115.33, 113.37, 77.16 ppm. ESI MS : 274.136 [$M^{+}$] Calc: 274.111

### 3.4.8: Synthesis of 3.6

**2.6** (25 mg, 0.038 mmol) and **3.2** (11 mg, 0.038 mg) were dissolved in DMF (1 mL), and the solution was heated to 135 $^{o}$C for 4 h. This resulting mixture was cooled, the solvent removed and the residue extracted with $CHCl_3$ (20 mL), washed with HCl (2M 2 x 20 mL), dried over $MgSO_4$, filtered, the solvent was removed and the residue purified *via* column chromatography (silica [$CHCl_3$:EtOAc 9:1]) to give **3.6** (29 mg, 0.033 mmol, 86 %) as a pink powder.

$^{1}$H NMR (400 MHz, Chloroform-*d*) δ 11.93 (s, 1H), 8.88 – 8.81 (m, 2H), 8.56 (d, *J* = 7.8 Hz, 1H), 7.58 – 7.32 (m, 11H), 7.08 (dd, *J* = 7.5, 1.7 Hz, 2H), 6.97 – 6.85 (m, 4H), 6.43 (dd, *J* = 8.1, 1.3 Hz, 2H), 2.72 (dt, *J* = 16.8, 6.9 Hz, 4H), 1.25 – 1.13 (m, 26H) ppm. $^{13}$C NMR (101 MHz, Chloroform-*d*) δ 166.89, 163.42, 162.99, 150.35, 145.67, 145.60, 143.92, 140.01, 136.67, 132.46, 130.86, 130.45, 130.18, 130.07, 128.45, 127.27, 127.20, 126.78, 126.34, 125.71, 124.66, 124.45, 124.34, 123.31, 122.48, 121.88, 117.65, 101.91, 77.48, 77.16, 76.84, 29.86, 29.42, 24.21, 24.17, 24.11 ppm. FD MS :874.35601 [$M^{+}$] Calc: 874.35528

**Crystal Data** for $C_{66}H_{84}Cl_6N_4O_{12}S$ ($M$ =1370.13 g/mol): orthorhombic, space group $P2_12_12_1$ (no. 19), $a$ = 13.9099(6) Å, $b$ = 16.2937(9) Å, $c$ = 25.4691(10) Å, $V$ = 5772.4(5) Å$^3$, $Z$ = 4, $T$ = 120(2) K, μ(CuKα) = 3.655 mm$^{-1}$, $Dcalc$ = 1.577 g/cm$^3$, GooF = 1.087, 31326 reflections measured (6.44° ≤ 2Θ ≤ 147.646°), 11431 unique ($R_{int}$ = 0.0961, $R_{sigma}$ = 0.0975) which were used in all calculations. The final $R_1$ was 0.1124 (I > 2σ(I)) and $\omega R_2$ was 0.3515 (all data).

## 3.4.9: Synthesis of 3.7

**2.6** (25 mg, 0.038 mmol) and **3.5** (11 mg, 0.039 mmol) were dissolved in DMF (1 mL), this was then heated to 135 °C for 4 h. This was cooled the solvent removed and the residue extracted with $CHCl_3$ (20 mL), washed with HCl (2M 2 x 20 mL), dried over $MgSO_4$, filtered the solvent was removed and the residue purified column chromatography (silica [$CHCl_3$:EtOAc 9:1]) to give **3.7** (20 mg, 0.024 mmol, 62%) as a pink powder.

$^1$H NMR (400 MHz, Chloroform-*d*) δ 11.94 (s, 1H), 8.89 – 8.82 (m, 2H), 8.58 (d, *J* = 7.8 Hz, 1H), 7.61 – 7.31 (m, 10H), 6.72 – 6.59 (m, 6H), 5.99 (dd, *J* = 7.6, 1.7 Hz, 2H), 2.73 (dt, *J* = 16.9, 6.8 Hz, 4H), 1.29 – 1.12 (m, 26H) ppm. $^{13}$C NMR (101 MHz, Chloroform-*d*) δ 166.92, 163.39, 162.99, 150.24, 145.67, 145.59, 144.09, 137.80, 137.28, 134.22, 132.85, 132.50, 130.62, 130.42, 130.15, 130.09, 130.06, 128.49, 126.80, 126.46, 126.17, 124.70, 124.46, 124.35, 123.52, 121.76, 121.70, 115.71, 113.43, 102.11, 29.85, 29.43, 24.21, 24.17, 24.11 ppm. FD MS : 858.37867 Calc[M$^+$]: 858.37812

**Crystal Data** for $C_{69}H_{99}Cl_3N_4O_{17}$ ($M$ =1362.87 g/mol): orthorhombic, space group $P2_12_12_1$ (no. 19), $a$ = 13.7486(5) Å, $b$ = 15.9651(9) Å, $c$ = 25.3392(12) Å, $V$ = 5561.9(5) Å$^3$, $Z$ = 4, $T$ = 120(2) K, μ(CuKα) = 2.219 mm$^{-1}$,*Dcalc* = 1.628 g/cm$^3$, GooF = 1.001, 28533 reflections measured (6.544° ≤ 2Θ ≤ 147.344°), 10919 unique ($R_{int}$ = 0.0886, $R_{sigma}$ = 0.1020) which were used in all calculations. The final $R_1$ was 0.0959 (I > 2σ(I)) and $\omega R_2$ was 0.2994 (all data).

## 3.4.10: Synthesis of 3.8 and 3.9

**2.7** (200 mg, 0.269 mmol) and **3.2** (117 mg, 0.404 mmol) were dissolved in DMF (5 mL) and heated to 135 $^o$C for 4 h. The solvent was removed and the residue purified *via* column chromatography (silica [$CHCl_3$:EtoAc 9:1]) to give **3.8** (119 mg, 0.125 mmol, 47 %) as a pink powder and **3.9** (23 mg, 0.019 mmol, 7 %) as a blue powder.

**3.8**: $^1$H NMR (400 MHz, Chloroform-*d*) δ 11.92 (s, 1H), 9.09 (s, 1H), 8.91 (s, 1H), 7.60 – 7.34 (m, 10H), 7.12 (dd, *J* = 7.5, 1.7 Hz, 2H), 7.01 – 6.87 (m, 4H), 6.47 (dd, *J* = 8.1, 1.3 Hz, 2H), 2.80 – 2.65 (m, 4H), 1.26 – 1.16 (m, 24H) ppm. $^{13}$C NMR (101 MHz, Chloroform-*d*) δ 166.89, 163.42, 162.99, 150.35, 145.67, 145.60, 143.92, 140.01, 136.67, 132.46, 130.86, 130.45, 130.18, 130.07, 128.45, 127.27, 127.20, 126.78, 126.34, 125.71, 124.66, 124.45, 124.34, 123.31, 122.48, 121.88, 117.65, 101.91, 77.48, 77.16, 76.84, 29.86, 29.42, 24.21, 24.17, 24.11 ppm. MALDI MS : 952.29 Calc[M$^+$]: 952.26

**3.9**: $^{1}$H NMR (500 MHz, Toluene-$d_8$) δ: 8.93 (s, 2H), 7.22 (m, 6H), 6.90 (m, 6H), 6.75 – 6.71 (m, 4H), 6.63 – 6.55 (m, 10H), 3.06 – 3.02 (m, 4H), 1.29 – 1.24 (m, 24H).

$^{13}$C NMR (126 MHz, Toluene-$d^8$) δ: 167.64, 163.08, 147.55, 146.43, 145.03, 138.79, 138.48, 132.79, 132.47, 132.35, 131.61, 127.53, 127.46, 124.83, 124.73, 123.30, 121.64, 117.01, 30.24, 24.69.

FD MS : 1162.42718 Calc[$M^+$]: 1162.42740

## 3.4.11: Synthesis of 3.10

**2.7** (120 mg, 0.17 mmol) and **3.5** (60 mg, 0.22 mmol) were dissolved in DMF (2 mL) and heated to 135 $^{o}$C for 4 h. The solvent was removed and the residue purified *via* column chromatography (silica [$CHCl_3$: EtOAc 9:1]) to give **3.10** (141 mg, 0.150 mmol, 89 %) as a pink powder.

$^{1}$H NMR (300 MHz, Chloroform-*d*) δ 11.89 (s, 1H), 9.06 (s, 1H), 8.87 (s, 1H), 7.62 – 7.30 (m, 10H), 6.73 – 6.57 (m, 6H), 6.03 – 5.94 (m, 2H), 2.80 – 2.58 (m, 4H), 1.25 – 1.11 (m, 24H) ppm. $^{13}$C NMR (101 MHz, Chloroform-*d*) δ 166.92, 163.39, 162.99, 150.24, 145.67, 145.59, 144.09, 137.80, 137.28, 134.22, 132.85, 132.50, 130.62, 130.42, 130.15, 130.09, 130.06, 128.49, 126.80, 126.46, 126.17, 124.70, 124.46, 124.35, 123.52, 121.76, 121.70, 115.71, 113.43, 102.11, 77.48, 77.16, 76.84, 29.85, 29.43, 24.21, 24.17, 24.11 ppm.

FD MS : 936.28882 Calc[$M^+$]: 936.28863

### 3.4.12: Synthesis of 3.11

**2.7** (20 mg, 0.027 mmol) and **3.5** (16.2 mg, 0.059 mmol) were dissolved in DMF (0.5 mL) and heated to 135 $^{o}$C for 4 h. The solvent was removed and the residue purified *via* column chromatography (silica [$CHCl_3$: EtOAc 9:1]) to give **3.11** (15 mg, 0.013 mmol, 49 %) as a blue powder.

$^{1}$H NMR (500 MHz, Toluene-$d_8$) δ: 8.99 (s, 2H), 7.30 – 7.25 (m, 6H), 6.77 – 6.67 (m, 4H), 6.56 – 6.42 (m, 10H), 3.13 – 3.04 (m, 4H), 1.33 – 1.29 (m, 24H). $^{13}$C NMR (126 MHz, Toluene-$d_8$) δ: 166.90, 146.70, 145.67, 144.24, 134.38, 132.22, 121.43, 115.53, 113.37, 29.96, 23.93, 20.60, 20.51, 20.36, 20.21, 20.05, 19.96.FD MS: 1130.47356 Calc[$M^+$]: 1130.47308

### 3.4.13: Synthesis of 3.12

**3.8** (50 mg, 0.052 mmol) and **3.5** (15 mg, 0.052 mg) was dissolved in DMF (1 mL) and heated to 135 $^{o}$C for 2 h. the solvent was removed and the residue purified *via* column chromatography (silica [$CHCl_3$:EtOAc 19:1]) to give **3.12** (28 mg, 0.024 mmol, 46 %) as a blue powder.

$^{1}$H NMR (500 MHz, Toluene-$d_8$) δ 8.94 (s, 2H), 7.25 – 7.20 (m, 6H), 6.74 – 6.68 (m, 6H), 6.67 – 6.62 (m, 4H), 6.61 – 6.57 (m, 4H), 6.51 – 6.38 (m, 10H), 3.06 – 3.00 (m, 4H), 1.27 – 1.21 (m, 24H). $^{13}$C NMR (126 MHz, Tol) δ 145.68, 144.28, 144.24, 134.37, 132.22, 132.04,

130.84, 129.63, 126.71, 126.58, 124.31, 123.99, 123.28, 122.55, 121.43, 121.18, 37.31, 32.09, 29.97, 23.93.

FD MS : 1146.45047 Calc[$M^+$]: 1146.45024

### 3.4.14: Synthesis of 3.13

**3.8** (50 mg, 0.053 mmol) and morpholine (10 µL, 0.11 mmol) was dissolved in DMF (0.5 mL) and heated to 135 $^oC$ for 2 h. the solvent was removed and the residue purified *via* column chromatography (silica [$CHCl_3$:EtOAc 19:1]) to give **3.13** (27 mg, 0.028 mmol, 52 %) as a blue powder.

$^1H$ NMR (400 MHz, Chloroform-*d*) δ 11.52 (s, 1H), 8.86 (s, 1H), 8.55 (s, 1H), 7.58 – 7.46 (m, 4H), 7.42 – 7.31 (m, 6H), 6.70 – 6.58 (m, 6H), 5.99 (dd, *J* = 7.6, 1.7 Hz, 2H), 3.97 – 3.91 (m, 4H), 3.45 – 3.39 (m, 4H), 2.81 – 2.64 (m, 4H), 1.23 – 1.14 (m, 24H) ppm. $^{13}C$ NMR (101 MHz, Chloroform-*d*) δ 166.86, 162.88, 161.93, 152.14, 147.44, 145.66, 145.48, 144.08, 138.57, 136.30, 134.34, 132.61, 130.98, 130.43, 130.04, 129.85, 127.74, 125.73, 125.38, 125.33, 124.99, 124.54, 124.43, 124.31, 123.52, 121.63, 121.11, 115.63, 113.44, 111.80, 103.13, 77.48, 77.16, 76.84, 66.94, 52.76, 29.41, 24.26, 24.21, 24.17, 24.07 ppm. FD MS : 959.40831 Calc[$M^+$]: 959.40804

### 3.4.15: Synthesis of 3.14

**3.10** (50 mg, 0.053 mmol) and morpholine (10 uL, 0.11 mmol) was dissolved in DMF (0.5 mL) and heated to 135 $^oC$ for 2 h. The solvent was removed and the residue purified *via* column chromatography

(silica [$CHCl_3$:EtOAc 19:1]) to give **3.14** (50 mg, 0.023 mmol, 99 %) as a blue powder.

$^1$H NMR (400 MHz, Chloroform-*d*) δ 11.53 (s, 1H), 8.87 (s, 1H), 8.55 (s, 1H), 7.56 – 7.31 (m, 10H), 7.05 (dd, *J* = 7.4, 1.7 Hz, 2H), 6.90-6.82 (m, 4H), 6.36 (dd, *J* = 8.1, 1.3 Hz, 2H), 3.94 (t, *J* = 4.5 Hz, 4H), 3.42 (t, *J* = 4.5 Hz, 4H), 2.72 (dt, *J* = 21.0, 6.8 Hz, 4H), 1.36 – 1.12 (m, 26H) ppm. $^{13}$C NMR (101 MHz, Chloroform-*d*) δ 166.72, 162.75, 161.80, 151.97, 147.39, 145.53, 145.36, 144.01, 138.62, 137.71, 131.44, 130.87, 129.89, 129.70, 127.61, 127.04, 126.96, 125.55, 124.78, 124.29, 124.17, 122.88, 121.44, 121.04, 116.87, 81.31, 77.34, 77.02, 76.71, 66.80, 52.63, 29.27, 24.12, 24.06 ppm. FD MS : 943.43062 Calc[$M^+$]: 943.43088

**Crystal Data** for $C_{252}H_{242}Cl_{36}N_{20}O_{25}$ (*M* =5226.84 g/mol): monoclinic, space group C2/c (no. 15), *a* = 41.9250(10) Å, *b* = 8.9649(4) Å, *c* = 33.8452(7) Å, *β* = 105.265(2)°, *V* = 12272.0(7) Å$^3$, *Z* = 2, *T* = 120(2) K, μ(CuKα) = 4.213 mm$^{-1}$, *Dcalc* = 1.414 g/cm$^3$, GooF = 1.026, 31610 reflections measured (7.804° ≤ 2Θ ≤ 147.512°), 12090 unique ($R_{int}$ = 0.0246, $R_{sigma}$ = 0.0231) which were used in all calculations. The final $R_1$ was 0.0527 (I > 2σ(I)) and $\omega R_2$ was 0.1373 (all data).

## 3.4.16: Synthesis of 3.15

Under an atmosphere of $N_2$ 4-bromobenzealdehyde (2.0 g, 10.8 mmol), copper iodide (82 mg, 0.43 mmol), bistriphenylpalladium(II)chloride (210 mg, 0.30 mmol), tetrahydrofuran (10 mL) and triethylamine (3.3 mL, 2.39 g, 23,7

mmol) were combined. Over 1 h ethynyltrimethylsilane (4.0 mL, 28.3 mmol) in THF (5 mL) was added. This was stirred overnight at 60 °C the solvent was removed and the residue extracted with hexane, filtered through kielselguhr (hexane), and purified *via* sublimation under vacuum at 60 °C to yield a yellow powder (2.1g, 10.6 mmol, 98%).

$^{1}$H NMR (400 MHz, Chloroform-*d*) δ 9.99 (s, 1H), 7.81 (d, *J* = 8.3 Hz, 2H), 7.60 (d, *J* = 8.3 Hz, 2H), 0.27 (s, 9H) ppm. $^{13}$C NMR (101 MHz, Chloroform-*d*) δ 191.55, 135.71, 132.61, 129.56, 103.96, 99.15, -0.08, -0.38 ppm. ESI MS : 202.0819 Calc[$M^+$]: 202.0813

### 3.4.17: Synthesis of 3.16

**3.15** (500 mg, 2.48 mmol) was dissolved in methanol (30 mL) and dichloromethane (1 mL) then $K_2CO_3$ (500 mg, 3.61 mmol) was added, this was stirred at RT for 1.5 h. $Et_2O$ (50 mL) was added and the solution washed with water (2 x 50 mL) and dried on $MgSO_4$ yielding **3.16** as a yellow powder (0.258 g, 1.98 mmol, 80%).

$^{1}$H NMR (400 MHz, Chloroform-*d*) δ 10.03 (s, 1 H) 7.85 (d, *J*=8.3 Hz, 2 H) 7.65 (d, *J*=8.3 Hz, 2 H) 3.30 (s, 1 H) ppm. $^{13}$C NMR (101 MHz, Chloroform-*d*) δ 191.01, 135.63, 132.37, 129.14 ,127.97, 82.29, 80.71 ppm. EI MS :130.0413 Calc[$M^+$]: 130.0418

### 3.4.18: Synthesis of 3.17

**3.16** (258 mg, 1.98 mmol) was dissolved in pyrrole (20 mL) under $N_2$. To this trifluoroacetic acid (0.01 mL, 0.13 mmol) was added, the

mixture was stirred at RT for 5 min then NaOH (500 mg, 5 mmol) was added and the mixture was stirred for 2 m. Following filtration, the solvent was removed *in vacuo.* The resulting product was purified by column chromatography (silica, [$CH_2Cl_2$: Hexane] [1:1]) and triturated with pentane yielding **3.17** as a white powder (53%).

$^1$H NMR (400 MHz, Chloroform-*d*) δ 7.93 (br. s., 2 H) 7.44 - 7.48 (m, 2 H) 7.16 - 7.20 (m, 2 H) 6.72 (td, *J*=2.63, 1.61 Hz, 2 H) 6.17 (q, *J*=2.63 Hz, 2 H) 5.91 (dd, *J*=3.33, 2.52 Hz, 2 H) 5.49 (s, 1 H) 3.07 (s, 1 H) ppm. $^{13}$C NMR (101 MHz, Chloroform-*d*) δ 142.97, 132.43, 131.88, 128.43, 120.76, 117.49, 108.57, 107.46, 83.45, 77.25, 43.86 ppm. ESI MS formula expected, obtained: ESI MS: 246.1106 Calc[$M^+$]: 246.1157

### 3.4.19: Synthesis of 3.18

**3.17** (246 mg,1 mmol) was dissolved in dichloromethane (20 mL) and cooled to 0 $^o$C. 2,3-Dichloro-5,6-dicyano-1,4-benzoquinone (330 mg, 1.1 mmol ) in dichloromethane (80 mL) was added slowly and the mixture stirred for 2 h. Triethylamine (6.3 mL, 45.5 mmol) and boron trifluoride diethyl etherate (6 mL, 4.86 mmol) were added rapidly, the mixture was warmed to RT stirred for 6 h. The solution was washed with water (200 mL), dried over $MgSO_4$, filtered and the solvent removed *in vacuo*. The resulting product was purified by column chromatography (silica, [$CH_2Cl_2$:Hexane ] [1:1]) to yield **3.18** (0.143 g, 0.49 mmol, 49%) as a red powder.

$^{1}$H NMR (400 MHz, Chloroform-*d*) δ 7.96 (s, 2 H) 7.66 (d, *J*=8.41 Hz, 2 H) 7.55 (d, *J*=8.41 Hz, 2 H) 6.92 (d, *J*=4.14 Hz, 2 H) 6.57 (d, *J*=1.00 Hz, 2 H) 3.27 (s, 1 H) ppm. $^{13}$C NMR (101 MHz, Chloroform-*d*) δ 144.48, 140.47, 134.71, 134.03, 132.12, 131.38, 130.40, 124.85, 118.73, 82.52, 79.87 ppm. ESI MS= 293.1048 (MH+) 315.0872 (M +Na) Calc: 293.1061

**Crystal Data** for $C_{17}H_{11}BF_2N_2$ (*M* =292.09 g/mol): triclinic, space group P-1 (no. 2), *a* = 7.6808(6) Å, *b* = 7.7447(6) Å, *c* = 12.2054(11) Å, *a* = 81.837(7)°, *β* = 75.361(7)°, *γ* = 75.384(6)°, *V* = 677.36(10) Å$^3$, *Z* = 2, *T* = 120(2) K, μ(CuKα) = 0.862 mm$^{-1}$, *Dcalc* = 1.432 g/cm$^3$, GooF = 1.033, 3885 reflections measured (11.85° ≤ 2Θ ≤ 147.17°), 2582 unique ($R_{int}$ = 0.0202, $R_{sigma}$ = 0.0241) which were used in all calculations. The final $R_1$ was 0.0387 (I > 2σ(I)) and $wR_2$ was 0.1048 (all data).

## 3.4.20: Synthesis of 3.19

Under an atmosphere of $N_2$ **3.8** (100 mg, 0.105 mmol), **3.18** (31 mg, 0.105 mmol), copper iodide (5 mg, 0.026 mmol) and palladium (0) tetrakistriphenylphosphine (30 mg, 0.026 mmol) were dissolved in dry degassed THF (20 mL). To this triethylamine (2 mL, 14.0 mmol) was added, this was heated to reflux for 16 h. The solution was filtered through kieselguhr, poured into HCl (2M, 100 ml) and extracted into $CHCl_3$ (3 x 30 mL) dried over $MgSO_4$, filtered and the solvent removed. The residue was purified *via* column

chromatography (silica [$CHCl_3$]) to give **3.19** (37 mg, 0.032 mmol, 31%) as a pinkish red powder.

$^1$H NMR (400 MHz, Chloroform-d) δ 11.94 (s, 1H), 9.04 (s, 1H), 8.88 (s, 1H), 7.95 (s, 2H), 7.77 (d, J = 8.3 Hz, 2H), 7.59 – 7.34 (m, 14H), 7.10 (dd, J = 7.5, 1.6 Hz, 2H), 7.00 – 6.85 (m, 7H), 6.56 (d, J = 6.2 Hz, 2H), 6.45 (dd, J = 8.2, 1.3 Hz, 2H), 2.81 – 2.69 (m, 4H), 1.25 – 1.19 (m, 24H) ppm. $^{13}$C NMR (101 MHz, Chloroform-d) δ 162.50, 145.67, 144.55, 143.85, 140.29, 138.25, 132.37, 131.56, 130.69, 130.57, 130.43, 127.33, 127.21, 125.81, 125.69, 124.53, 124.39, 123.40, 122.80, 122.25, 118.91, 117.87, 102.02, 91.26, 77.48, 77.16, 76.84, 29.85, 29.48, 24.31, 24.24, 24.15, 24.09 ppm. FD MS : 1164.43826 Calc[$M^+$]: 1164.43796

### 3.4.21: Electrochemical and Optical Investigations

UV/visible absorption spectra were recorded on Perkin-Elmer Lambda 25 spectrometer. Cyclic voltammetric and coulometric studies were conducted using an Autolab PGSTAT20 potentiostat. DCM was dried *via* distillation under nitrogen on calcium hydride. Standard cyclic voltammetry was carried out under an atmosphere of argon using a three electrode arrangement in a single compartment cell. Electrodes used in the cell were as follows; A glassy carbon working electrode, a Pt wire secondary electrode and a calomel reference electrode, chemically isolated from the test solution *via* a bridge tube containing electrolyte solution and fitted with a porous vycor frit. The solutions were $10^{-3}$ M in molecule of interest and 0.4

M in $[Bu_4N][BF_4]$ as the supporting electrolyte. Redox potentials are quoted versus the ferrocenium-ferrocene couple used as an internal reference. Compensation for internal resistance was not applied.

The UV/vis spectroelectrochemical experiments were carried out with and optically transparent electrochemical cell (modified quartz cuvette, optical pathlength: 0.5 mm). A three electrode configuration, consisting of Pt/Rh gauze working electrode, a Pt wire secondary electrode (in a fritted PTFE sleeve) and a saturated calomel electrode, as reference, chemically isolated from the test solution *via* a bridge tube containing electrolyte solution and terminated in a porous frit, was used in the cell. The potential at the working electrode was controlled by a Sycopel scientific Ltd DD10M potentiostat. The UV/vis spectra were recorded on a Perkin Elmer Lambda 16 spectrophotometer. The cavity was purged with dinitrogen and temperature control at the sample was achieved by flowing cooled dinitrogen across the surface of the cell.

## 3.5: References


(1) C. Wang, W. Hu, Y. Liu, D. Zhu *Chem. Rev,* **2012**, *112*, 2208.
(2) J. E.Anthony, *Chem. Rev,* **2006**, *106*, 5028.
(3) M. Mottaghi, G.Horowitz, *Org Electron,* 2006, 7, 528
(4) G. Bernard, P. Christophe, *Polym. Int,* **2006**, *55*.
(5) A. C.Bernanose, P. *J.*Vouaux, *Chim. Phys* **1953**, *50*, 64.
(6) C. W.Tang, S. A.VanSlyke, *Appl. Phys. Lett,* **1987**, *51*, 913.
(7) M. R. Wasielewski, *Acc. Chem. Res,* **2009**, *42*, 1910.
(8) K.Susumu, P. R.Frail, P. J.Angiolillo, M. J.Therien, *JACS,* **2006**, *128*, 8380.
(9) V.Lloveras, J.Vidal-Gancedo, T. M.Figueira-Duarte, J.-F.Nierengarten, J. J.Novoa, F.Mota, N.Ventosa, C.Rovira, J.Veciana, *JACS,* **2011**, *133*, 5818.
(10) N.Sakai, R.Bhosale, D.Emery, J.Mareda, S.Matile, *JACS,* **2010**, *132*, 6923.
(11) P. W.Anderson, P. A.Lee, M.Saitoh, *Solid State Commun,* **1973**, *13*, 595.
(12) R. Pfattner, M. Jaggi, S. Liu, S. Decurtins, G. Bratina, J. Veciana, M. Mas-Torrent, C. Roviraa *J Mater Chem,* **2013**, *1*, 3985.
(13) E. A.Weiss, M. J.Ahrens, L. E.Sinks, A. V.Gusev, M. A.Ratner, M. R.Wasielewski, *JACS,* **2004**, *126*, 5577.
(14) C. E.Smith, S. O.Odoh, S.Ghosh, L.Gagliardi, C. J.Cramer, C. D.Frisbie, *JACS,* **2015**, *137*, 15732.
(15) M.Kuss-Petermann, O. S.Wenger, *JACS,* **2016**, *138*, 1349.
(16) K.Hasharoni, H.Levanon, S. R.Greenfield, D. J.Gosztola, W. A.Svec, M. R.Wasielewski, *JACS,* **1996**, *118*, 10228.
(17) S. R.Greenfield, W. A.Svec, D.Gosztola, M. R.Wasielewski, *JACS,* **1996**, *118*, 6767.
(18) M. P.Debreczeny, W. A.Svec, E. M.Marsh, M. R.Wasielewski, *JACS,* **1996**, *118*, 8174.
(19) M. E.El-Khouly, J. H.Kim, K.-Y. Kay, C. S.Choi, O.Ito, S.Fukuzumi, *Chem. Eur. J,* **2009**, *15*, 5301.
(20) D.Villamaina, S. V.Bhosale, S. J.Langford, E.Vauthey, *PCCP,* **2013**, *15*, 1177.
(21) N.Banerji, S. V.Bhosale, I.Petkova, S. J.Langford, E.Vauthey, *PCCP,* **2011**, *13*, 1019.
(22) D.Villamaina, M. M. A. Kelson, S. V.Bhosale, E.Vauthey, *PCCP,* **2014**, *16*, 5188.
(23) A.Granzhan, T.Riis-Johannessen, R.Scopelliti, K.Severin, *Angew. Chem. Int. Ed*, **2010**, *49*, 5515.
(24) M. F.Jacobsen, M. M.Knudsen, K. V.Gothelf, *J. Org. Chem,* **2006**, *71*, 9183.

(25) V. J.Richards, A. L. Gower, J. E Smith, E. S.Davies, D.Lahaye,; A. G Slater, W.Lewis, A. J.Blake, N. R.Champness, D. L.Kays, *Chem. Commun,* **2012**, *48*, 1751.

# Chapter 4 : Toward synthesis of a light harvesting NDI rotaxane

# 4.1: Introduction

## 4.1.1: Molecular Interlocked Molecules

Molecularly interlocked systems have generated a lot of interest as synthetic targets; in order to produce them a complex puzzle must be solved. Causing two molecules to interact with each other without forming a chemical bond may seem impossible to control. However this sort of higher order interaction is used by nature commonly in species such as proteins. It is therefore reasonable to think these interactions can be controlled, though it may require precise tuning.

The first reported molecular interlocked system was a macrocycle sitting around a rod molecule known as a rotaxane, which was generated via a statistical approach.[1] This approach involved attaching the macrocycle to a solid support resin which was then treated with two halves of a dumbbell molecule 70 times, the support being washed between each reaction. This led to a 6 % yield of the desired rotaxane. This low yield is not unexpected as there is no driving force to cause the dumbbell to form within the macrocycle, instead relying purely on the statistical chance of the two dumbbell half-units uniting within the cavity of the macrocycle, then removing all those which did not. This example proved that these species could be generated. However relying on the statistical approach would never allow for large quantities of these species to be obtained.

Since then work on the synthesis of these species has revolved around how to gain more control exploiting host-guest chemistry[2] to direct the components to assemble around each other. The most common approach involves engineering systems which utilise intermolecular interactions such as π-π interactions,[3] hydrogen bonding[4,5] and the hydrophobic effect[5] to select for the thermodynamic minima of the system when the components are associated with each other. These components can then be trapped in this state (e.g. by using large end caps of a rotaxane to block the macrocycle from slipping off) allowing the interlocked species to exist outside of the reaction conditions. Through exploitation of these interactions complex systems such as rotaxanes, Borromean rings[6] (Figure 4-1), knotanes[7,8] and extended catenane species such as Olympiadane,[9] have been prepared.

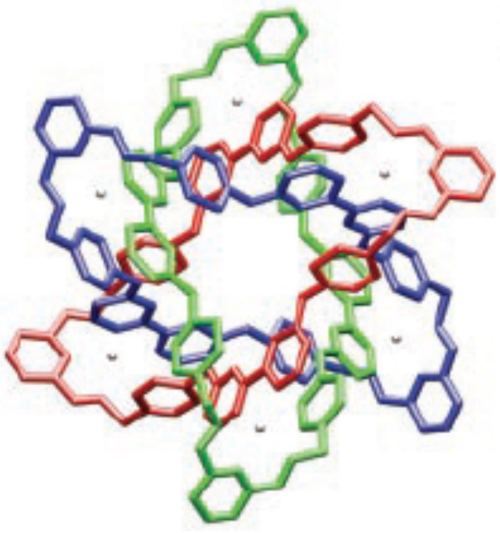

Figure 4-2: A molecular modelling image of the Borromean ring produced by Stoddart and co-workers[6]

### 4.1.2: Utilising Rylene diimide intermolecular interactions

The planar aromatic core of rylene diimides represents an easily exploitable building block for the construction of molecularly interlocked systems. The aromatic surface functions in two ways to generate favourable intermolecular interactions; the electron poor π clouds encourage the formation of π-π interactions and this large aromatic area is hydrophobic potentially driving molecular interactions.

The favourable intermolecular interactions of rylene diimides are expressed most noticeably by their poor solubility, preferring to interact with themselves rather than with solvent. It is also common for these molecules to self-assemble into ordered molecular arrays through intermolecular interactions with themselves.[10] This can be utilised to cause them to assemble into structures such as nanotubes[11] and in a similar fashion these tubular structures can be used to generate gels[12-14] (Figure 4-3). These gels are the result of higher order interactions allowing these species to be adopt complex structures comparable to those found in nature such as vesicles and β-sheets giving a greater understanding of how these species operate.

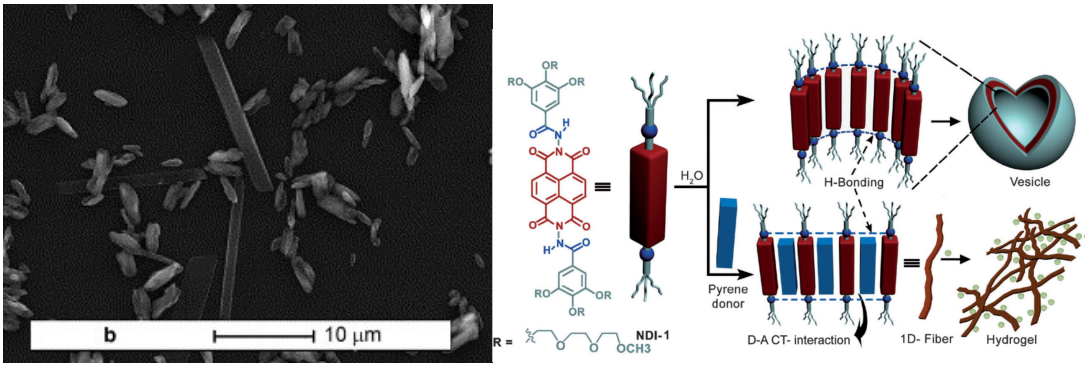


Figure 4-4: Environmental scanning electron microscopy image of a NDI based nanotube (left).[11] A diagram showing mechanisms by which NDI can assemble into higher order structure's (right).[14]

There are also several examples of rylene interactions being used to make more intimate molecularly interlocked systems. These systems typically involve the interaction of the aromatic core of the rylene with a complementary yet distinct molecular entity. By utilising such interactions, macrocycles can be directed to encircle rylene diimides which can then be locked into place to generate mechanically bound species. This allows for species such as catenanes[15,16] to be synthesised (Figure 4-6). These species are created by using an electron rich naphthalene crown ether which is complimentary to the electron poor NDI, encouraging them to interact and the species can be interlocked.

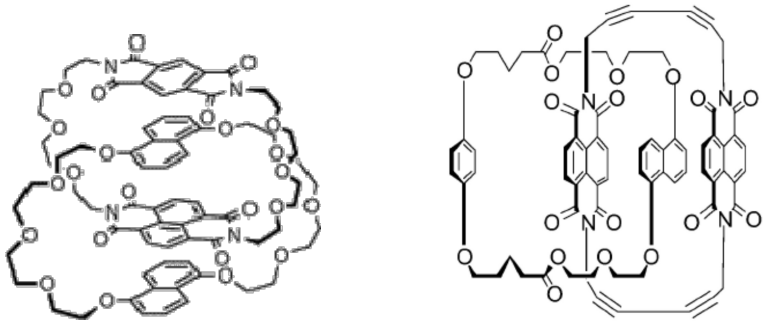

Figure 4-5: Two catenanes which have been prepared using NDIs and crown ether macrocycle (left,[15] right[16])

Using a similar approach rotaxanes can be synthesised, by utilising a crown ether macrocycle and a rylene diimide furnished with bulky stopper groups resembling a molecular dumbbell. Such a molecule has been prepared previously within the Champness group (Figure 4-7) Utilising a perylene diimide furnished with stopper groups based on a tetraphenylmethane framework as the guest for the macrocycle.[17] The rotaxane was formed by using elevated temperature to slip[18] the macrocycle over the bulky stoppers, where it became trapped upon the aromatic core. The redox properties of the molecule were found to change upon complexation, the first reduction generating a radical anion, a switchable state of the rotaxane, while the second reduction caused dethreading due to electronic repulsion between the components.

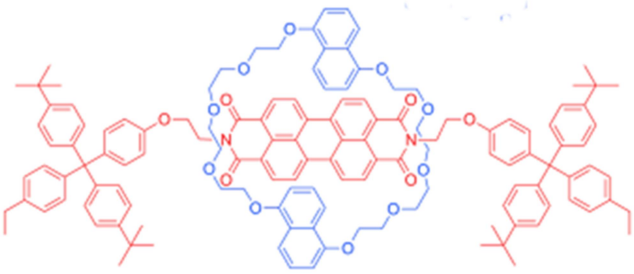

Figure 4-8: Perylene diimide crown ether rotaxane prepared by the Champness group[17]

### 4.1.3: Light harvesting systems utilising BODIPY

The BODIPY family of molecules have attracted a lot of attention as an excellent candidate to act as a light harvester in many molecular systems[19-23] where visible light is typically utilised to initiate electron transfer in photovoltaic systems. This is in part due to their narrow, highly absorbing bands within the visible region, low Stokes shift (so little loss of energy) and finally the excellent synthetic mutability of these species.

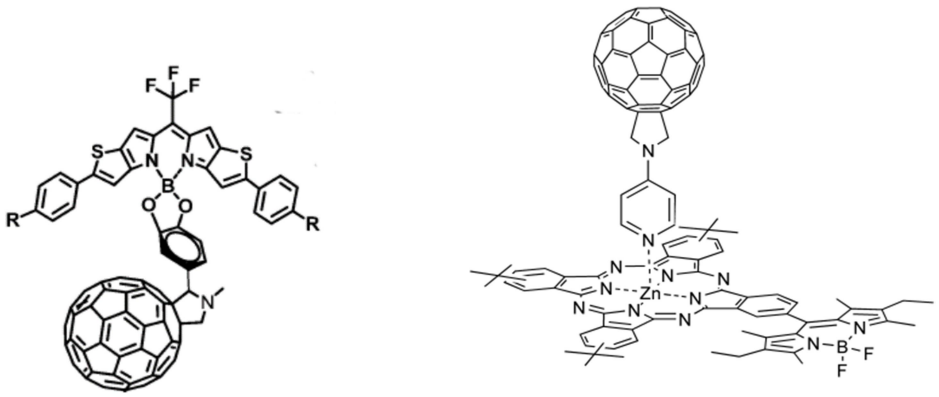


Figure 4-9: Structures of the BODIPY fullerene dyad[26] (left) and the BODIPY–zinc phthalocyanine furnished with a fullerene[27] (Right)

A number of light harvesting donor acceptor species have utilised the absorbing properties of BODIPY, allowing electron transfer to occur using visible light. A series of anthracene BODIPY "cassettes"[24,25] have been shown to readily undergo energy transfer from the BODIPY to the anthracene after photoexcitation. There are also examples of BODIPYs acting within donor acceptor species when substituted with fullerenes. Examples of this include the core substituted BODIPY fullerene dyad (Figure 4-10), which was seen to

undergo ultrafast PET with slow charge recombination in transient absorption studies.[26] Another example is a BODIPY–zinc phthalocyanine dyad coordinated to pyridyl-fullerene,[27] which upon photoexcitation of the BODIPY, the energy is transferred and causes an electron transfer between the phthalocyanine and the fullerene.

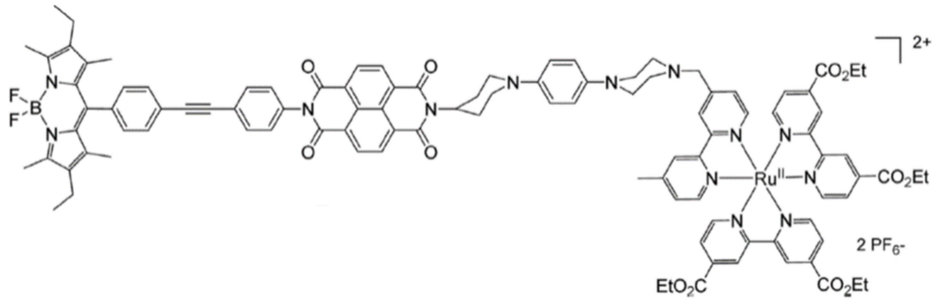


Figure 4-11: The structure of a bodipy NDI tetrad[28]

BODIPYs have been shown to undergo electron transfer to NDIs after photoexcitation, an NDI-BODIPY tetrad (Figure 4-12)[28] exhibits this phenomenon. After excitation; the BODIPY transfers an electron to the NDI generating a charge separated state, which unusually can be excited a second time to generate a second charge separated state, with the electron transferring to the Ru unit. This dual charge separation uniquely imitates those observed with chlorophyll photosystems.

## 4.2: Aim and Objectives

The intention of this project was to create a rotaxane based off the NDI rod (**4.3**, Figure 4-13) and crown ether macrocycle architecture (**4.8**, Figure 4-14). In this case however the NDI would incorporate BODIPY units to attempt to act as the stopper units. This would allow testing of the robustness of the macrocycles ability to encapsulate the NDI while seeing if the BODIPY units were suitable caps.

BODIPY is also interesting as it functions as an excellent visible light harvester and it has been postulated that the energy absorbed could be transferred to an NDI exciting it. This excitation could be enough to cause a disruption in the host guest interactions of the NDI and macrocycle which could perhaps be utilised to initiate a shift in the position of the macrocycle.

Furthermore the electronic orbitals of the NDI rod could be changed via thionation of its carbonyls (**4.10**-**4.13**, Figure 4-15). This would lower the energy needed to excite the NDI making the excitation easier to achieve. This would also allow for an exploration of the photophysics of these species, hopefully resulting in insight as to how the electronics of the NDI species can be manipulated for more efficient energy transfer.

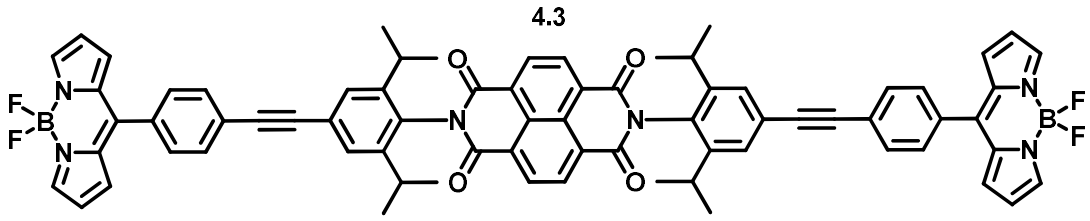


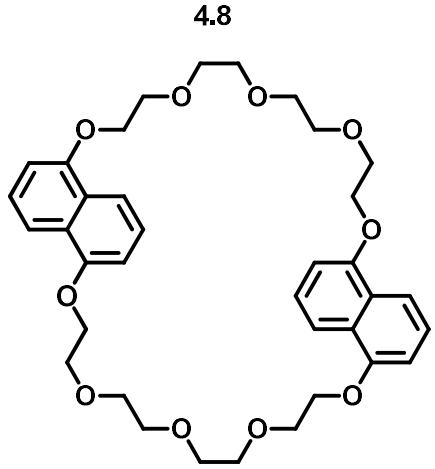


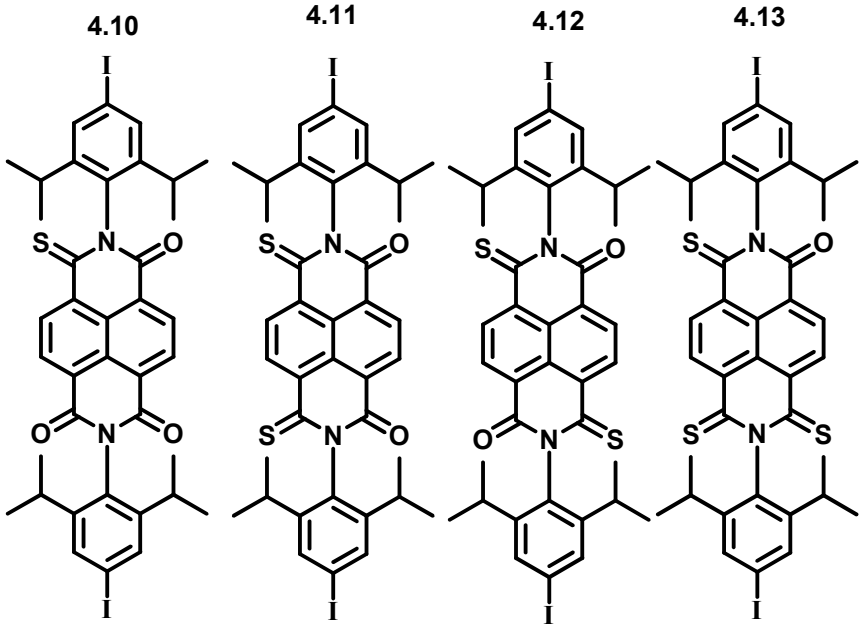


Figure 4-16: Target molecules of Chapter 4

## 4.3: Results and discussion

### 4.3.1: Synthesis

In order to allow further synthetic modification of the NDI, so that more complexity could be added at a later date, a broadly reactive amine species **4.1** was selected, there are large libraries of coupling reactions available for aryl bromides. **4.1** was prepared via bromination of 2,6-diisoproylaniline following a literature procedure[29] (Scheme 4-1).

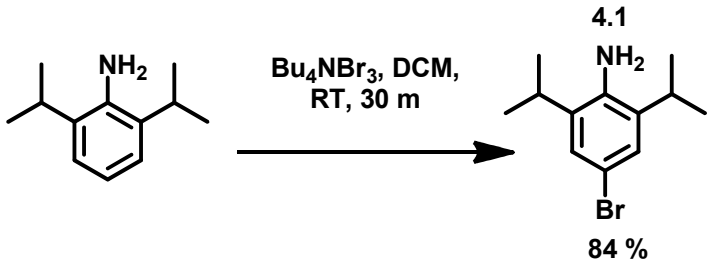


Scheme 4-1: Synthesis of **4.1**

**4.1** was then used to imidise NDA to create **4.2** (Scheme 4-2), this was performed at high temperature using imidazole as the solvent. These conditions overcame the less nucleophilic character of the aryl amine and also the steric effects of the isopropyl groups whose bulky nature limit the possible angles of successful nucleophilic attack.

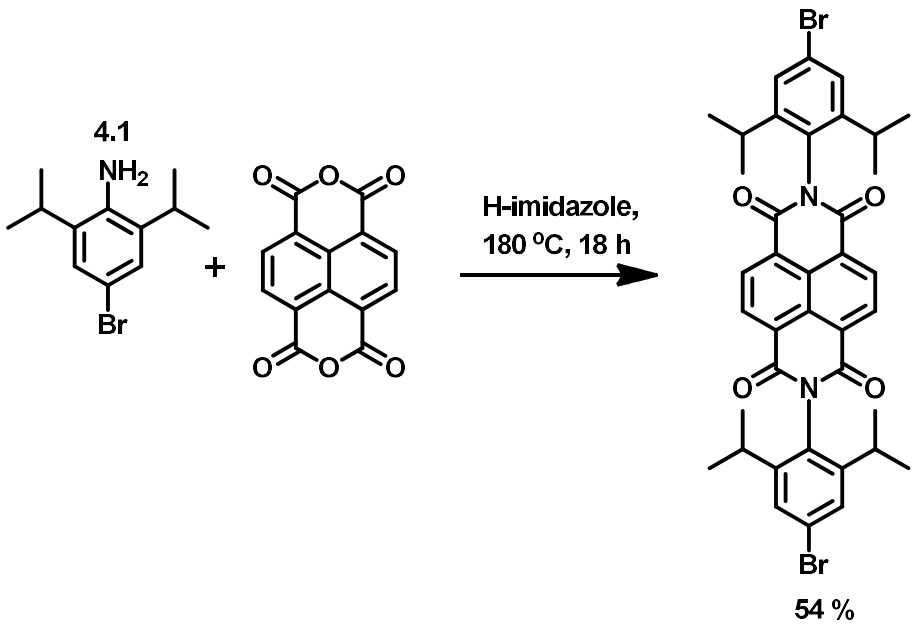


Scheme 4-2: Synthesis of **4.2**

Attempts were made to functionalise **4.2** via reaction at the aryl bromide. Sonogashira reaction conditions were used to couple with **3.18** in order to prepare **4.3** (Scheme 4-3). Unfortunately these conditions did not generate the desired product, instead leaving the unreacted NDI starting material. One example of this reaction is described in the literature as "somewhat erratic"[30], often giving low yields; despite repeated attempts **4.3** was not obtained. This is likely due to low reactivity of the aryl bromide, as the unreacted bromide was still present after several days of reaction. A strategy to probe and overcome this low reactivity was made by trying convert the bromide into a more reactive azide, which could then undergo click chemistry to couple to the BODIPY. **4.2** also proved to be unreactive towards sodium azide and the starting material was recovered from the reaction mixture.

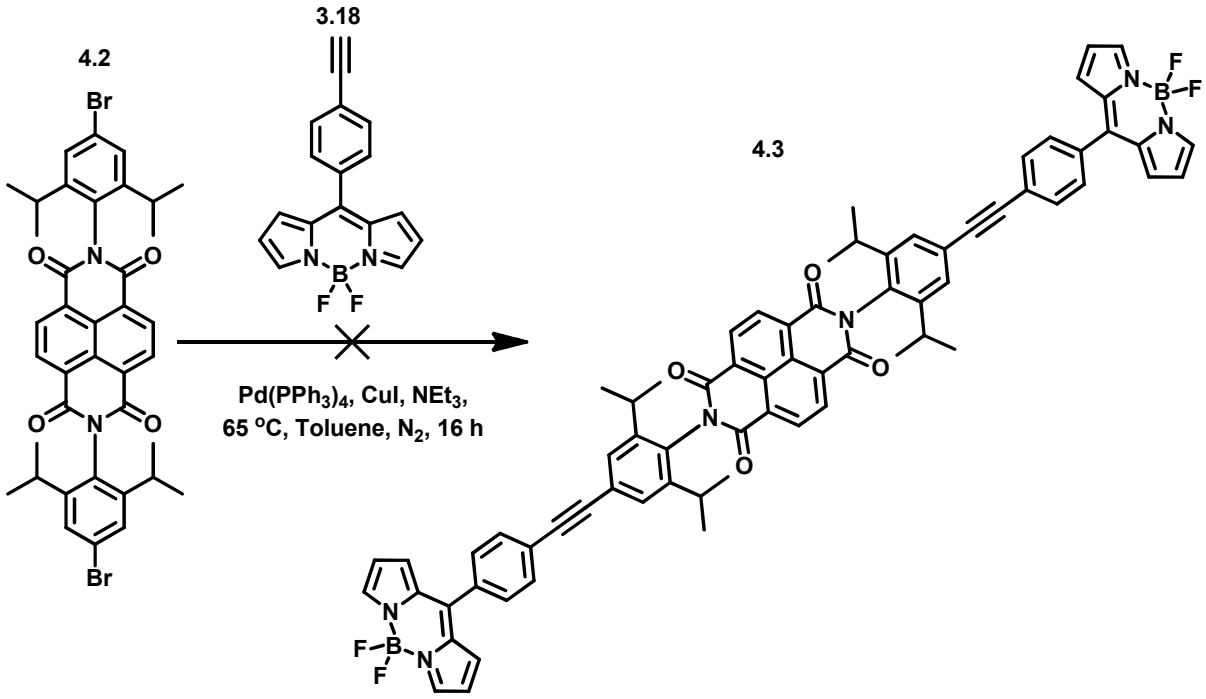


Scheme 4-3: Attempted synthesis of **4.3**

A more reactive precursor was required to improve coupling efficiency, to this end the aryl iodide **4.4** was proposed. Once again the starting point for this product was 2,6-diisoproylaniline which was iodinated using standard literature conditions[31] (Scheme 4-4**Error! Reference source not found.**) to generate **4.4** this was then reacted with NDA, using the same conditions used to generate **4.2**, to yield **4.5**.

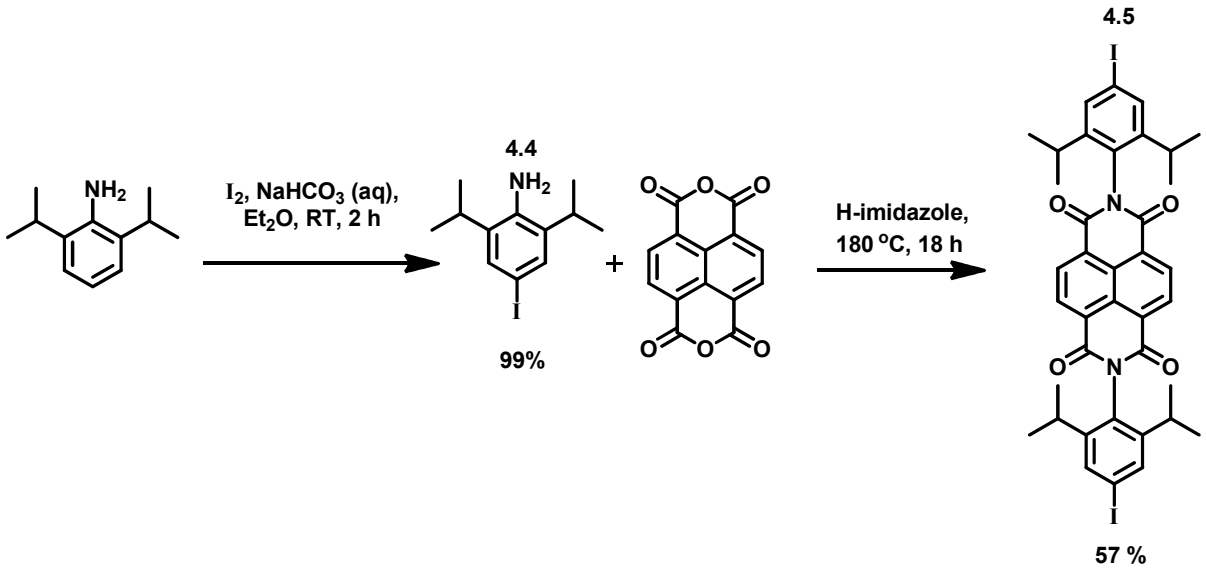


Scheme 4-5: Synthesis of **4.4** and **4.5**

As iodine is a more reactive leaving group than bromine, it was expected that the Sonogashira reaction would proceed more successfully, the oxidative addition step occurring more readily. The same Sonogashira conditions for the attempted reaction of **4.2** were used with **4.5.** The increased reactivity of the aryl iodide allowed for the reaction to successfully proceed and as such **4.3** was isolated and characterised (Scheme 4-6). Single crystals suitable for X-Ray Diffraction of **4.3** were grown via vapour diffusion of MeOH into a solution of **4.3** in chloroform (Figure 4-17).

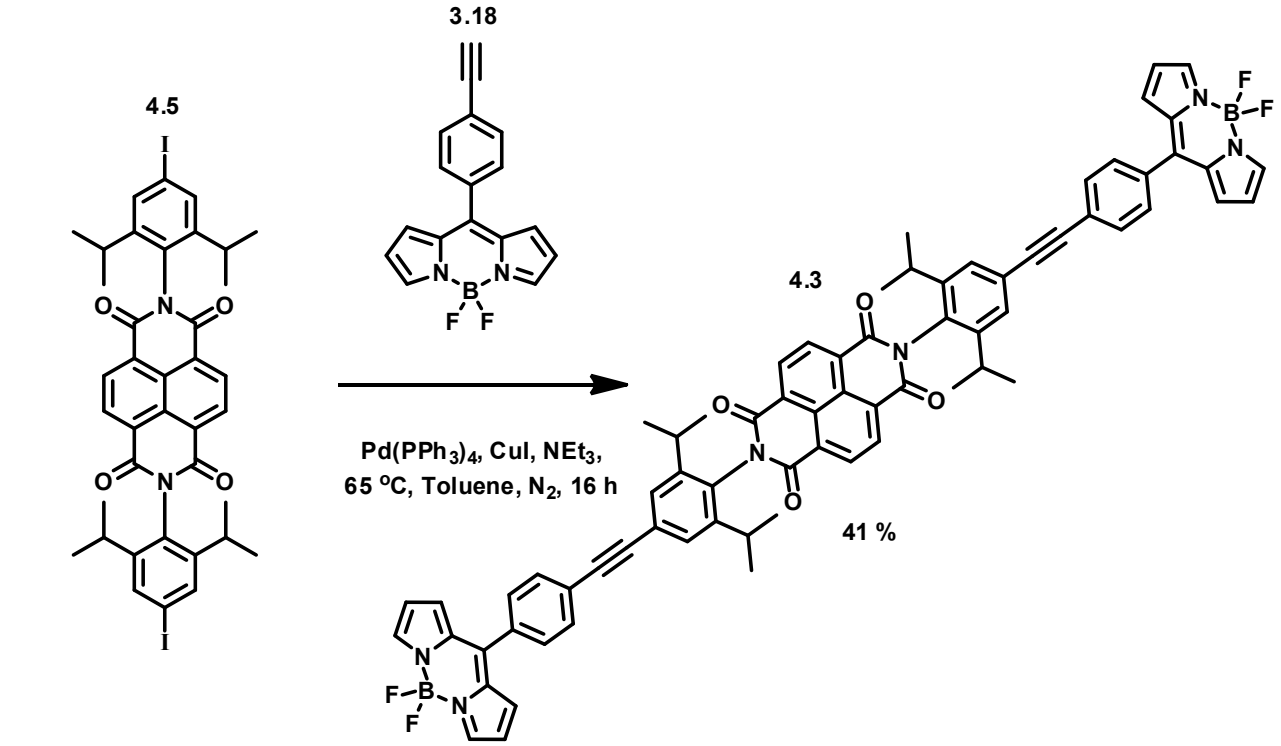


Scheme 4-7: Synthesis of **4.3**

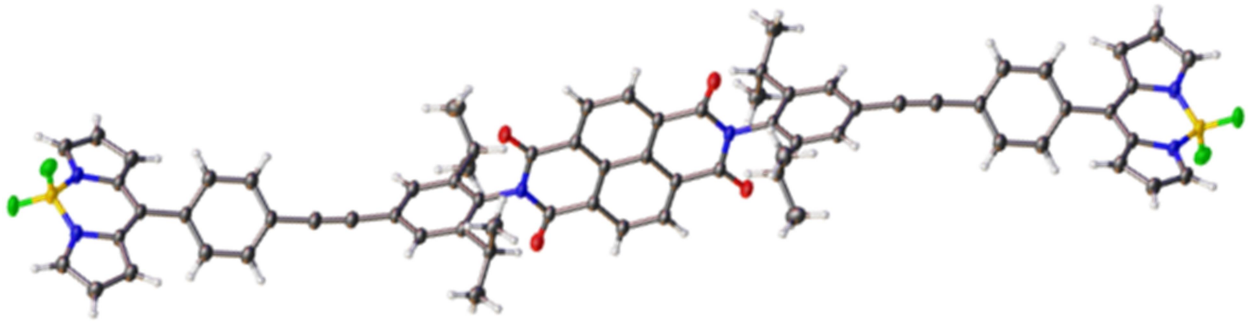

Figure 4-18: X-ray crystal structure of **4.3**

In order to prepare a rotaxane, a macrocycle that has been shown to strongly interact with the NDI aromatic core was selected **4.8**. This crown ether macrocycle has been used to generate NDI catenanes and rotaxanes, and with PDIs by slipping onto the rylene at elevated temperature.[32]

This macrocycle was prepared following a literature procedure,[33] by first furnishing tetraethylene glycol with two tosyl groups *via* reaction with tosyl chloride to produce **4.6** (Scheme 4-8). Reaction with 1,5-dihydroxynaphthalene was carried out under high dilution conditions to help selection of the desired di glycol functionalised product **4.7** rather than a polymeric product. **4.7** was then reacted with a second equivalent of 1,5-dihydroxynaphthalene, once again under high dilution conditions to avoid polymerisation, closing the macrocyclic ring and creating **4.8**.

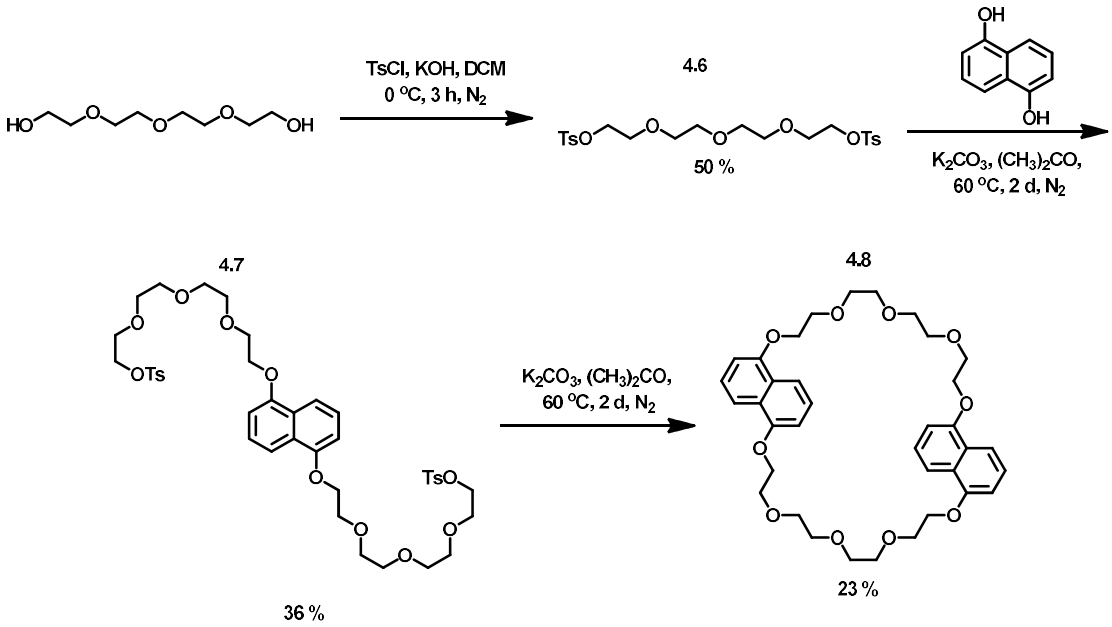


Scheme 4-9: Synthesis of **4.6**-**4.8**

Binding of the macrocycle to **4.3** was attempted using a slipping procedure. This involves using a mixture of $CHCl_3$ and MeOH to encourage formation of the rotaxane. The highly polar MeOH was anticipated to promote the interaction between the macrocycle and the non-polar aromatic core of the NDI, limiting the hydrophobic surface area of the NDI, while $CHCl_3$ acts only to solubilise the NDI. LiBr was added to further promote the macrocycle-rod interaction. The reaction was carried out at 70 °C in a pressure tube over 14 days (Scheme 4-10). Unfortunately no trace of the desired rotaxane was observed.

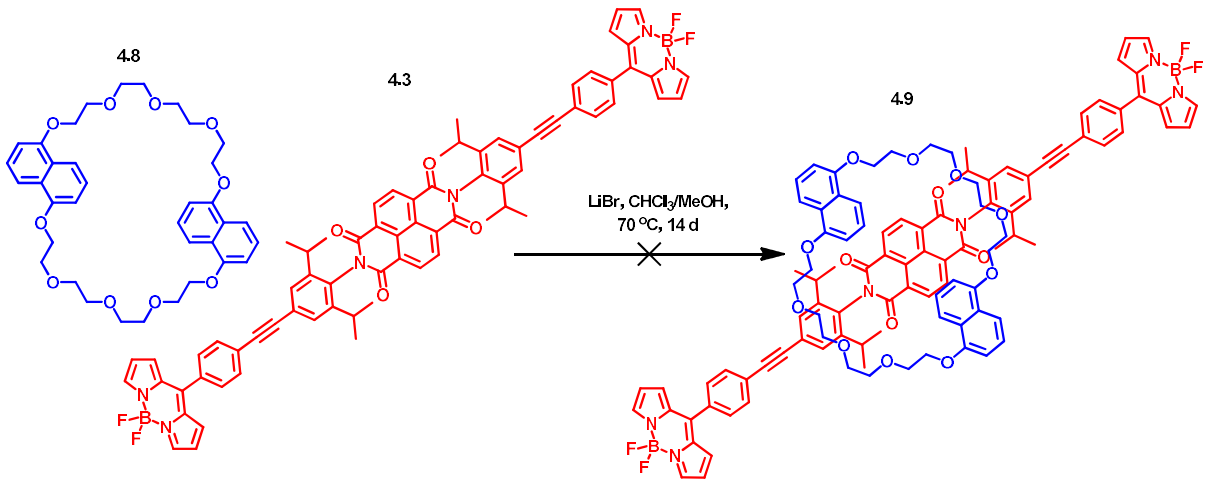


Scheme 4-11: Attempted synthesis of **4.9**

There are several reasons postulated for the absence of the desired product. First there is a possibility that the BODIPY unit being used to cap the rotaxane was simply to small, allowing the macrocycle to easily de-thread in ambient conditions despite this association being expected to be the lowest energy state of the system. Another consideration is that the rotaxane may not represent a

thermodynamic minimum, as there are several differences between this system and other interlocked NDI systems reported in the literature. For instance the isopropyl groups are positioned above and below NDI aromatic core, which may have also reduced efficient π-π interactions between the macrocycle and the NDI aromatic core. Unfortunately the failed attempted synthesis of the rotaxane showed that major modifications to the architecture of the molecule would have to be undertaken in order to attempt to resolve the problems encountered. This would involve removal of isopropyl groups which allowed for the molecule to be synthesised in the first instance and an entirely new series of molecules be created via different synthetic methods. Rather than have a multi-step synthetic investigation be entirely wasted further effort was made to probe this system to see if the molecule had interesting exploitable optical and electronic properties.

In order to produce further interesting species based on **4.3** an effort was to modulate the electronics of **4.3.** Via thionation the electronics of the NDI could be altered, this would create a series of molecules which had the potential to undergo photoinduced electron transfer, as thionation makes NDIs more readily reducible,[34] the BODIPYs could act as donor species. Direct thionation of **4.3** using Lawesson's reagent in refluxing toluene however did not give rise to any of the expected thionated products. Instead what was observed was

primarily the decomposition of **4.3**, none of the decomposition species were isolated however small amounts of **4.3** were recovered**.**

It was assumed that the decomposition was the result of an unexpected reaction with the BODIPY species. In order to avoid this problem it was proposed that first **4.5** be thionated then **3.18** be coupled to the now thionated NDIs. **4.5** was thionated using the same conditions as the attempted thionation of **4.3**: Lawesson's reagent refluxing in toluene (Scheme 4-12). The thionation gave rise to a series of partially thionated NDIs **4.10**-**4.13.** Despite the reaction now yielding the desired products, the overall yield was low, with 50 % of the starting material being recovered and 23 % being lost to decomposition. The major product of the reaction was the mono-thionated species **4.10**, around 10 times less of the two observed di-thionated isomers (**4.11** and **4.12**) were created none of the third possible isomer was generated. The tri-thionated species **4.13** was observed with MALDI-MS however was not isolated, due to the reaction generating only trace amounts of this species. It should also be noted that thionation of this species seems to be highly unfavourable due to the low overall yield and the low conversion to the higher thionated species. Increased reaction times did show a marginal increase in the yield of di-thionated products (by around 1 %), however lowered the total yield of thionated products and increased the amount of starting material that was lost to decomposition.

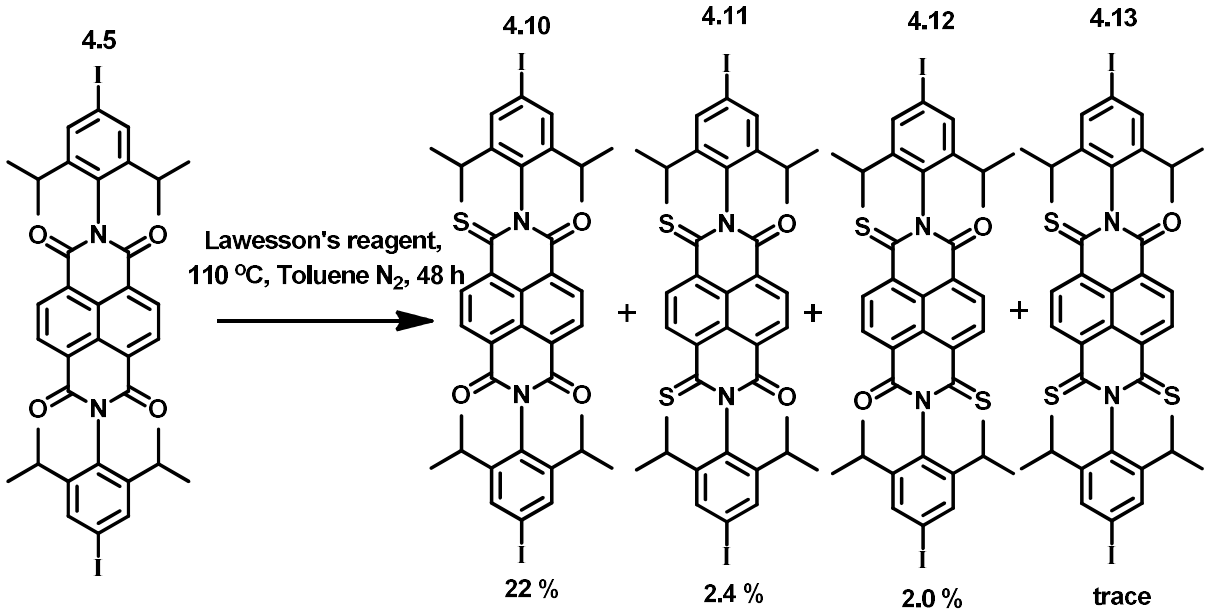


Scheme 4-13: Synthesis of **4.10-4.13**

**4.10** was selected to create a thionated analogue of **4.3,** primarily as it was the main product of the thionation reaction so a suitable amount of it could be accessed. A Sonogashira coupling between **4.10** and **3.18** was performed (Scheme 4-14), using the conditions which successfully created **4.3**. **4.14** was detected via MLADI MS of the crude reaction mixture. However when purification was attempted it became clear that **4.14** was unstable and was decomposing as the impurities were regenerated following purification, TLC confirming the instability of the species, possibly due to light initiated decomposition. Unfortunately **4.14** was not isolated and over time the sample decomposed into multiple unidentifiable species.

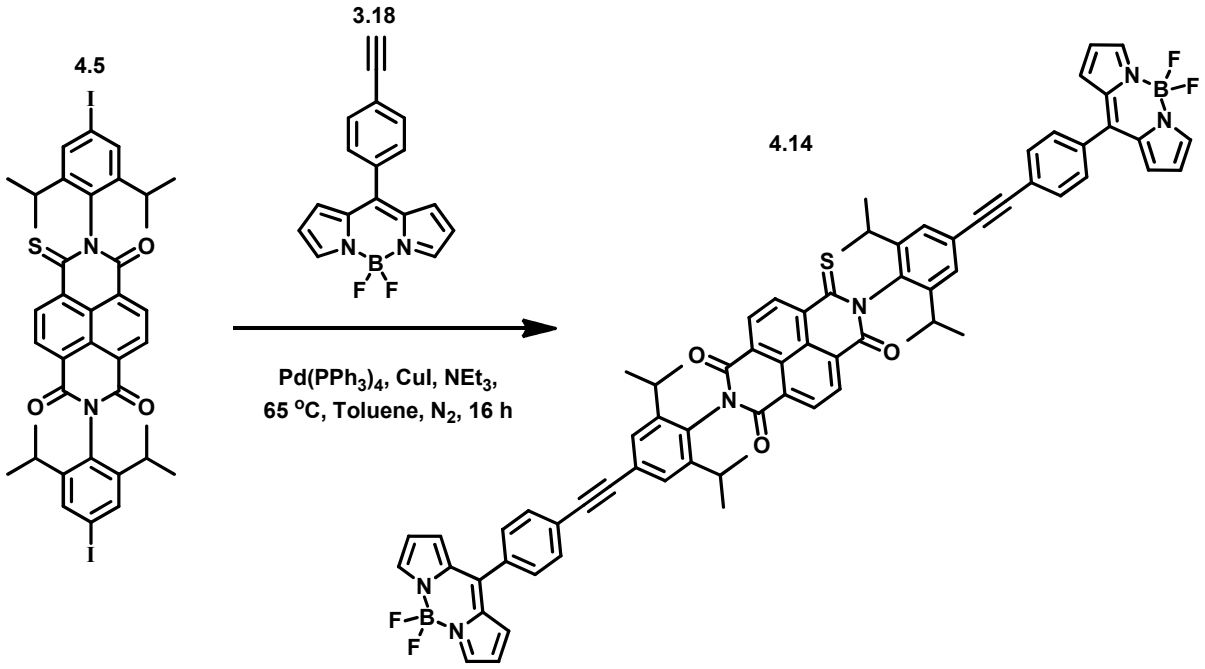


Scheme 4-15: Synthesis of **4.14**

## 4.3.2: Cyclic voltammetry

The redox properties of **4.3** were investigated using cyclic voltammetry. Though no reversible oxidative processes were detected, 3 distinct reductions were clearly observed (Figure 4-20).

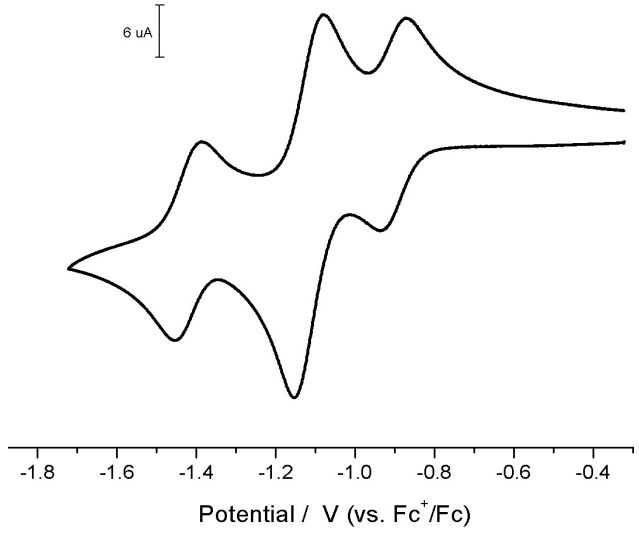


Figure 4-19: Cyclic voltammogram of **4.3** in DCM with 0.4 M $[Bu_4N][BF_4]$supporting electrolyte, at a scan rate of 100 $mVs^{-1}$ at room temperature

These reductions can easily be assigned, the first single electron reduction is related to the first reduction of the NDI core, at -0.901 V vs $Fc^+/Fc$, a potential typical for an NDI. After this can clearly be seen a two electron reduction (having twice the current response), which is assigned to the two BODIPY units being reduced at the same potential, -1.12 V vs $Fc^+/Fc$. Finally, the last reduction is assigned to the second reduction of the NDI core, at -1.42 V vs $Fc^+/Fc$, again at a potential typical of the second reduction of an NDI. The fact that the NDI's redox properties are not greatly perturbed is due to an electronic node at the nitrogen of the imide in the NDI molecular orbital[35] separating the NDI core from the BODIPY appendages.

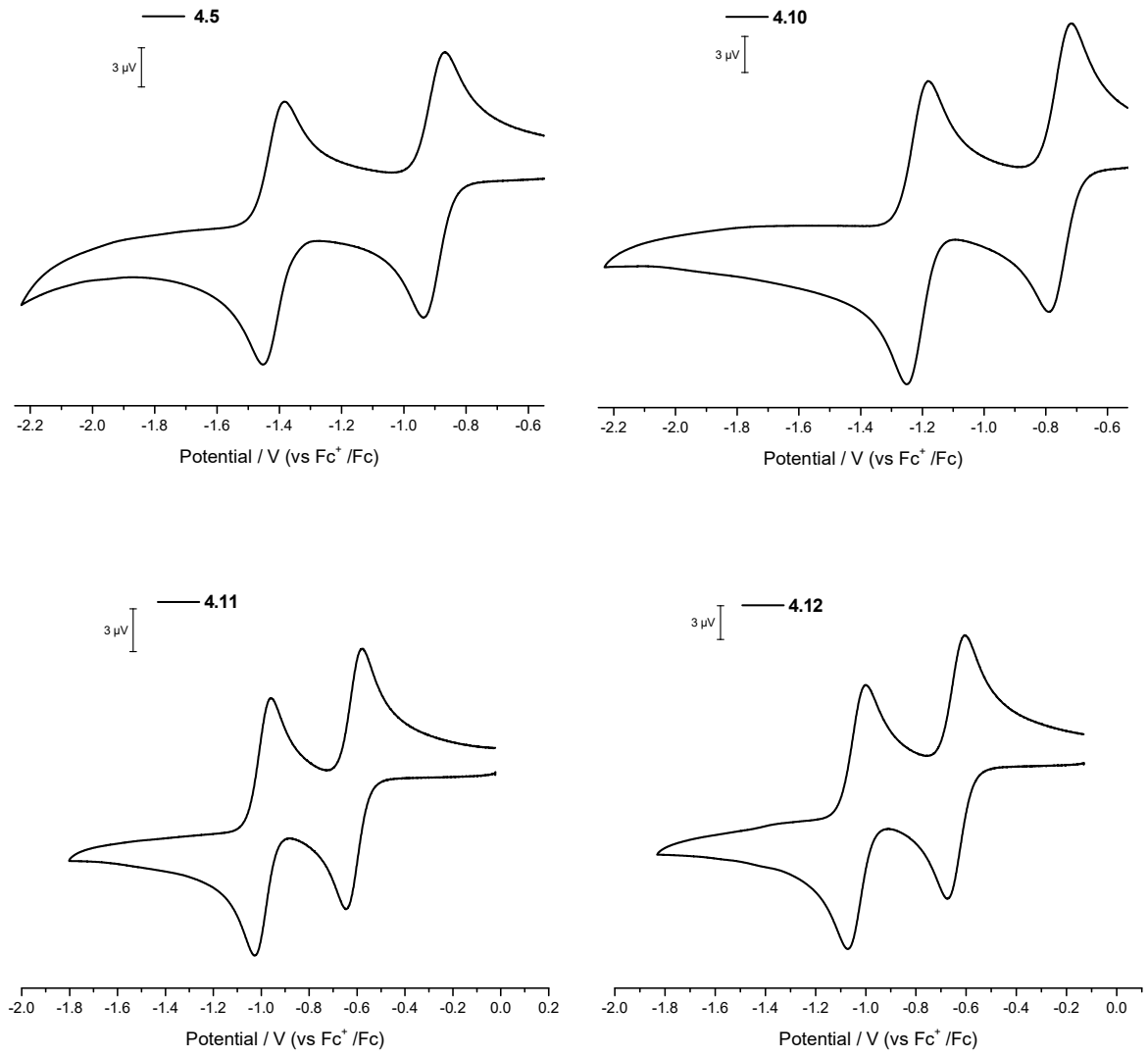


Figure 4-21: Cyclic voltammograms of **4.5**, **4.10**, **4.11** and **4.12** in DCM with 0.4 M $[Bu_4N][BF_4]$ supporting electrolyte, at a scan rate of 100 $mVs^{-1}$ at room temperature

In order to see how the redox properties of **4.5** had been altered via thionation **4.5**, **4.10**, **4.11** and **4.12** were also probed using cyclic voltammetry (Figure 4-22). As can be seen clearly, each of the species retained their typical two reversible one electron reductions. However upon viewing the potentials for these reductions a clear trend following increasing thionation can be observed. As the NDI becomes more thionated the reduction potentials of the species become more

positive. This change in potential seems to be around 140 mV for each sulphur in relation to the first reduction and about 200 mV for each sulphur for the second reduction (Table 4-1). This can be explained as each additional sulphur lowers the energy of the LUMO, making reduction easier.

Interestingly however, although the number of sulphur substituents plays the major role in the value for these potentials it seems that also the location of the substitution plays a role. When comparing the two di substituted isomers **4.11** and **4.12** this dependence is revealed as these two molecules do not share identical reduction potentials (Table 4-2). In both cases **4.12** is found to have more negative reduction potentials; a difference of 0.028 V for the first reduction and a difference of 0.047 V for the second. This is due to the ability of the sulphurs to modify the energies of the NDI molecular orbitals.

| **Molecule** | **1st Reduction $E_{1/2}$ / V** | **2nd Reduction $E_{1/2}$ / V** | **3rd Reduction $E_{1/2}$ / V** |
|---|---|---|---|
| **4.3** | -0.901 | -1.12 | -1.42 |
| **4.5** | -0.901 | -1.42 | - |
| **4.10** | -0.753 | -1.22 | - |
| **4.11** | -0.612 | -0.993 | - |
| **4.12** | -0.640 | -1.04 | - |

Table 4-3: Reduction potentials of **4.3**, **4.5**, **4.10**, **4.11** and **4.12.** Potentials recorded relative to the internal standard $E_{1/2}$ $Fc^+/Fc$ at a scan rate of 100 $mVs^{-1}$ at room temperature.

### 4.3.3: Spectroelectrochemistry

The optical behavior of **4.3** upon reduction was examined via spectroelectrochemical methods (Figure 4-23). The progress of the reductions of the molecule were followed utilizing UV/vis spectroscopy. These measurements were all carried out using DCM as the solvent. After undergoing the initial one electron reduction, the main bands related to the neutral species reduce in intensity and new red shifted bands correlating to the monoanionic species are generated concurrently (Table 4-4). The two bands at 363 nm and 384 nm are seen to deplete and so are related to the neutral NDI species. Two highly absorbing bands at 481 nm and 505 nm, within the visible range are produced, one overlapping the BODIPY's absorbance band, making this anion strongly absorbing at around 500 nm. Also a series of 3 broad low energy bands are generated at 607 nm, 699 nm and 778 nm these bands are also typical of a monoanionic NDI. Under these conditions the reduction was found to be entirely reversible.

| $\lambda_{abs}$ / nm ($\varepsilon$ x $10^{-3}$/ $mol^{-1}dm^3cm^{-1}$) | | |
|---|---|---|
| **4.3** | **$4.3^{1-}$** | **$4.3^{3-}$** |
| 282 (64.4), 296 (59.1), 363 (52.5), 384 (72.4), 485 (43.2), 505 (103.8) | 271 (68.8), 284 (69.0), 300 (62.6), 384 (35.6), 402 (36.9), 481 (88.5), 505 (127.1), 607 (14.0), 699 (4.9), 778 (8.3) | 271 (68.8), 289 (66.3), 304 (69.5), 336 (28.8), 418 (27.1), 456 (43.5), 479 (57.4), 546 (34.2), 608 (22.4), 667 (11.4), 777 (8.5) |

Table 4-5 Spectroelectrochemical data for **4.3** for neutral, monoanionic and trianionic states

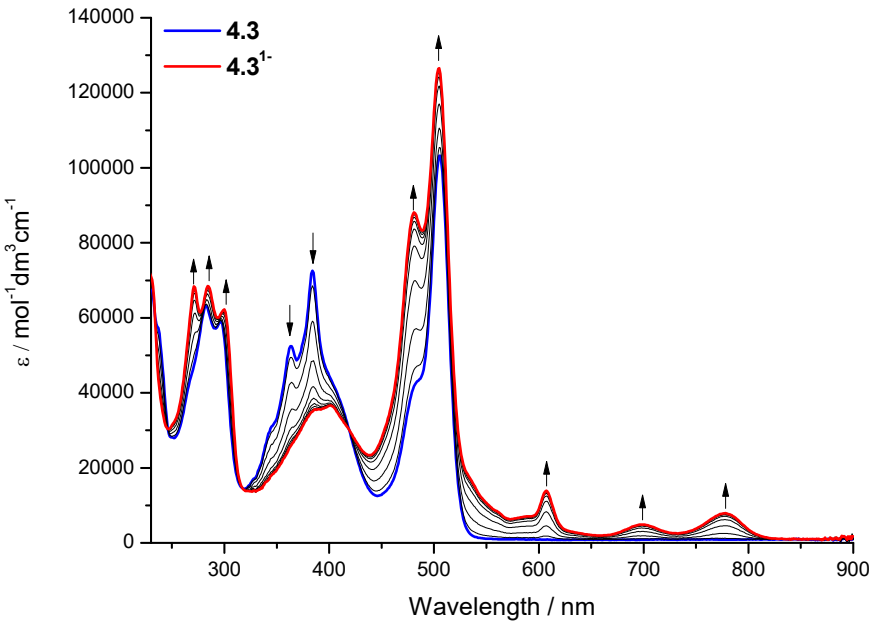


Figure 4-24: UV/vis absorption spectra recorded in DCM containing $[Bu_4N][BF_4]$ (0.4 M) using spectroelectrochemical methods for **4.3** at 243 K showing the inter-conversion of **4.3** (blue) to **4.3**$^{1-}$ (red). Arrows show the progress of the reduction.

Following the progress of the second reduction (Figure 4-25) the narrow band at 505 nm can be seen to deplete, as BODIPYs typically have narrow absorption bands this observation supports the idea that this reduction is related to the BODIPY units. These bands are then replaced by a band at 336 nm and several broad bands at lower energy (608 nm and 667 nm) along with a broad absorption profile centred around 777 nm, these bands add to the previous ones generated by the NDI anion. The fact that the band at 778 nm isn't perturbed shows that this second reduction is occurring on separate parts of the molecule. The two species, NDI and BODIPY, are reduced separately and maintain their separate anionic nature.

Unfortunately upon regeneration of the mono reduced species after the second reduction there was seen a markedly reduced intensity of the absorption of the sample. This is mostly likely due to the chemical decomposition of the BODIPY species upon being reduced, which is not uncommon for BODIPY molecules under these conditions. This unfortunately meant that the final reduction of this compound could not be investigated as the spectra generated could not be assigned to solely the reduced species and bands produced may be due to the decomposition of **4.3**.

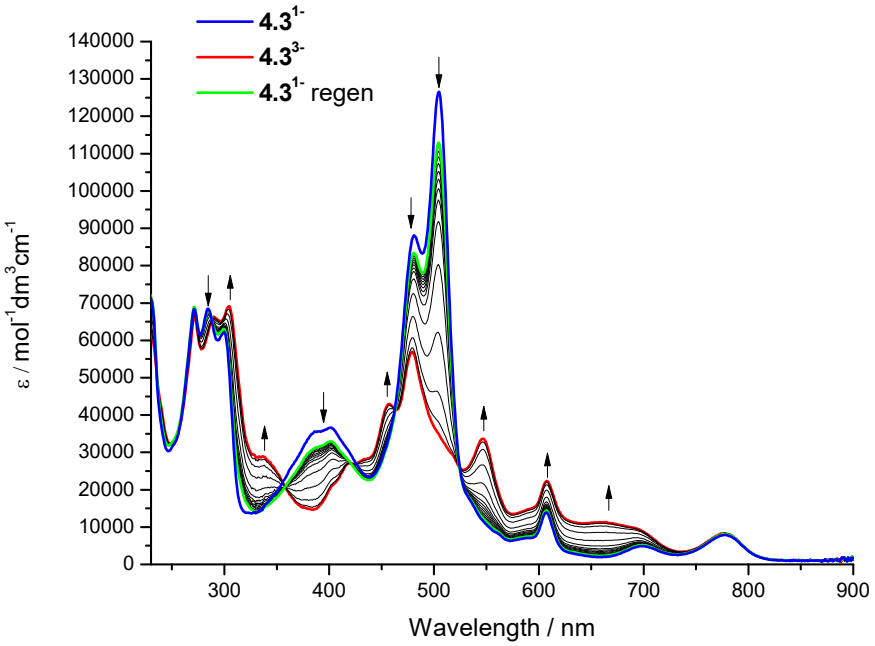


Figure 4-26: UV/vis absorption spectra recorded in DCM containing $[Bu_4N][BF_4]$ (0.4 M) using spectroelectrochemical methods for **4.3** at 243 K showing the inter-conversion of **4.3**$^{1-}$ (blue) to **4.3**$^{3-}$ (red). Arrows show the progress of the reduction. The regenerated spectra of **4.3**$^{1-}$ after reduction is also included (green).

## 4.4: Conclusions

Though unfortunately a rotaxane based upon and NDI-BODIPY architecture was not generated, the attempted synthesis of this molecule helped gain more understanding into these systems. Conditions which allow for coupling onto NDIs have been explored, and a troublesome coupling reaction has been made more reliable, allowing for it to be used towards the synthesis of other target molecules.

The electronic and optical properties of the BODIPY NDI rod was investigated. The BODIPY units were proven to be non-communicating to the NDI core. The ability of the species to absorb visible light was enhanced dramatically via the addition of the BODIPY antenna.

In addition to this work thionation of the rod was also attempted, to see how altering the frontier orbitals would affect energy transfer from the BODIPY to the NDI. However this lead to decomposition of the BODIPY antenna. Thionation of the unsubstituted NDI lead created a series of thionated products. The thionation caused a change in the energies of the frontier orbitals, noted by their absorbance of visible light. Unfortunately upon attempting to undergo the coupling reaction the species decomposed. This case is an illustration of the relative instability of thionated NDIs.

Future work within this area would do well to avoid using thionation of NDIs to manipulate their frontier orbitals, due to the erratic behaviour of them during synthesis. Perhaps a better way to peruse this goal would be via substitution onto the aromatic core. This allows for control of the frontier orbitals while generally forming stable species which could have their properties investigated.

## 4.5: Experimental

### 4.5.1: General procedures

All starting materials were purchased form Sigma Aldrich or Fisher Scientific and used without further purification. Column chromatography was conducted using silica gel (merck silica gel 60, 0.2-0.5 mm, 50-130 mesh). The $^{1}H$ and $^{13}C$ NMR spectra were obtained on a Bruker 400 MHz spectrometer. MALDI MS spectra were collected with a Bruker Ultraflex III mass spectrometer using trans-2-[3-(4-tert-butylphenyl)-2-methyl-2-propenylidene]malononitrile as the matrix. FD MS spectra were measured with a JOEL AccuTOF GCX spectrometer. Single crystal X-ray diffraction experiments were performed on an Oxford Diffraction Supernova CCD area detector diffractometer at 120 K using monochromated Cu K α radiation (λ = 1.54184 Å); on Agilent GV1000 AtlasS2 and TitanS2 CCD area detector diffractometers at 120 K using monochromated Cu K α radiation (λ = 1.54184 Å). Absorption corrections were applied using analytical numerical methods using either ShelXS or ShelXT and refined with ShelXL using a least squares method. In all instances, Olex2 software was used as the solution refinement and analysis program. All hydrogen atoms were placed in geometrically calculated positions; non-hydrogen atoms were refined with anisotropic displacement.

### 4.5.2: Synthesis of 4.1

2,6-Diisopropylanaline (4.69 g, 5 mL, 26.5 mmol) was dissolved in DCM (250 ml), tetrabutylammonium (12.8 g, 26.5 mmol) in DCM (250 ml) was added the solution was stirred at RT for 30 mins. Solvent was removed *in vacuo* and the residue re-dissolved in diethyl ether (150 ml), washed with 2M sodium hydroxide (150 ml x2), water (150 ml) and brine (150 ml). The solvent was removed, yielding a yellow oil. This was purified by column chromatography (silica, chloroform) to yield **4.1** (5.70 g, 22.26 mmol, 84 %) as a yellow oil. $^{1}$H NMR (400 MHz, Chloroform-*d*) δ 10.09 (bs, 2 H), 7.35 (s, 2 H), 3.73-3.65 (m, 2 H), 1.28 ppm (d, *J*=6.4 Hz, 12 H). $^{13}$C NMR (101 MHz, Chloroform-*d*) δ 145.0, 128.0, 123.9, 123.8, 29.0, 24.2 ESI MS: *:*255.2681for calc [*M*]$^{+}$: 255.0623;.

### 4.5.3: Synthesis of 4.2

Under a $N_2$ atmosphere, on activated 4 Å molecular sieves, H-imidazole (20 g), 1,4,5,8-naphthalenetetracarboxylic dianhydride (1 g, 3.73 mmol) and **4.1** (2.10 g, 8.20 mmol) was heated to 180 $^{o}$C for 18 h. This was cooled to room temperature and extracted into chloroform (2x 30 mL) then washed with 2 M HCl (3 x 60 mL), $Na_2CO_3$ (60 mL) and brine (60 mL). This was dried over $MgSO_4$, filtered and the solvent removed *in vacuo*. The product was purified by column chromatography (silica, [$CHCl_3$ : Hexane] [1:1]) to yield **4.2** (1.35 g, 1.82 mmol, 54 %) as a beige powder. $^{1}$H NMR (400 MHz, Chloroform-*d*) δ 8.89 (s, 4H), 7.47 (s, 4H), 2.66 (sep, *J*=6.9 Hz, 4H),

1.15 (d, *J*=6.9 Hz, 24H). $^{13}$C NMR (101 MHz, Chloroform-*d*) δ 162.7, 147.9, 131.7, 129.1, 127.8, 127.6, 126.8, 124.4, 29.4, 23.7. MALDI-MS: 743.40 calc[*M*]$^{+}$: 743.09

### 4.5.4: Synthesis of 4.4

Iodine (6.00 g, 23.3 mmol) was added to a solution of 2,6-diisopropylaniline (4 mL, 3.6 mmol) in diethyl ether (20 mL). Sodium bicarbonate solution (60 mL, 2 M) was added and the mixture stirred for 2 h. Sodium thiosulfate (3.00 g, 18.99 mmol) was added and the mixture stirred for a further 10 min. The mixture was extracted into diethyl ether (2 x 30 mL) and the organic layer washed with water (60 mL). The organic extract was dried over $MgSO_4$, filtered, the solvent removed *in vacuo* and the product purified by column chromatography (silica, [$CH_2Cl_2$: Hexane] [1:1]) to yield **4.1** as a colourless oil (6.41 g, 21.23 mmol, 99%). $^{1}$H NMR (400 MHz, Chloroform-*d*) δ 7.31 (s, 2 H) 3.75 (br. s., 2 H) 2.87 (sep, *J*= 6.80 Hz, 2 H) 1.27 (d, *J*=6.87 Hz, 12 H). $^{13}$C NMR (101 MHz, Chloroform-*d*) δ 140.03, 134.94, 131.64, 81.04, 27.81, 22.19. ESI MS: 304.0547 calc [MH$^{+}$]: 304.0562

### 4.5.5: Synthesis of 4.5

Under a $N_2$ atmosphere, on activated 4 Å molecular sieves, H-imidazole (20.00 g), 1,4,5,8-napthalenetetracarboxylic dianhydride (1.77 g, 6.60 mmol) and **4.4** (6.00 g, 19.8 mmol) was heated to 180 $^{o}$C for 18 h. This was cooled to room temperature and extracted into chloroform (2 x 30 mL) then washed with HCl (2M, 3 x 60 mL),

$Na_2CO_3$ (60 mL) and brine (60 mL). The organic extract was dried over $MgSO_4$ filtered and the solvent removed *in vacuo*. The product was purified by column chromatography (silica, [$CHCl_3$ :Hexane] [1:1]) to yield **4.2** as a beige powder ( 846 mg, 1.01 mmol, 57 %).

$^1$H NMR (400 MHz, Chloroform-*d*) δ 8.89 (s, 4 H) 7.67 (s, 4 H) 2.62 (sept, *J*=6.83 Hz, 4 H) 1.12 - 1.18 (m, 24 H). $^{13}$C NMR (101 MHz, Chloroform-*d*) δ 162.69, 147.97, 133.85, 131.73, 130.04, 127.64, 126.78, 96.75, 29.23, 23.76. MALDI MS = 838.673 Calc[$M^+$]: 838.0764.

### 4.5.6: Synthesis of 4.3

Under an atmosphere of $N_2$ **4.5** (566 mg 0.675 mmol), **3.18** (394 mg, 1.35 mmol), tetrakis-triphenylphosphine palladium (80 mg 0.068 mmol), copper iodide (20 mg, 0.1 mmol) was dissolved in a mixture of toluene (15 mL) and triethylamine (8 mL). The mixture was heated to 65 $^o$C for 24 h then cooled, extracted with toluene (40 mL) and filtered through kieselguhr. The filtrate was washed with HCl (2 M, 30 mL x 2), water (30 mL), brine (30 mL) and then dried over $MgSO_4$. The solvent was removed *in vacuo* and the crude product purified via column chromatography (silica, [$CH_2Cl_2$:Hexane] [95:5]) to yield **6** as a red powder (323 mg, 0.287 mmol, 41%).

$^1$H NMR (400 MHz, Chloroform-*d*) δ 8.93 (s, 4 H) 7.98 (s, 4 H) 7.76 (d, *J*=8.18 Hz, 4 H) 7.62 (d, *J*=8.18 Hz, 4 H) 7.58 (s, 4 H) 6.99 (d, *J*=3.95 Hz, 4 H) 6.60 (d, *J*=2.78 Hz, 4 H) 2.74 (sept, *J*=6.80 Hz, 4 H) 1.22 (d, *J*=6.72 Hz, 24 H). $^{13}$C NMR (101 MHz, Chloroform-*d*) δ 163.06 146.69

146.45 144.62 135.01 133.84 131.99 131.94 131.68 131.00 130.84 128.15 127.96 127.11 126.33 124.66 118.99 92.48 88.88 29.61 24.10. Hi-res MALDI MS: 1166.4478 Calc [$M^+$]: 1166.4485, 1147.4474 Calc [M –F]: 1147.4501

**Crystal Data** for $C_{72}H_{56}B_2F_4N_6O_4$ ($M$ =1166.84 g/mol): monoclinic, space group $P2_1/c$ (no. 14), $a$ = 21.7113(7) Å, $b$ = 8.9648(3) Å, $c$ = 15.3877(4) Å, $\beta$ = 104.521(3)°, $V$ = 2899.34(17) Å$^3$, $Z$ = 2, $T$ = 30(2) K, μ(Synchrotron) = 0.086 mm$^{-1}$, *Dcalc* = 1.337 g/cm$^3$, GooF = 1.042 32869 reflections measured (5.636° ≤ 2Θ ≤ 58.998°), 8490 unique ($R_{int}$ = 0.0535, $R_{sigma}$ = 0.0433) which were used in all calculations. The final $R_1$ was 0.0785 (I > 2σ(I)) and $wR_2$ was 0.2514 (all data).

## 4.5.7: Synthesis of 4.6

Tetraethyleneglycol (11.25 mL, 51 mmol) and *p*-toluenesulfonylchloride (19.38 g, 102 mmol) were dissolved in degassed DCM (51 mL). The solution was added dropwise to KOH (22.66 g, 404 mmol), at 0 °C, then stirred for 4 h. The mixture was extracted into DCM (50 mL) and washed with water (3 x 100 mL), dried over $MgSO_4$ filtered and the solvent removed *in vacuo*. The residue was purified via column chromatography (silica [$Et_2O$]) to yield **4.7** (11.29 g, 22.5 mmol, 50 %) as a white solid.

$^1$H NMR (400 MHz, d6-DMSO) δ 7.79 (d, $J$ 8.3 Hz, 4H), 7.34 (d, $J$ 8.3 Hz, 4H), 4.15 (t, $J$ 4.9 Hz, 4H), 3.68 (t, $J$ 4.9 Hz, 4H), 3.56 (s, 8H), 2.45 (s, 6H). $^{13}$C NMR (101 MHz, d6-DMSO) δ 144.79, 132.87,

129.78, 127.91, 70.65, 70.47, 69.21, 68.61, 21.59. ESI MS: 525.1328 Calc [$MNa^+$]: 525.1228

### 4.5.8: Synthesis of 4.7

Under $N_2$ **4.7** (11.3 g, 22.5 mmol) and 1,5-dihydroxynaphthalene (720 mg, 4.5 mmol) in dry acetone (125 mL) was added to $K_2CO_3$ (3 g, 21.7 mmol) in dry acetone (125 mL) at 60 $^oC$ over 3 h. This was then left for 3 d, filtered the solvent removed *in vacuo* and the residue extracted into $CH_2Cl_2$ (100 ml). This was washed with water (2 x 100 mL,) $NaOH_{(aq)}$ solution (2M. 3 x 100 mL) dried over $MgSO_4$ filtered and the solvent removed *in vacuo*. The crude material was purified via column chromatography (silica, $Et_2O$) to yield **4.8** (1.38 g, 1.65 mmol, 36 %) as a white powder.

$^1H$ NMR (400 MHz, Chloroform-*d*) δ 7.62 (q, *J* = 5.1 Hz, 2H), 7.53 (d, *J* = 8.3 Hz, 4H), 6.60 (q, *J* = 5.1 Hz, 2H), 4.08-4.03 (m, 4H), 3.90-3.87 (m, 2H), 3.59−3.53 (m, 4H), 3.49−3.40 (m, 14H), 3.37−3.32 (m, 4H) ppm. $^{13}C$ NMR (101 MHz, Chloroform-*d*) δ 155.1, 144.9, 140.2, 132.9, 129.8, 127.6, 124.9, 114.5, 105.6, 70.7, 70.3, 69.2, 68.6, 67.8, 21.6 ppm. ESI MS: 843.2708 Calc [$MNa^+$]: 843.2696

### 4.5.9: Synthesis of 4.8

Under $N_2$ **4.8** (1.3 g, 1.6 mmol) and 1,5-dihydroxynaphthalene (260 mg, 1.6 mmol) in dry acetone (110 mL) was added to $K_2CO_3$ (1.5 g, 10.9 mmol) in dry acetone (110 mL) at 60 $^oC$ over 3 h. This was left for 3 d, filtered to remove any solid material, the solvent removed *in*

*vacuo* and the residue extracted into $CH_2Cl_2$ (100 ml). This was washed with water (2 x100 mL) NaOH solution (2M, 3 x 100 mL) dried over $MgSO_4$ filtered and the solvent removed *in vacuo*. The crude material was purified via column chromatography (silica, EtOAc) to yield **4.9** as a white powder.

$^1$H NMR (400 MHz, Chloroform-*d*) δ 7.79 (d. 4H. *J* - 8 Hz), 7.19 (t. 4H. *J* - 8 Hz), 6.50 (d, 4H.] - 8 Hz), 4.06 (m. 8H), 3.93 (m, 8H). 3.78 (m. 8H), 3.75 (m, 8H). $^{13}$C NMR (101 MHz, Chloroform-*d*) δ 154.1, 126.6, 125.0, 114.4, 105.4, 70.9, 69.7, 67.7. ESI MS: 659.2893 Calc [$MNa^+$]: 659.2832

## 4.5.10: Synthesis of 4.10-4.12

**4.5** (1 g, 1.19 mmol) and Lawesson's reagent (3 g, 7.41 mmol) were refluxed in toluene (100 ml) for 48 h. This was cooled, washed with NaOH solution (2M, 2 x 100 mL), then water (2 x 100 mL), dried over $MgSO_4$, filtered and the solvent was removed *in vacuo*. This was then filtered through a kieselguhr plug ($CHCl_3$). The solvent was removed *in vacuo* and the crude material was purified via column chromatography (silica [$CH_2Cl_2$:Hexane, 1:1]). This yielded **4.10** (220 mg, 0.26 mmol, 22 %), **4.11** (26 mg, 0.024 mmol, 2.4 %) and **4.12** (21 mg, 0.024 mmol, 2.0 %) as green powders.

**4.10:** $^1$H NMR (400 MHz, Chloroform-*d*) δ 9.14 (d, *J* = 7.9 Hz, 1H), 8.86 (s, 2H), 8.78 (d, *J* = 7.9 Hz, 1H), 7.64 (d, *J* = 7.0 Hz, 4H), 2.67 – 2.52 (m, 4H), 1.15 – 1.11 (m, 24H). $^{13}$C NMR (101 MHz, Chloroform-*d*) δ 193.28, 162.99, 160.13, 148.00, 147.17, 135.92, 134.92,

134.14, 133.86, 131.91, 131.74, 131.31, 130.27, 130.13, 127.89, 127.07, 126.43, 125.99, 125.51, 96.74, 96.35, 77.34, 77.02, 76.70, 29.26, 29.15, 24.13, 23.82, 23.77. MALDI MS: 854.21 Clac: 854.05

**4.11:** $^{1}$H NMR (400 MHz, Chloroform-*d*) δ 9.04 (s, 2H), 8.84 (s, 2H), 7.63 (s, 4H), 2.61 – 2.49 (m, 4H), 1.15 – 1.07 (m, 24H). $^{13}$C NMR (101 MHz, Chloroform-*d*) δ 193.41, 160.42, 147.19, 135.49, 134.12, 131.94, 129.80, 129.00, 127.98, 126.74, 125.09, 96.33, 77.34, 77.02, 76.70, 29.71, 29.15, 24.13, 23.81. MALDI MS: 870.32 Clac: 870.03

**Crystal Data** for $C_{38}H_{36}I_2N_2O_2S_2$ ($M$ =870.61 g/mol): monoclinic, space group Ia (no. 9), $a$ = 16.7101(6) Å, $b$ = 9.4970(3) Å, $c$ = 23.2404(9) Å, $\beta$ = 101.294(4)°, $V$ = 3616.8(2) Å$^3$, $Z$ = 4, $T$ = 120(2) K, μ(CuKα) = 15.012 mm$^{-1}$, *Dcalc* = 1.599 g/cm$^3$, GooF = 1.132, 19727 reflections measured (7.758° ≤ 2Θ ≤ 133.156°), 6345 unique ($R_{int}$ = 0.0539, $R_{sigma}$ = 0.0479) which were used in all calculations. The final $R_1$ was 0.0560 (I > 2σ(I)) and $\omega R_2$ was 0.1548 (all data).

**4.12:** $^{1}$H NMR (400 MHz, Chloroform-*d*) δ 9.15 (d, $J$ = 8.0 Hz, 3H), 8.77 (d, $J$ = 8.0 Hz, 2H), 7.66 (s, 8H), 2.63 – 2.53 (m, 4H), 1.13 (t, $J$ = 7.1 Hz, 26H). $^{13}$C NMR (101 MHz, Chloroform-*d*) δ 193.49, 160.50, 147.17, 136.00, 134.12, 131.56, 131.41, 129.81, 126.21, 96.31, 77.34, 77.02, 76.70, 29.71, 29.15, 24.12, 23.81. MALDI MS: 870.431 Clac: 870.03

**Crystal Data** for $C_{40}H_{37}Cl_6I_2N_2O_2S_2$ ($M$ =1108.33 g/mol): triclinic, space group P1 (no. 1), $a$ = 8.7155(3) Å, $b$ = 11.8026(4) Å, $c$ = 12.6123(5) Å, $\alpha$ = 115.873(4)°, $\beta$ = 101.873(3)°, $\gamma$ = 99.253(3)°, $V$ = 1095.12(7) Å$^3$, $Z$ = 1, $T$ = 120(2) K, μ(CuKα) = 15.830 mm$^{-1}$, *Dcalc* = 1.681 g/cm$^3$, v GooF= 1.030, 7926 reflections measured (8.196° ≤ 2Θ ≤ 147.782°), 5035 unique ($R_{int}$ = 0.0306, $R_{sigma}$ = 0.0413) which were used in all calculations. The final $R_1$ was 0.0320 (I > 2σ(I)) and $wR_2$ was 0.0796 (all data).

## 4.5.11: Electrochemical and Optical Investigations

UV/visible absorption spectra were recorded on Perkin-Elmer Lambda 25 spectrometer. Cyclic voltammetric and coulometric studies were conducted using an Autolab PGSTAT20 potentiostat. $CH_2Cl_2$ was dried *via* distillation under nitrogen on calcium hydride. Standard cyclic voltammetry was carried out under an atmosphere of argon using a three electrode arrangement in a single compartment cell. Electrodes used in the cell were as follows; A glassy carbon working electrode, a Pt wire secondary electrode and a calomel reference electrode, chemically isolated from the test solution *via* a bridge tube containing electrolyte solution and fitted with a porous vycor frit. The solutions were $10^{-3}$ M in molecule of interest and 0.4 M in $[Bu_4N][BF_4]$ as the supporting electrolyte. Redox potentials are quoted versus the ferrocenium-ferrocene couple used as an internal reference. Compensation for internal resistance was not applied.

The UV/vis spectroelectrochemical experiments were carried out with and optically transparent electrochemical cell (modified quartz cuvette, optical pathlength: 0.5 mm). A three electrode configuration, consisting of Pt/Rh gauze working electrode, a Pt wire secondary electrode (in a fritted PTFE sleeve) and a saturated calomel electrode, as reference, chemically isolated from the test solution *via* a bridge tube containing electrolyte solution and terminated in a porous frit, was used in the cell. The potential at the working electrode was controlled by a Sycopel scientific Ltd DD10M potentiostat. The UV/vis spectra were recorded on a Perkin Elmer Lambda 16 spectrophotometer. The cavity was purged with dinitrogen and temperature control at the sample was achieved by flowing cooled dinitrogen across the surface of the cell.

## 4.6: References


(1) I. T.Harrison, S.Harrison, *JACS,* **1967**, *89*, 5723.

(2) Jean-Marie, L. *Angewandte Chemie International Edition* **1988**, *27*, 89.

(3) C. G. Claessens, J. F. Stoddart, *J. Phy. Org.Chem,* **1997**, *10*, 254.

(4) G. R.Desiraju, *Acc. Chem. Res,* **1996**, *29*, 441.

(5) F.Biedermann, W. M. Nau, H. Schneider, *Angew. Chem. Int. Ed*, **2014**, *53*, 11158.

(6) K. S.Chichak, S. J.Cantrill, A. R.Pease, S.-H.Chiu, G. W. V.Cave, J. L.Atwood, J. F.Stoddart, *Science,* **2004**, *304*, 1308.

(7) A. M.Albrecht-Gary, M.Meyer, C. O.Dietrich-Buchecker, J. P.Sauvage, J.Guilhem, C.Pascard, *Recl. Trav. Chim. Pays-Bas*, **1993**, *112*, 427.

(8) O.Lukin, F.Vögtle, *Angew. Chem. Int. Ed,* **2005**, *44*, 1456.

(9) D. B.Amabilino, P. R.Ashton, A. S.Reder, N.Spencer, J. F.Stoddart, *Angew. Chem. Int. Ed,* **1994**, *33*, 1286.

(10) B. A. Ikkandaa, B. L. Iverson, *Chem.Commun,* **2016**, *52*, 7752.

(11) M.Tomasulo, D. M.Naistat, A. J. P.White, D. J.Williams, F. M.Raymo, *Tetrahedron Lett,* **2005**, *46*, 5695.

(12) H.Shao, J. R.Parquette, *Chem. Commun,* **2010**, *46*, 4285.

(13) J.Zheng, W.Qiao, X.Wan, J. P.Gao, Z. Y.Wang, *Chem. Mater,* **2008**, *20*, 6163.

(14) M. R.Molla, S.Ghosh, *Chem. Eur. J,* **2012**, *18*, 9860.

(15) G. D.Fallon, M. A. P. Lee, S. J.Langford, P. J.Nichols, *Org.Lett,* **2004**, *6*, 655.

(16) J. G.Hansen, N.Feeder, D. G.Hamilton, M. J.Gunter, J.Becher, J. K. M.Sanders, *Org. Lett,***2000**, *2*, 449.

(17) B. J.Slater, E. S.Davies, S. P.Argent, H.Nowell, W.Lewis, A. J.Blake, N. R.Champness, *Chem. Eur. J,* **2011**, *17*, 14746.

(18) M. Asakawa, P. R. Ashton., R.Ballardini, V. Balzani, M. Bělohradský, M. T. Gandolfi, O. Kocian, L. Prodi, F. M. Raymo, J. F. Stoddart, M. Venturi, *JACS* **1997**, *119*, 302.

(19) Z.Kostereli, T.Ozdemir, O.Buyukcakir, E.U.Akkaya, *Org. Lett,* **2012**, *14*, 3636.

(20) W.Li, Z.Xie, X.Jing, *CatalCommun,* **2011**, *16*, 94.

(21) S.Erten-Ela, M. D.Yilmaz, B.Icli, Y.Dede, S.Icli, E. U.Akkaya, *Org. Lett,* **2008**, *10*, 3299.

(22) R.Ziessel, G.Ulrich, A.Haefele, A.Harriman, *JACS,* **2013**, *135*, 11330.
(23) C.Zhang, J.Zhao, S.Wu, Z.Wang, W.Wu, J.Ma, S.Guo, L.Huang, *JACS,* **2013**, *135*, 10566.
(24) C.-W.Wan, A.Burghart, J.Chen, F.Bergström, L. B. Å.Johansson, M. F.Wolford, T. G.Kim, M. R.Topp, R. M. Hochstrasser, K.Burgess, *Chem. Eur. J,* **2003**, *9*, 4430.
(25) A.Burghart, L. H.Thoresen, J.Chen, K.Burgess, F.Bergstrom, L. B. A.Johansson, *Chem. Commun,* **2000**, 2203.
(26) V.Bandi, S. K.Das, S. G.Awuah, Y.You, F.D'Souza, *JACS,* **2014**, *136*, 7571.
(27) Y.Rio, W.Seitz, A.Gouloumis, P.Vázquez, J. L.Sessler, D. M.Guldi, T.Torres, *Chem. Eur.J,* **2010**, *16*, 1929.
(28) L.Favereau, A.Makhal, Y.Pellegrin, E.Blart, J.Petersson, E.Göransson, L.Hammarström, F.Odobel, *JACS,* **2016**, *138*, 3752.
(29) Y.Schramm, F.Barrios-Landeros, A.Pfaltz, *Chem. Sci,* **2013**, *4*, 2760.
(30) A.Mayr, M.Srisailas, Q.Zhao, Y.Gao, H.Hsieh, M.Hoshmand-Kochi, N.St. Fleur, *Tetrahedron* **2007**, *63*, 8206.
(31) A.Hospital, C.Gibard, C.Gaulier, L.Nauton, V.Thery, M.El-Ghozzi, D.Avignant, F.Cisnetti, A.Gautier, *Dalton Trans,* **2012**, *41*, 6803.

(32) H.P. J. de Rouville, J. Iehl, C. J.Bruns, P. L.McGrier, M.Frasconi, A. A.Sarjeant, J. F. Stoddart, *Org. Lett* **2012**, *14*, 5188.

(33) C. J. Bruns, S.Basu, J.F.Stoddart, *Tetrahedron Lett.* **2010**, *51*, 983.

(34) L. M.Kozycz, C.Guo, J. G. Manion, A. J. Tilley, A. J.Lough, Y.Li, D. S. *J* .Seferos, *Mater. Chem. C* **2015**, *3*, 11505

(35) S. P.Jarvis, A. M.Sweetman, I.Lekkas, N. R.Champness, L.Kantorovich, P. *J.*Moriarty, *Phys. Condens. Matter* **2015**, *27*, 54004.

# Chapter 5 : Conclusion

This thesis explores how NDIs can be manipulated to absorb visible light. Visible light is the most abundant light on the surface of the planet due to other wavelengths being absorbed by the atmosphere. NDIs have high absorbtion coefficients, typically found in the UV region. By changing the wavelength of energies absorbed these high coefficients could be utilized to efficiently absorb visible light energy. This, along with their modest reduction potential, would enable them to be good candidates for photovoltaic devices.

Core substitution onto naphthalene diimides has been investigated in depth throughout this thesis. Within Chapter 2 a synthetic pathway that allows for the synthesis of cNDIs is developed and used to create a series of morpholine substituted cNDIs. This substitution caused the absorbtion of the NDI to be shifted to the visible range. The redox and optical properties of these molecules were examined and a good deal of information upon how this substitution affects the molecular orbitals is gathered. From this the properties of the molecules were rationalized.

This chapter work creates a foundation from which new cNDIs could be synthesized. In addition it expands upon the knowledge of how a NDIs frontier orbitals can be modified, providing an example were the geometry of the substituents plays a role upon the how the affect them.

Within Chapter 3 the synthetic pathway devised in Chapter 2 is used to generate cNDIs substituted with phenothiazine and phenoxazine.

These electron rich species pair with the electron poor NDI, to make a series of electron donor-acceptor systems. This required a new synthetic method for substitution onto phenonazine to be developed. This method should be robust enough to allow for easy synthesis of many other aryl N-substituted phenoxazine species.

These donor-acceptor systems highlight how the ability to change the energy of the frontier orbitals of NDIs could be put to practical use. The additional benefit of substituting the donor species onto the core of the NDI is that the NDIs frontier orbitals are modulated to the point where they absorb visible light. This in turn means that they become good candidates for photovoltaic devices. Excitation of the NDI by visible light may generate a charge separated state, which could be used to generate a current allowing for visible light to be transferred into electricity.

This study also showcases that the frontier orbitals of the NDI systems can be further modified by further substitution. This allows for a great degree of freedom in regards to the frontier orbitals of the NDI. As only one site is required to attach the donor species other sites on the core can be used to tweak the NDIs frontier orbitals to be complementary to the donor species and ultimately make accessing a charge separated state more efficient.

The molecules synthesized throughout this study would certainly benefit from further study. DFT calculations could be used to gain a greater insight into the transitions observed. Also time resolved

spectroscopy could be used to gain further insight into the molecules synthesized. These techniques could access whether the species undergo PET to generate a charge separated state, the lifetime and efficiently of this charge transfer could be accessed.

Within Chapter 4 are examples of synthetic problems that still need to be better understood and overcome in NDI chemistry. Primarily the selectivity of thionation of NDI remains unselective. Also thionated NDIs are shown to be unstable under certain conditions. This work would hope to inform future work as to the instability of thionated NDI and synthetic routes which should be avoided.

Overall this body of work explores how the frontier orbitals of NDI can be controlled. The hope is that this work could assist and inspire the increased use of NDI as a tunable chromophore. In this way the NDI could act as an excellent light harvester. Currently the majority of photovoltaic devices are based ion costly silicon chips. By replacing these with a cheaper organic alternative, solar cells could be created more readily at a smaller cost. This work hopes to highlight ways in which NDIs could be used to fill this role. This would hopefully create an avenue to a cheap, green and renewable energy source to help cope with the energy demands of the future.